Evaluation of timber-concrete composite floors

Andreas Manaridis

Avdelningen för Konstruktionsteknik
Lunds Tekniska Högskola
Lund Universitet, 2010

Rapport TVBK - 5187

Avdelningen för Konstruktionsteknik
Lunds Tekniska Högskola
Box 118
221 00 LUND

Department of Structural Engineering
Lund Institute of Technology
Box 118
S-221 00 LUND
Sweden

Evaluation of timber-concrete composite floors

Utvärdering av samverkansbjälklag av trä och betong

Andreas Manaridis

2010

Abstract

An inevitable consequence of the increasingly larger buildings that we see around us is the demand for lighter construction components. Since floor slabs constitute the main part of the overall weight of multistory buildings, reducing their weight is a key step in reducing the overall weight of the construction. Usually this is done by using hollow core slabs or other types of all-concrete solutions.

This thesis brings attention to an alternative solution. A timber-concrete composite deck reduces the weight several times compared to a standard concrete deck, without compromising the bending stiffness. Additional benefits include architectural considerations, possibilities of longer spans as well as free space between the timber components. With the aim of evaluating different timber-concrete composite solutions, an extensive literature review on the field was conducted. Vital construction parts and existing timber-concrete composite solutions were studied. Finally, two full scale composite deck specimens were tested.

The fruit of this work is the presentation of a timber-concrete composite solution that can either be prefabricated or semi-prefabricated. The obvious field of application is multistory office buildings, where the solution offers an answer to demands of reduced overall weight, large open spaces and architectural benefits.

Rapport TVBK-5187
ISSN 0349-4969
ISRN: LUTVDG/TVBK-10/5187+131p

Examensarbete
Handledare: Tord Isaksson
Juli 2010

Acknowledgements

I would like to thank the people who have made this master thesis possible.
First I would like to thank my supervisor Sven Thelandersson, professor at the department of structural engineering at “Lunds Tekniska Högskola”, for his advice and patient guidance during my efforts to compile this master thesis. I also want to thank the Setra Group for financing my experiments. Last but not least I would like to thank Tero Korhonen and Dominic Sieber at SFS Intec for offering their help and providing me with connectors and documentation.

Table of contents

1 Introduction

1.1 Background

Concrete is undoubtedly one of the greatest inventions in the field of constructional engineering and it brought with it fantastic possibilities. Nevertheless, ever since it was invented, its low tensile capacity has constituted an obstacle. In concrete floorings, the solution to this day has been the adding of steel reinforcement to the structure.

However, in order for a floor to develop a sufficient amount of moment capacity, the resultants of compression- and tensile forces need to be kept at a certain distance from one another. Practically and somewhat simplified, this means that about half the amount of concrete in traditional concrete floors, fills merely the function of keeping the steel reinforcement at a convenient distance from the compression zone in the upper part of the slab.

With demands for increasingly larger buildings, the weight of the extra concrete needed to keep reinforcement in place has become an issue in itself. Since floor slabs constitute the main part of the overall weight of a building, reducing their weight is a key step in reducing the overall weight. Thus far, this has been achieved using hollow core slabs or other types of all-concrete solutions.

An alternative approach that has gained more attention recently is the use of timber as a part of the structure. Timber beams have a high tensile capacity in the grain direction and provided a stiff connection, an efficient composite structure constituted by a thin concrete slab at the top and timber beams at the bottom can be created. In such a structure, the concrete slab will mainly be exposed to compressive forces, while the tensile forces are concentrated in the timber beams.

Without the extra concrete needed to keep the reinforcement in place, a considerable amount of weight can be saved without compromising the bending stiffness. Additional benefits that follow include the possibility to use longer spans as well as aestetical gains or alternatively the utilization of the free space between the timber beams. The extra cost of timber as a part of the structure is compensated by the fact that the timber components function as permanent formwork, thus enabling work to take place underneath at an earlier stage. When compared to a steel-concrete composite, benefits of a timber-concrete composite involve reduced weight, cost and energy consumption during the manufacturing.

Considering the above advantages, it seems logical to invest more research in this field, so that an effective timber-concrete composite floor could be

introduced on a large scale. A possible field of application could be multistory office buildings, where timber-concrete composite floors offer an answer to the demands of reduced overall weight, large open spaces and architectural benefits.

1.2 Objectives

There are two main objectives for this master thesis:

- To evaluate timber-concrete composite floor solutions
- To present an efficient timber-concrete composite solution for floors in office buildings

1.3 Outline of the thesis

Chapter 2 is a literature review and serves as the foundation for this master thesis. It deals primarily with the function and design of a composite floor but it also contains 3 surveys, concerning tested shear connectors (the vital part in a composite floor), currently employed timber-concrete solutions as well as some possible methods for enhancing the performance of a timber-concrete composite floor. The purpose of the surveys is to facilitate the evaluation that constitutes the first objective of this thesis.

Chapter 3 aims to fulfil the first objective of this thesis. It is an evaluation of different timber-concrete composite floor solutions, based on the surveys presented in chapter 2.

Chapter 4 accounts for the full scale bending tests that were conducted as a part of this master thesis.

Chapter 5 aims to fulfil the second objective of this thesis. Based on the evaluation and the full scale bending tests, chapter 5 presents a timber-concrete composite solution that is suitable for multi-storey office buildings. The presentation includes design procedure and method of construction among other things.

Chapter 6 states the conclusions drawn from this work, together with a short discussion.

2 Litterature Review

2.1 Function of a timber-concrete composite

2.1.1 General

If a concrete slab is cast freely on top of a beam and the friction is assumed to be negligible, the beam and the slab will act separately to resist flexural action, see figure 2.1 c. Their separate actions will give rise to a slip between the slab and the beam upon loading. By interconnecting concrete and timber however, that slip can be reduced. Preventing slip inevitably results in reduced vertical displacement as well. Thus, by interconnecting two elements, their combined bending stiffness can be increased. This phenomenon of two components working together as opposed to acting separately is known as composite action.

Of course, the degree of composite action achieved increases with the stiffness of the connection. The degree of composite action may vary from no composite action for no connection, to full composite action for an infinitely stiff connection.

The taller cross section of a composite element compared to the cross sections of its individual sub-elements results in a longer internal moment arm. Consequently, the normal strains resulting from an arbitrary external load are reduced within the structure. For a very stiff connection, the result is a state where the concrete slab is mainly exposed to compression forces, while tensile stresses are concentrated in the wooden part, see figure 2.1 a. This means that the materials, concrete with its high compression capacity and wood with its high tensile capacity in the grain direction, are being used effectively.

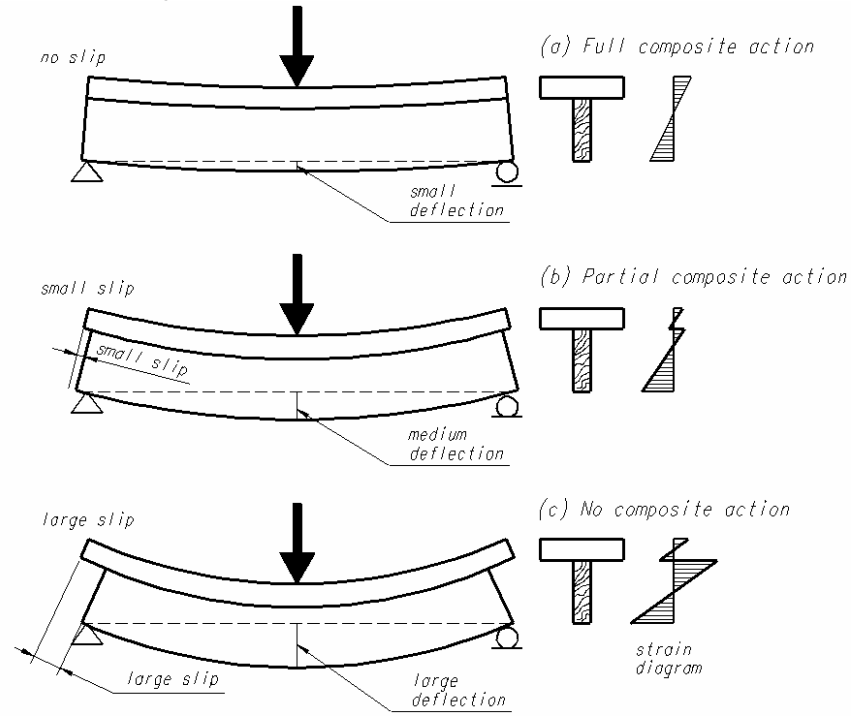

Figure 2.1 The concept of composite action (Lukaszewska, 2009)

It should be emphasized that the correlation between the bending stiffness of a composite structure - often referred to as the effective bending stiffness - and the stiffness of the connection is not linear. Dias presents the following graphical representation of the correlation between the stiffness of the connection and the effective bending stiffness of a composite beam, see figure 2.2 (Dias, 2005).

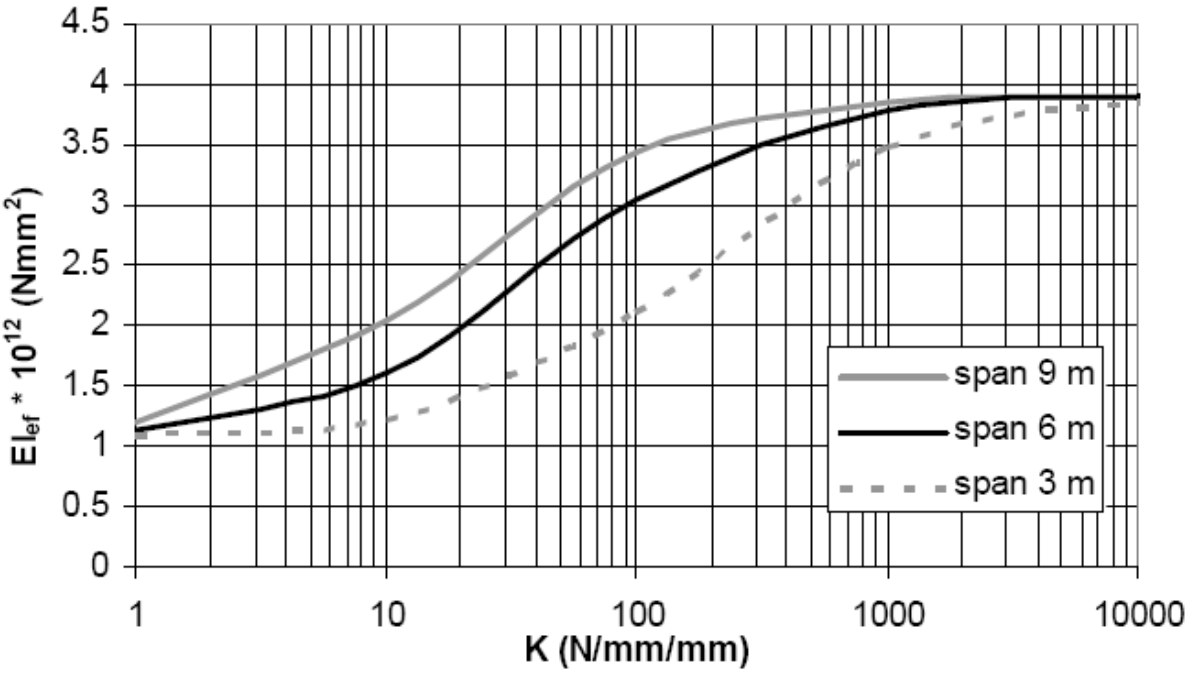

Figure 2.2 Graphical representation of the correlation between stiffness of a shear connection and the effective bending stiffness of a composite floor (Dias, 2005)

It is evident from figure 2.2 that making efforts to increase the stiffness of the connection past a certain limit becomes useless since it has no significant impact on the effective bending stiffness. Similarly, for a connection to serve any purpose, its stiffness must be above a certain limit. Van der Linden also concluded that the bending stiffness could be increase up to a maximum of 4 times by introducing composite action. This was only possible given an infinitely stiff connection and certain combinations of geometric and material properties. (Dias, 2005)

2.1.2 Shear connector

It is apparent that the critical part of any composite structure is the connection between the elements. This component is usually referred to as the shear connector because of the shear forces that it must absorb. Indeed, apart from being stiff, a shear connector needs to have a certain strength, or shear capacity, in order not to fail. A failure of the shear connectors in a composite floor could lead to a global collapse of the floor if the individual sub-elements lack the capacity needed to resist the load on their own. The stiffer the shear connector is, the stronger it needs to be since the exposure to shear forces increases with stiffness.

Thus, the stiffness and strength of a timber-concrete composite beam is dependant on both the stiffness and strength of its connectors. A lack of stiffness and strength of the shear connectors could be compensated by increasing the total number of connectors along the beam, but a very small spacing between the connectors is usually synonymous with more work resulting in higher construction costs.

Apart from a high level of stiffness and strength, a good post peak behaviour is also desirable for a shear connector. The post-peak behavior can be defined as "the connector's behavior under loading after failure has occurred". As for construction in general, a good post peak behavior for the connectors is considered to be ductile. A ductile failure gives users a warning in case of an imminent collapse. Since the failure mode of concrete as well as the tensile/bending-failure mode of wood can be considered brittle, as a last resort it would be desirable to have failure occur in shear-connectors with a ductile post peak behavior. This would lead to a slow increase in deflection before the final failure.

Strength, stiffness and post-peak behavior of a connector are often investigated by conducting symmetrical or asymmetrical shear tests. These are commonly referred to as push out tests, since they involve the "pushing out" of one of the components constituting the test specimens. Figure 2.3 shows the principal setup of a symmetrical push-out test, where the horizontal lines symbolize shear connectors.

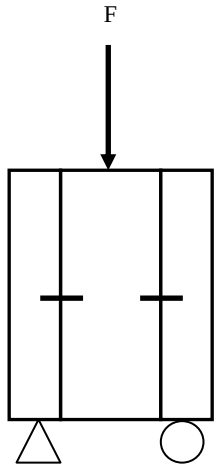

Figure 2.3 Setting of a symmetrical push-out test

After conducting the push-out tests, the shear capacity, stiffness and post peak behavior of the connectors can be assessed from studying the load-displacement curves. The shear capacity is equal to the peak value of the load in the load-displacement curve and the stiffness is assessed by determining the slip modulus k [N/mm], of the connector. The best connector from a structural perspective is characterized by a curve with a long and steep first section (indicating high stiffness and strength) followed by a second slightly declining plateau-like section (indicating good post peak behavior), before the curve drops (final failure). Figure 2.4 illustrates the principal load-displacement curves for desirable and undesirable connectors respectively.

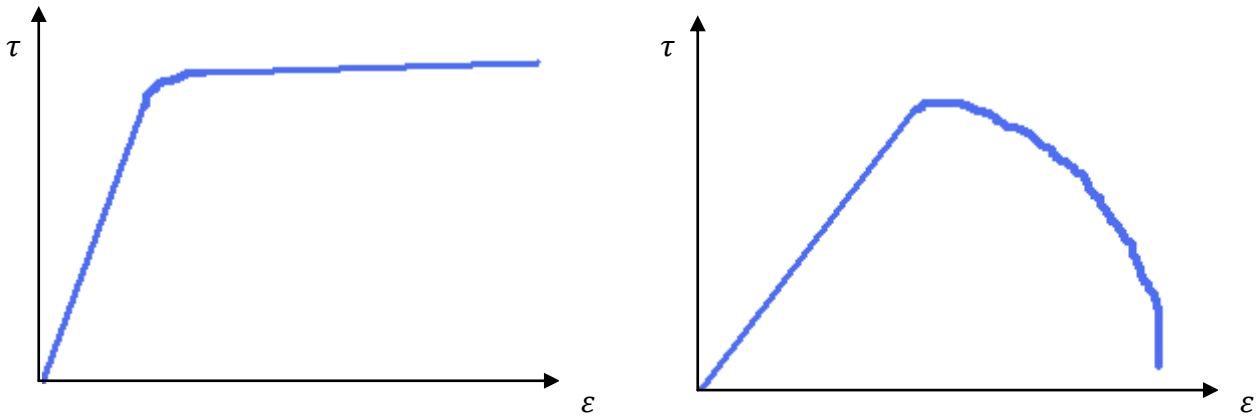

Figure 2.4 Left: Desirable connector, Right: undesirable connector

2.2 Design procedure of a timber-concrete composite

2.2.1 Historical background

The first design model applicable for composite beams resulted from small scale testing in the U.S. during the 1940's. Later, during the 1950's, Newmark and Möhler presented a linear model based on previously derived equations of equilibrium that took into account the interlayer slip between two mechanically interconnected materials. This model today known as the γ-method was originally developed for simply supported beams, but the use of recommended effective beam lengths allowed for continuous beams to be analyzed as well. Its easy use made the γ-method widely spread. (Lukaszewska, 2009)

In 1984 Goducky et al. presented a model that like the γ-method took into account the interlayer slip, but also accounted for long term effects through the assumption of time-dependant declines of the elasticity moduli. The progress continued in 1989 & 1996 when Stevanovic presented a method of analysis for floors subjected to transversal as well as axial loading. Stevanovic's model included section forces, connector-shear forces and element deflection. The same was achieved by Girhammar & Gopu in 1991, but their approach differed from Stevanovic's in that their Euler-Bernoulli-based theory considered second order effects as well. Two years later, Girhammar & Gopu presented exact first- and second order functions for timber-concrete composite beams with partial interaction. With the aim of deriving an exact closed form solution for characteristic equations within the Euler-Bernoulli beam theory, Girhammar & Gopu extended and generalized their work in 2007. Just a year later, due to the very cumbersome second order analysis, Girhammar developed a simplified approach applicable for design purposes in 2008. (Lukaszewska, 2009)

Due to its easy use, the approach described in the European code today, is the γ-method. However, Girhammar has recently been promoting the inclusion of his simplified approach in building codes. Apart from being superior to the γ-method for various boundary conditions, the simplified approach is easier to use according to Girhammar. Unlike the γ-method's recommended effective beam lengths, Girhammars simplified approach assumes effective beam lengths equal to the Euler buckling lengths for corresponding columns. This has resulted in small error margins of about 5%, in contrast to the approximately 27% of the γ-method. The simply supported case constitutes the exception of course, for which the two methods give exactly the same result. (Girhammar, 2009)

2.2.2 Short- and long-term verifications

As with any structure, the design of a timber-concrete composite structure involves two types of analyses; ultimate limit state analyses and serviceability limit state analyses. The first implies a control of the cross-sectional normal stresses, while the latter implies a control of the vertical displacement. For concrete and timber respectively, the controls are,

$$\sigma_{ccd} + \sigma_{cmd} \leq f_{ccd} \quad \text{(Eq. 2.1)}$$

$$\frac{\sigma_{ttd}}{f_{ttd}} + \frac{\sigma_{tmd}}{f_{tmd}} \leq 1 \quad \text{(Eq. 2.2)}$$

$$\delta \leq L/(\sim 250) \quad \text{(Eq. 2.3)}$$

where,

σ_{ccd}	Normal stress in concrete due to compression
σ_{cmd}	Normal stress in concrete due to bending
f_{ccd}	Compressive strength of concrete
σ_{ttd}	Normal stress in timber due to tension
f_{ttd}	Tensile capacity of timber
σ_{tmd}	Normal stress in timber due to bending
f_{tmd}	Bending capacity of timber
δ	Deflection
L	Length of composite beam

Conducting these controls in practice is a repetitive procedure in which a cross section is first assumed, and then analyzed. This continues until a cross section is found that fulfills the requirements. Fortunately, with modern day technology, this can be executed quickly.

The stresses and the displacement in equations 2.1-2.3 can be found using a number of different methods, refer to chapter 5.1. In this thesis, the methods accounted for are the γ-method and Girhammar's simplified approach (section 2.2.3-2.2.4). Regardless of the method used, the stresses will depend on the applied load, the Young's modulus of the sub-elements and the slip modulus of the shear connector.

Since the behavior of the shear connector is typically non-linear, two separate slip moduli are used for design purposes. Usually $k_u=k_{60}$, corresponding to the secant value at 60% of the shear connector's load carrying capacity, is used for ultimate limit state analysis, while $k_{ser}=k_{40}$ is used for serviceability state calculations, see figure 2.5. (Lukaszewska, 2009)

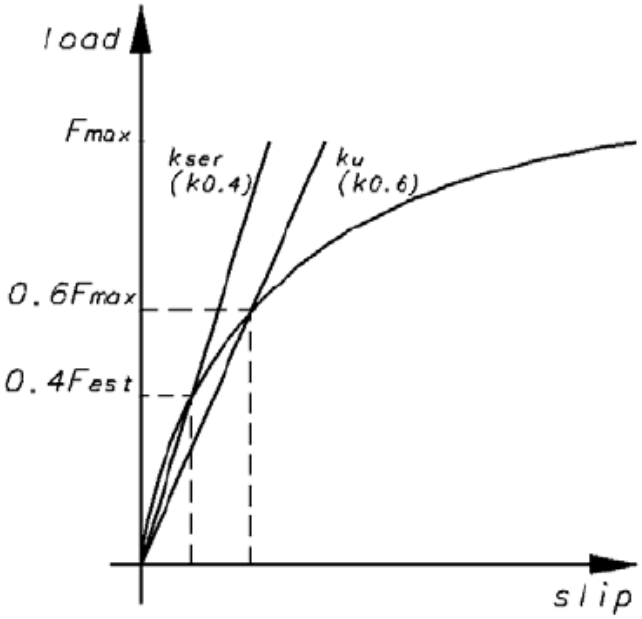

Figure 2.5 k_u & k_{ser} (Lukaszewska, 2009)

It is important that the controls (Eq. 2.1-2.3) are carried out both in the short- and long term. This is to take into consideration effects such as thermal strains, shrinkage and creep of the concrete, as well as creep and mechano-sorption of the timber and connector. (Lukaszewska, 2009)

In spite of numerical programs that have been proposed to provide accurate solutions, or various proposals of recommended elastic moduli-reductions, no consensus have been reached among researchers of how to conduct the long-term verification. The current recommendation from the European code is to use a method known as the effective modulus method. This method uses so called creep factors developed from load-duration studies to estimate the long term elastic moduli of the involved materials. It can be summarized as follows (Lukaszewska, 2009):

A general long term effect such as stress or displacement can be considered to consist of two parts; one that is due to the quasi-permanent load (the time-average of loading) (i), and one that is due to the difference between the short term design load and the quasi-permanent load (ii).

The part of the general effect that is due to (i) is determined using so called effective moduli, while the part that is due to (ii) is determined using mean values of the Young's moduli. The total general effect is the sum of the effects obtained.

The effective moduli for concrete, timber and shear connectors are calculated using equations 2.4-2.6 (Lukaszewska, 2009). The index *fin* refers to "final modulus", for which long term effects are considered. Appendix C accounts for how the creep coefficients ($\phi(t,t_0)$, k_{def}) are determined.

$$E_{c,fin} = \frac{E_{cm}(t_0)}{1+\phi(t,t_0)} \quad \text{(Eq. 2.4)}$$

$$E_{t,fin} = \frac{E_{0,mean}}{1+k_{def,t}} \quad \text{(Eq. 2.5)}$$

$$k_{fin} = \frac{k}{1+k_{def,f}} \quad \text{(Eq. 2.6)}$$

where,

$E_{cm}(t_0)$	Mean value of the Young's modulus for compression of concrete at the time of loading, t_0
$\phi(t,t_0)$	Creep coefficient for concrete at time t given initial time of loading t_0
$E_{0,mean}$	Mean value of the Young's modulus for tension of timber in the grain direction
$k_{def,t}$	Creep coefficient for timber/connectors at time t
k	Slip modulus corresponding to the secant value at 60 or 40 % of the shear connector's load carrying capacity, depending on which limit state control is being conducted.

Hence, the general approach that is recommended by the European code for short- and long term limit state verifications can be summarized as follows:

Short term verification:
The short term effect in terms of stress "σ_{inst}" can be expressed as a function in the following form:

$$\sigma_{inst} = \sigma^{F_{d,u}}(E_{cm}, E_{0,mean}, k_u)$$

Where $F_{d,u}$ designates the ultimate limit state load combination.

The short term effect in terms of vertical displacement "u_{inst}" can be expressed

$$u_{inst} = u^{F_{d,r}}(E_{cm}, E_{0,mean}, k_u)$$

Where $F_{d,r}$ designates the rare load combination

Long term verification:
The long term effect in terms of stress "σ_{fin}" can be expressed as

$$\sigma_{fin} = \sigma^{F_{d,p}}\left(E_{c,fin}, E_{t,fin}, k_{ser,fin}\right) + \sigma^{F_{d,u}-F_{d,p}}(E_{cm}(t), E_{0,mean}, k_u)$$

Where $F_{d,p}$ designates quasi-permanent load combination and $F_{d,u}$ designates the ultimate limit state load combination .

The long term effect in terms of vertical displacement "u_{fin}" can be expressed as

$$u_{fin} = u^{F_{d,p}}(E_{c,fin}, E_{t,fin}, k_{ser,fin}) + u^{F_{d,r}-F_{d,p}}(E_{cm}(t), E_{0,mean}, k_{ser})$$

Where $F_{d,r}$ designates the rare load combination

The load combinations for ultimate limit state-, rare-, frequent- and quasi permanent loading prescribed by EN 1990:2002 (Basis of structural design), are as follows:

$$F_{d,u} = \sum \gamma_{G,j} * G_{k,j} + \gamma_{Q,1} * Q_{k,1} + \sum \gamma_{Q,i} * \psi_{0,i*} Q_{k,i} \quad \text{(Eq. 2.7)}$$

$$F_{d,r} = \sum G_{k,j} + Q_{k,1} + \sum \psi_{0,i} * Q_{k,i} \quad \text{(Eq. 2.8)}$$

$$F_{d,f} = \sum G_{k,j} + \psi_{1,1*} Q_{k,1} + \sum \psi_{2,i} * Q_{k,i} \quad \text{(Eq. 2.9)}$$

$$F_{d,p} = \sum G_{k,j} + \sum \psi_{2,i} * Q_{k,i} \quad \text{(Eq. 2.10)}$$

Where,

G_k,Q_k	Characteristic values of permanent and variable actions
ψ_0	Combination factor for ultimate limit state values of variable actions
ψ_1	Combination factor for frequent values of variable actions
ψ_2	Combination factor for quasi permanent values of variable actions

2.2.3 The γ-method

In order for the γ-method to be applied, the following assumptions must be satisfied according to EN 1995-1-1 (2002) (Design of timber structures);

1. Beams are simply supported with a span *l*. For continuous or cantilever beams, *l* must be modified as follows:
   - $l = 0{,}8*l$ for continuous beams
   - $l = 2*l$ for cantilevered beams
2. The individual wooden parts are either full length or made with glued end joints
3. The individual parts are connected by mechanical fasteners with a slip modulus K
4. The spacing "s" between the fasteners is constant or varies uniformly according to the shear force, between s_{min} and s_{max} with $s_{max} \leq 4*s_{min}$
5. The load is acting in the z-direction resulting in a moment M=M(x) varying sinusoidally or parabolically, and a shear force V=V(x)

Given the satisfaction of these assumptions, an effective beam bending stiffness can be calculated according to equation 2.11;

$$(EI)_{eff} = \sum_{i=1}(E_i I_i + \gamma_i E_i A_i a_i^2) \qquad \text{(Eq. 2.11)}$$

where,

E_i	The mean value of the elasticity modulus of the i:th sub-element
$I_i = \frac{b_i h_i^3}{12}$	The second moment of inertia of the i:th sub-element
$A_i = b_i h_i$	The cross sectional area of the i:th sub-element
$\gamma_i = \frac{1}{1 + \frac{\pi^2 E_i A_i s_i}{K_i l^2}}$	Parameter describing composite action (for *i*=1 and *i*=3)
$\gamma_2 = 1$	
a_i	The distance from the centroid of the i:th sub-element to the neutral layer of the composite section

Figure 2.6 shows the sub-elements and interaction surfaces of composite sections for different configurations. When the bending stiffness according to equation 2.11 has been calculated, the loading on the shear connectors and the cross sectional normal stresses resulting from compression, tension and bending, can be obtained using equations 2.12-2.14.

$$\sigma_{i=} \frac{\gamma_i E_i a_i M}{(EI)_{eff}} \qquad \text{(Eq. 2.12)}$$

$$\sigma_{m,i} = \frac{0{,}5 E_i h_i M}{(EI)_{eff}} \qquad \text{(Eq. 2.13)}$$

$$F_i = \frac{\gamma_i E_i A_i a_i s_i}{(EI)_{eff}} V \qquad \text{(For } i\text{=1 and } i\text{=3)} \qquad \text{(Eq. 2.14)}$$

Deflection is calculated by replacing the bending stiffness in standard expressions with the calculated effective bending stiffness.

(1)

(2)

(3)

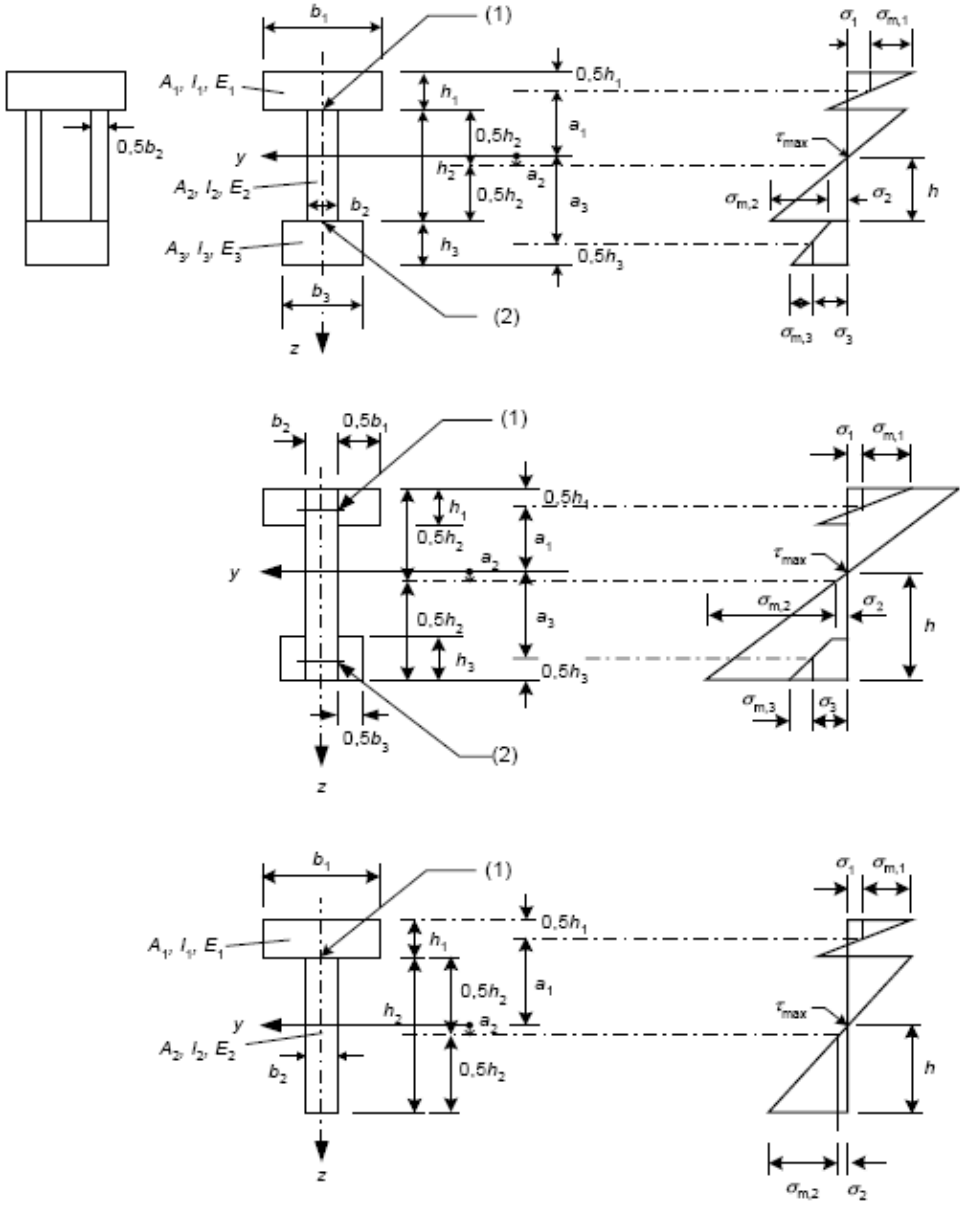

Figure 2.6.Quantities of the γ−method (EN 1995-1-1, Design of timber structures)

In the case of a timber-concrete composite T-beam, illustrated in figure 2.6 (3), equation 2.11 becomes;

$$(EI)_{eff} = E_1 I_1 + \gamma E_1 A_1 a_1^2 + E_2 I_2 + E_2 A_2 a_2^2 \qquad \text{(Eq. 2.15)}$$

where index 1 refers to the concrete sub-element and index 2 refers to the timber element. γ and a are obtained using equations 2.16-2.18.

$$\gamma = \gamma_1 = \frac{1}{1+\frac{\pi^2 E_1 A_1 s}{kl^2}} \qquad \text{(Eq. 2.16)}$$

$$a_2 = \frac{\gamma E_1 A_1 (h_1 + h_2)}{2(\gamma E_1 A_1 + E_2 A_2)} \qquad \text{(Eq. 2.17)}$$

$$a_1 = \frac{h_c + h_t}{2} - a_2 \qquad \text{(Eq. 2.18)}$$

The fastener load and normal stresses are calculated using equations 2.12-2.14.

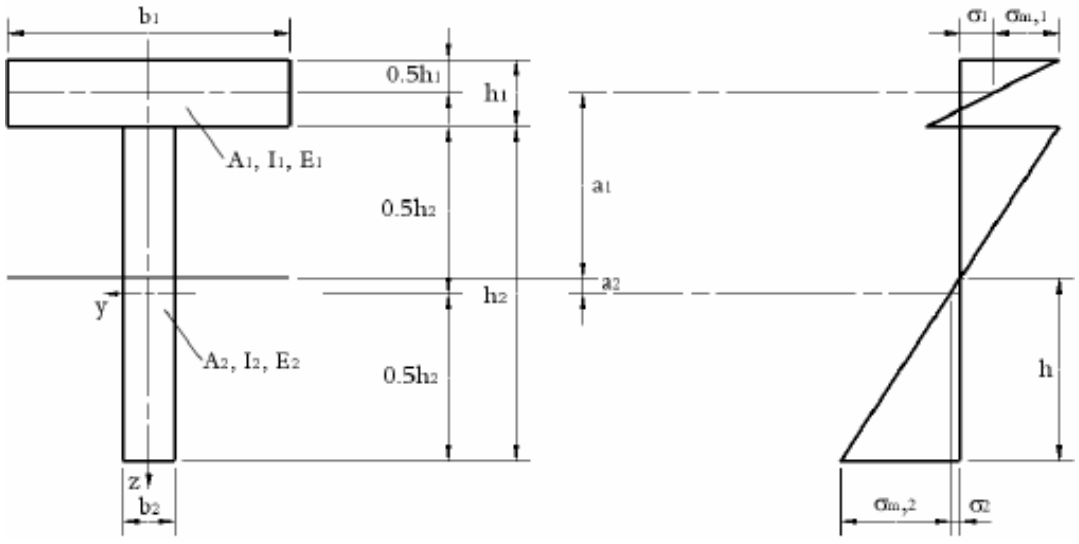

Figure 2.7 Timber-concrete composite T-beam (Lukaszewska, 2009)

2.2.4 Girhammar's simplified approach

In order for the method to be applicable, the following assumptions must be satisfied (Girhammar, 2009):

1. The mechanical shear connectors are evenly spaced and produce uniformly distributed slip forces with a constant slip modulus K
2. The x-axis is located in the centroid of the fully composite section. The displacements in the x- and z-directions are denoted u and w, respectively

If these assumptions apply, the effective bending stiffness of a composite T-beamcan be calculated using equation 2.19.

$$EI_{eff} = \frac{\mu_\infty^2}{\mu^2}\left[1 + \frac{EI_\infty/EI_0 - 1}{1+(\mu/\pi)^2(\alpha L)^2}\right]^{-1} EI_\infty \qquad \text{(Eq. 2.19)}$$

Where,

μ	The buckling length coefficient for partially composite beams.
μ_∞	Buckling length of the fully composite beam (corresponding to the standard Euler-buckling length coefficient)
$\alpha L = \sqrt{\frac{Kr^2}{EI_0(1 - EI_0/EI_\infty)}}L$	The non-dimensional shear connector parameter
$EI_0 = E_1I_1 + E_2I_2$	The bending stiffness of the corresponding non-composite section
$EI_\infty = EI_0 + \frac{EA_pr^2}{EA_0}$	The bending stiffness of the corresponding fully-composite section, where r denotes the distance between the centoids of the sub-elements
$EA_0 = E_1A_1 + E_2A_2$	The sum of the axial stiffness of each sub-element
$EA_p = E_1A_1 * E_2A_2$	The product of the axial stiffness of the sub elements

Since the buckling length coefficients for partially composite beams are practically the same as the Euler buckling length coefficients for most boundary conditions, equation 2.19 can be reduced to:

$$EI_{eff} \approx \left[1 + \frac{EI_\infty/EI_0 - 1}{1+(\mu/\pi)^2(\alpha L)^2}\right]^{-1} EI_\infty \qquad \text{(Eq. 2.20)}$$

When the effective bending stiffness has been calculated, the internal actions can be obtained using equations 2.21-2.25. As before, r denotes the distance between the centroids of the sub-elements. r_i is the distance from the centroid of the i:th sub-element to the neutral layer of the composite section.

$$N_{1,eff} = -\left(1 - \frac{EI_0}{EI_{eff}}\right)\frac{M}{r} \quad \text{(Eq. 2.21)}$$

$$N_{2,eff} = \left(1 - \frac{EI_0}{EI_{eff}}\right)\frac{M}{r} \quad \text{(Eq. 2.22)}$$

$$M_{i,eff} = \pm\frac{E_i I_i}{EI_{eff}} M \quad \text{(Eq. 2.23)}$$

$$V_{s,eff} = \left(1 - \frac{EI_0}{EI_{eff}}\right)\frac{V}{r} \quad \text{(Eq. 2.24)}$$

$$V_{i,eff} = \frac{E_i I_i}{EI_{eff}} V + V_{s,eff} r_i \quad \text{(Eq. 2.25)}$$

$V_{s,eff}$ refers to the slip/shear force at the interlayer between the sub-elements, while $V_{i,eff}$ refers to the shear force acting on the cross section of sub-element i, see figure 2.8. The load on the shear connector can easily be obtained by multiplying the interlayer slip force with the fastener spacing, see equation 2.26. The interlayer slip is obtained using equation 2.27.

$$F_{s,eff} = V_{s,eff} s \quad \text{(Eq. 2.26)}$$

$$\Delta u = V_{s,eff}/K \quad \text{(Eq. 2.27)}$$

The deflection is obtained by replacing the effective bending stiffness in the standard equations with the effective bending stiffness calculated according to equation 2.20. (Girhammar, 2009)

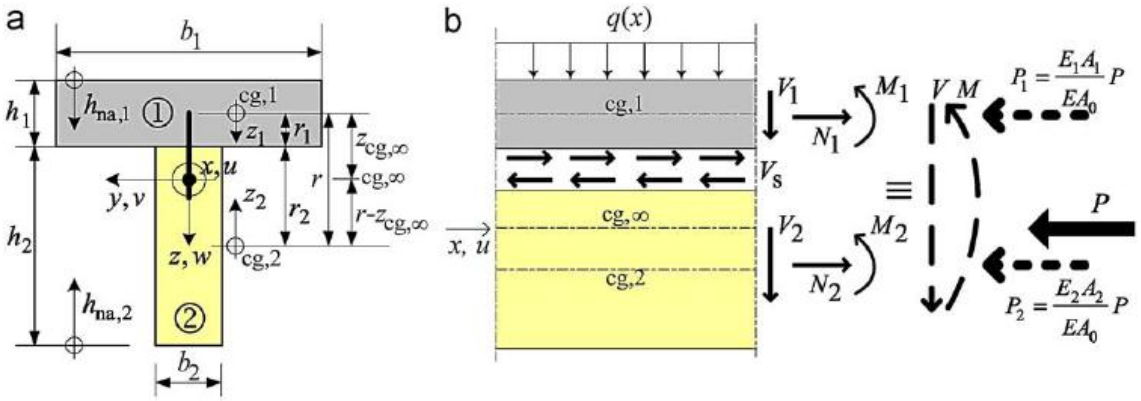

Figure 2.8. Quantities used in Girhammar's simplified method (Girhammar, 2009)

2.3 Survey of tested shear-connectors

Since the connector plays such an important role, choosing the right shear connector is critical for the structural performance of a composite floor. This survey presents various objects that could potentially be used as shear connectors and lists the results from tests that have been performed on them. The survey serves as a basis for the evaluation of timber-concrete composites solutions in chapter 3.

2.3.1 Nails

Nails represent the simplest type of shear connector, see figure 2.9. They are used by pounding them partway into the timber, enabling the top to become embedded in the concrete upon casting of the slab. Several tests have been carried out on nails as shear connectors.

Figure 2.9 Typical Nail

Push-out tests have shown that the penetration of a nail into the wood should be approximately eleven times the diameter in order to reach maximum efficiency. Further more, full scale bending tests with nails penetrating to this depth show that the load carrying capacity of a floor can be doubled while at the same time decreasing deflection when using nails as shear connectors. (Weaver, 2002)

Branco, Cruz and Piazza performed shear tests on pairs of smooth round nails, using lightweight concrete and a 2 mm plywood interlayer. The nails were 70 mm long with a diameter of 3,4 mm. An average shear capacity of 8,06 kN per two nails with a corresponding slip of 9,85 mm was determined. The slip modulus $k_{0,4}$ per two nails was established to 14,65 kN/mm (Branco, Cruz & Piazza, 2009).

In 1998, nails of similar size to those tested by Branco, Cruz and Piazza was approved by the German institute for building technique for employment as shear connectors in floors made of standard concrete and timber. According to the approval that concerned 60 mm long nails with a diameter of 3,4 mm, penetrating the wood to a depth of approximately 11*d, the characteristic and design shear capacity per nail should be set to $F_{max,k}$=1,2 kN and $F_{max,d}$=0,5 kN respectively. The approval also prescribed a slip modulus of $k_{0,4}$=1,2kN/mm, see table 2.1 (Aicher, Klöck, Dill-Langer, & Radovic, 2003).

	F_{max} [kN]	Slip [mm]	$k_{0,4}$ [kN/mm]
Branco, Cruz & Piazza(1)	4,03*	*9,85	7,32
German approvad(2)	1,2**	-	1,2

(1) Single nail, l=70mm, d=3,4mm.*Average values
(2) Single nail, l=60 mm, d=3,4 mm.**Characteristic values

Table 2.1 Mechanical parameters for nails

2.3.2 SFS-screw (VB 48-7,5x100)

The VB 48-7,5x100 produced by SFS Intec, commonly known as the SFS-screw, is a connector specifically developed for timber-concrete composite structures. Two heads allow for the lower part of the screw to be fixed in the wood while the top part is anchored in the concrete, see figure2.10.

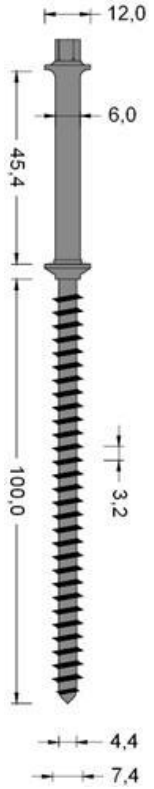

Fig. 2.10 The SFS-screw

The best performance is achieved when placing the screws pair-wise, inclining the screws within the pair at 45° and 135° respectively, see figure 2.11. This allows the screw tilted in the direction of the shear force to absorb tensile forces, while the screw tilted in the opposite direction acts as a stiffener. The screw is quickly installed using a power drive. Setting tools with angle-applications are also available. (SFS intec)

Several push-out tests have been conducted on the SFS-screw by various researchers. All push-out tests conducted with standard concrete of quality C25 and higher result in failure through either the pulling out of the wood or the shearing off of the screw. Using lightweight concrete results in failure of the concrete instead. (Faust & Selle, 1999).

Fig 2.11 Screws installed pair-wise at angels of $45^0$and 135^0

Deam, Fragiacomo & Buchanan performed push-out tests on a big variety of shear connectors, including the SFS-screw, using test specimens consisting of laminated veneer lumber and standard concrete. Tests were performed both with and without an interlayer and it was concluded that the screw was not significantly affected by an interlayer. (Deam, Fragiacomo, & Buchanan, 2008) Table 2.2 presents the mechanical parameters established through testing for one pair of SFS-screws, with the screws inclined in opposite directions.

	F_{max} [kN]	$k_{0,4}$ [kN/mm]	$k_{0,6}$ [kN/mm]	$k_{0,8}$ [kN/mm]	Slip [mm]
Standard concrete*	18,5	14,4	12,7	11,9	2,52
Lightweight concrete**	15,05	15,08	13,96	-	-

* (Deam, Fragiacomo, & Buchanan, 2008)
** (Steinberg, Selle, & Faust, 2003)

Table 2.2 Mechanical parameters for an SFS-screw-pair with the screws inclined in opposite directions

2.3.3 Insa Hilti

The Insa Hilti is a tubular connector developed specifically for use in timber-concrete composite floors, see figure 2.12 (Lukaszewska, 2009). The principal objective was to decrease the time needed for installation and to solve the problem of shearing, displayed by many traditional connectors such as nails and screws, of the connector upon fatigue loading. The connector is essentially a hollow cylinder with varying cross-section and wall thickness. When driven into the wood with a cartridge-powered pistol, it confines the fibers at the wood surface. This distributes the shear forces across a larger surface thus minimizing the risk of shearing off the wood. (Weaver, 2002)

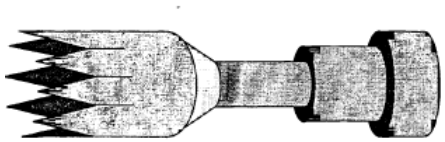

Figure 2.12 The Insa Hilti connector (Weaver, 2002)

The connector displayed great ductility in tests. The average load capacity was established to 161,5 kN per four connectors, with a corresponding average slip of 19 mm. (Lukaszewska, 2009). However, it is unclear if the Insa Hilti connector can still be obtained. Little information is available and when the Hilti staff in Sweden was asked about the product, they had not heard of it. It is possible that the production has ceased.

2.3.4 Lag screws

Lag screws can function as shear connectors in timber-concrete composite floors by being partway screwed into the wood. Deam, Fragiacomo & Buchanan tested lag screws having diameters of 12 and 16 mm (refer to section 2.3.2 for more specifics). The tests showed that failure was initiated by yielding of the screws, followed by the crushing of the wood at the interface. The Φ16-screw also caused the LVL to split longitudinally. The yielding of the steel and crushing of the wood resulted in excessively large deformations (22mm) before the peak strength was reached. This would prevent the screws from developing their full strength in a flooring system. (Deam, Fragiacomo, & Buchanan, 2008) The following strength parameters were determined from the tests, see table 2.3:

Fig. 2.13 Lag screw

	F_{max} [kN]	$k_{0,4}$ [kN/mm]	$k_{0,6}$ [kN/mm]	$k_{0,8}$ [kN/mm]	Slip [mm]
Φ12 lag screw	21,5	195,5	2,9	1,7	15
Φ16 lag screw	34,2	88,3	21,4	2,7	15

Table 2.3 Structural parameters for lag screws

2.3.5 Reinforcement bars

A section of a reinforcement bar, smooth or profiled, (see figure 2.14), can be used as a shear connector by forcing it into a predrilled hole in the wood.

Fig. 2.14 Section of reinforcement bar

According to Lukaszewska. 2009, the performance of two types of connections was studied by Gelfi and Giuriani; one using a smooth Φ16 bar with a wooden interlayer present, and one where the concrete was in direct contact with the wooden beams using a smooth Φ12 bar. Apart from concluding that wood insertion lengths more than 5 times the bar-diameter did not considerably improve the performance, they observed the following intervals of the strength parameters, see table 2.4 (Lukaszewska, 2009):

	F_{max} [kN]	v [mm]
Smooth Φ12 (no interlayer)	8,3-10,7	<3,5
Smooth Φ16 (with interlayer)	9,9-12,7	3-3,5

Table 2.4. Strength parameters for smooth reinforcement bars as concluded by Gelfi and Giuriani (Lukaszewska, 2009)

Lukaszewska also presents the results of another study on sections of reinforcement-bars that was carried out by Dias. According to Lukaszewska, he performed a large number of push-out tests on both smooth and profiled bars. Three types of timber and concrete were used; spruce, maritime pine and chestnut, and lightweight-, normal strength- and high strength-concrete. His results are presented in table 2.5 (Lukaszewska, 2009).

Connector	Timber	Concrete	F_{max} [kN]	k [kN/mm]
(1) smooth Φ8	spruce	normal strength	13,6	13,2
(1) smooth Φ10	spruce	normal strength	22,6	17,2
(1) smooth Φ10	spruce	high strength	23,6	15,7
(1) smooth Φ10	maritime pine	normal strength	25,5	26,4
(1) smooth Φ10	chestnut	normal strength	26,2	36,1
(1) smooth Φ10	spruce	lightweight	18,5	16,1
(2) profiled Φ10	spruce	normal strength	69,8	40,2
(2) *profiled Φ10	spruce	normal strength	63,3	26,2

(1)Two connectors, (2)Four connectors, *With 20 mm thick interlayer

Table 2.5. Strength parameters concluded by Dias (Lukaszewska, 2009)

2.3.6 Flat steel lock connector

The flat steel lock connector is essentially a flat and quadratic zinced steel plate with a 5*40 mm cross section. It is inserted into a sawing cut at an angle of 5^0 towards the shear force. This is illustrated in figure 2.15. (Aicher & Reinhardt, 2000)

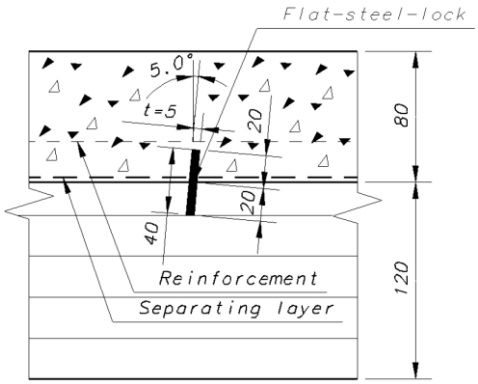

Fig. 2.15 Flat steel lock connector (Lukaszewska, 2009)

It has been concluded from tests that the spacing between the connectors can be kept relatively large compared to dowel-type connectors such as screws, bolts or bars. Also, tests show that failure is first initiated in the concrete surrounding the flat steel locks (Aicher & Reinhardt, 2000). The shear capacity for a pair of connectors has been established to approximately 100 kN with a corresponding slip of 4 mm, see table 2.6 (Lukaszewska, 2009).

	F_{max} [kN]	Slip [mm]
Flat steel lock connector	50,0	4

Table 2.6 Strength parameters for the flat steel-lock connector (Lukaszewska, 2009)

2.3.7 Dimple/plug

A very simple type of connector can be created by drilling holes/dimples in the timber beam, see figure 2.16. Upon casting of the concrete, a concrete plug is formed that has the ability to transfer shear forces between the concrete and the wood. A number of tests have been carried out on this simple connector-type.

Figure 2.16 Dimple
(Deam, Fragiacomo, & Buchanan, 2008)

Deam, Fragiacomo, & Buchanan (refer to section 2.3.2) tested a connection with dimples 20 mm deep and with diameters of 48,5 mm. As would be expected considering the nature of concrete, brittle failure was observed. The mechanical parameters determined by Deam, Fragiacomo & Buchanan are presented in table 2.7.

F_{max}[kN]	$k_{0,4}$ [kN/mm]	$k_{0,6}$ [kN/mm]	$k_{0,8}$[kN/mm]	Slip [mm]
13,2	83,1	42,6	36,9	0,62

Table 2.7 Mechanical parameters for circular dimples/concrete plugs
(Deam, Fragiacomo, & Buchanan, 2008)

Tests have also been performed on composite floors with a connection consisting of dimples/plugs on three sides of the wooden beams, see figure 2.17. This was made possible by the drilling of dimples in the top part of the beam and then embedding it in the concrete upon casting, as is illustrated in figure 2.17. The dimples were 10 mm deep with a diameter of 20 mm. It was shown that full composite action could be achieved utilizing this approach. (Lukaszewska, 2009)

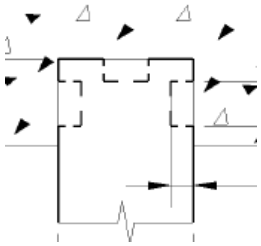

Figure 2.17 Dimples on three sides
(Lukaszewska, 2009)

2.3.8 Dimple/plug reinforced with lag screw

Deam, Fragiacomo, & Buchanan also studied the behavior of concrete plug-type connectors reinforced with a lag screw. In such a connection, shear forces are transferred between the sub-elements both through the bearing at the interface between the materials and through the dowel action provided by the lag screw.

Apart from observing a stronger connection than for the corresponding unreinforced plug, it was observed that the screw enhanced the post-peak performance by acting as a tensile anchor, holding the fractured concrete in the plug together after failure. Both rectangular and circular reinforced plugs were studied. The circular plug studied was 20 mm deep with a diameter of 48,5 mm, reinforced with a 150*12 mm lag screw. The lag screw penetrated 100 mm into the wood measured from the bottom of the dimple. The rectangular plug had a depth of 16,5 mm, and a width of 50 mm. The plug was cut from one side to the other of the 105 mm wide LVL-section. The same screw as for the circular dimples was used, this time penetrating 103 mm into the wood. In both cases a 9 mm hole was predrilled for the screw. The mechanical parameters determined from the push out tests are presented in table 2.8.

Figure 2.18 Top: Round reinforced concrete plug before casting. Bottom: Square reinforced concrete plug before casting (Deam, Fragiacomo, & Buchanan, 2008)

	F_{max}[kN]	$k_{0,4}$ [kN/mm]	$k_{0,6}$ [kN/mm]	$k_{0,8}$[kN/mm]	Slip [mm]
Round plug with screw	31,4	105,9	56,3	39,1	1,89
Rectangular plug with screw	54,9	297,0	197,3	148,5	1,35

Table 2.8 Mechanical parameters for concrete plug reinforced with coach screw

It was concluded that the stiffness and strength of a connector of this type is governed by the bearing surface area of the concrete plug, the cross sectional area of the plug and the flexural as well as the tensile strength of the screw. (Deam, Fragiacomo, & Buchanan, 2008)

2.3.9 Dimple/plug reinforced with steel pipe

Another type of reinforced plug tested by Deam, Fragiacomo, & Buchanan was the concrete plug reinforced with a steel pipe, see figure 2.19. The pipe was of the same diameter as the dimple and approximately three times as high. It was attached by simply forcing it into the hole.

The connection resulted in roughly the same shear capacity as the screw-type reinforcement. However, after the peak value was reached it was observed that both the concrete within the pipe and the compressed wood was crushed. Due to the lack of a top at the pipe end, holding fractured concrete together, the slip was much larger than for the case with the screw-type reinforcement. The mechanical parameters that were determined are presented in table 2.9. (Deam, Fragiacomo, & Buchanan, 2008)

Figure 2.19 Steel pipe reinforced dimple (Deam, Fragiacomo, & Buchanan, 2008)

	F_{max}[kN]	$k_{0,4}$ [kN/mm]	$k_{0,6}$ [kN/mm]	$k_{0,8}$[kN/mm]	Slip [mm]
Steel pipe	32,6	66,6	42,5	29,7	3,09

Table 2.9 Mechanical parameters for concrete plug reinforced with steel pipe

2.3.10 Dimple/plug reinforced with lag screw and steel pipe combined (CHS)

Benitez tested a connection consisting of a concrete plug reinforced with a lag screw in conjunction with a steel pipe, see figure 2.20. This connection type is often referred to as *circular hollow section* or simply CHS. The concrete used was of strength class C25 and the lag screw was a 150 mm long M16 screw. The concrete and timber were separated by a heavy-duty plastic membrane to prevent any friction action from disturbing the test results.

Figure 2.20 Circular hollow section (Benítez, 2000)

In contrast to plugs using just a steel pipe for reinforcement as those tested by Deam, Fragiacomo and Buchanan, the fractured concrete was held together with the CHS-connection.

Like Deam, Fragiacomo and Buchanan, Benitez also observed crushing of the compressed wood. The average maximum loading capacity observed in shear tests was 353,2 kN per two connectors, and the failure was classified as ductile. (Benítez, 2000)

No information was found about the actual slip and stiffness of this connector.

2.3.11 Punched metal plate fasteners (Nail-plates)

According to Aicher, Klöck, Dill-Langer, Radovic (2003), extensive research on nail-plates was carried out in Karlsruhe and Stuttgart, Germany in the 1990's. The studies carried out in Karlsruhe concerned the nail-plates MNP-A and GN 200, illustrated in figure 2.21. These were bent at mid-width and placed on top of the timber beams without the use of any interlayer and with the one side embedded in the concrete slab. The sub-elements consisted of C20 concrete and either solid wood or glulam sections. The nails were removed from the side of the nail-plate embedded in the concrete in order to avoid air pockets. (Aicher, Klöck, Dill-Langer, & Radovic, 2003)

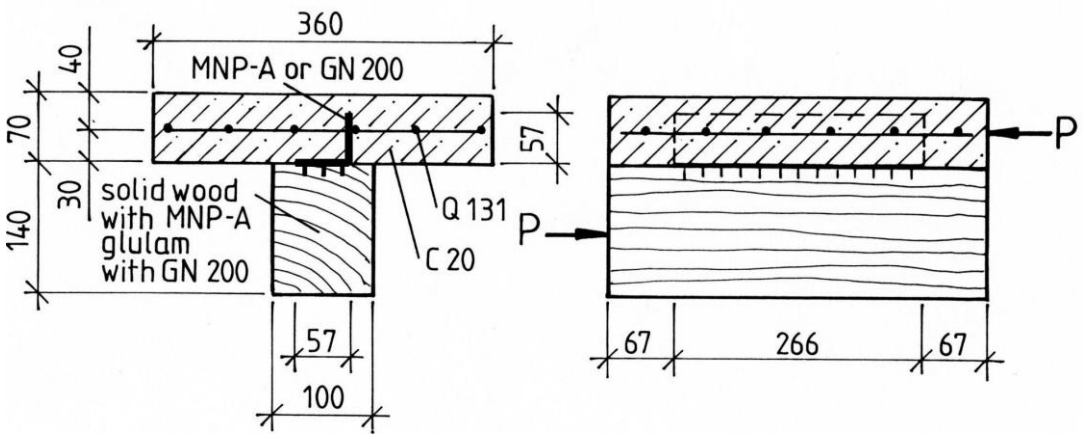

Figure 2.21 Nail-plates studied in Karlsruhe, Germany (Aicher, Klöck, Dill-Langer, & Radovic, 2003)

The study carried out in Stuttgart involved the *Wolf 15N* nail-plate, see figure 2.22. The sub-elements consisted of a lightweight concrete and duo-beams of solid wood. No interlayer was used. The nail-plates were not bent and had no nails removed. Instead two nail-plates were attached on each side of the timber beam, with roughly half their height embedded in the concrete slab. (Aicher, Klöck, Dill-Langer, & Radovic, 2003)

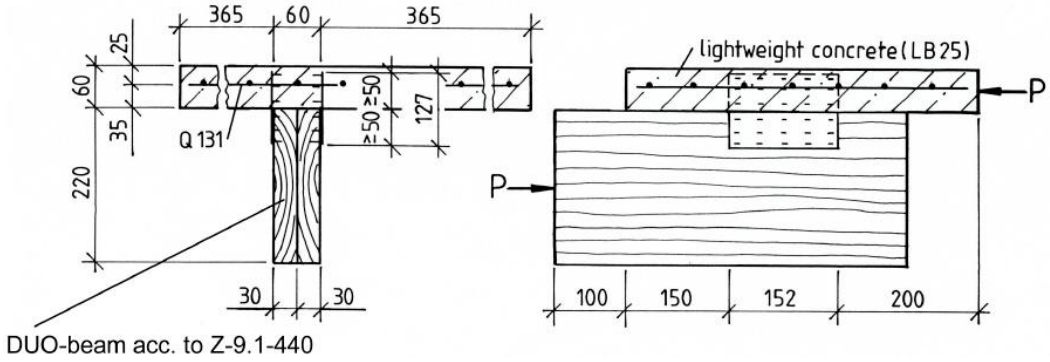

Figure 2.22 Nail-plates studied in Stuttgart, Germany (Aicher, Klöck, Dill-Langer, & Radovic, 2003)

The Karlsruhe and Stuttgart connectors had in common that failure occurred only in the nail-plates at the timber-concrete interface, resulting in a ductile failure mode typical for steel. Table 2.10 summarizes the results from the tests carried out in Germany. (Aicher, Klöck, Dill-Langer, & Radovic, 2003)

	Nail-plate	$k_{0,4}$ [kN/mm]	F_{max} [kN]
Karlsruhe	GN 200	50	53,5
	MNP-A	49	47,9
Stuttgart	Wolf 15N	28	31,5

Table 2.10 Mechanical parameters for nail-plates
(Aicher, Klöck, Dill-Langer, & Radovic, 2003)

Taking the size of the nail-plates into consideration, the Wolf 15N being roughly half of the size of the others, showed about the same characteristics as the GN 200 and the MNP-A per cm nail-plate.

2.3.12 Steel brace anchor

This type of connector was also included in the tests conducted by Deam, Fragiacomo, & Buchanan. The tests were carried out on a Pryda steel brace anchor (see figure 2.23), attached to the wood using four screws. The steel brace anchor was installed in various angles relative to the beam to investigate if it had any impact on the results. It was also investigated if rods installed horizontally in the holes of the vertical part of the connector had any effect on the outcome.

Figure 2.23Pryda steel brace anchor (Deam, Fragiacomo, & Buchanan, 2008)

Test results showed that the failure was concentrated in the screwed connection between the LVL and the steel brace anchor, explaining why neither the installation angle or the presence of horizontal steel rods seemed to have any significant impact on the mechanical performance. The failure modes for all test specimens were classified as brittle. Table 2.11 summarizes the mechanical parameters that were determined. (Deam, Fragiacomo, & Buchanan, 2008)

	F_{max} [kN]	$k_{0,4}$ [kN/mm]	$k_{0,6}$ [kN/mm]	$k_{0,8}$ [kN/mm]	v [mm]
$^{(1)}0^0$	16,6	156,9	125,8	20,6	6,89
$^{(1)*}0^0$	15,3	170,3	158,1	18,8	2,51
$^{(1)}45^0$	19,3	77,2	30,3	17,2	2,96
$^{(1)}90^0$	16,3	271,7	155,2	30,3	2,12

$^{(1)}$Angle relative to beam axis, *Horizontal rods added

Table 2.11 Mechanical parameters for Pryda steel brace anchor

2.3.13 Framing bracket

The final connector studied by Deam, Fragiacomo, & Buchanan was a Pryda framing bracket illustrated in figure 2.24. The framing bracket was attached to the wood using 6 nails each having a length of 40 mm and a diameter of 3 mm.

During the push-out tests, the slip was concentrated in the nailed connection. Turning the framing bracket in the opposite direction had no significant impact on the mechanical performance of the connection, and the mode of failure was classified as ductile for both cases. Table 2.12 presents the mechanical parameters that were determined (Deam, Fragiacomo, & Buchanan, 2008):

Figure 2.24 Pryda framing bracket (Deam, Fragiacomo, & Buchanan, 2008)*:*

	F_{max} [kN]	$k_{0,4}$ [kN/mm]	$k_{0,6}$ [kN/mm]	$k_{0,8}$ [kN/mm]	Slip [mm]
$^{(1)}0^0$	16,8	27,8	9,6	4,7	15,0
$^{(1)*}180^0$	15,8	37,8	13,1	7,1	12,29

$^{(1)}$Angle relative to beam axis

Table 2.12 Mechanical parameters for Pryda framing bracket

2.3.14 Universal column (UC)

The tests carried out by Benitez included a connection consisting of a universal column-section. In such a connection, the web and flanges of the universal column provides shear resistance while the top flange contributes with withdrawal resistance. The universal column section was attached to the wood using 4 lag screws penetrating the bottom flange as illustrated in figure 2.25. (Weaver, 2002)

Benitez concluded that using a universal column section as shear connector results in full composite action between the materials. The connection could also sustain large forces even after 100 000 loading cycles. The failure was due to the pulling out of the lag screws and the failure was classified as ductile. The average maximum load capacity determined from Benitez's tests was 344 kN per two connectors. (Benítez, 2000)

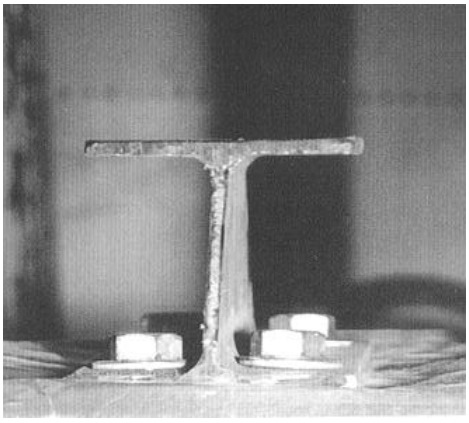

Figure 2.25 Universal column-section (Benítez, 2000)

2.3.15 Shaped perforated steel sheet

This continuous, shaped and perforated steel sheet was studied by Piazza and Ballerini. It was made of a 2 mm thick steel sheet and equipped with holes for better interaction with the concrete. The steel sheet was attached using 120 mm long screws placed on each side at a small spacing of 20 mm. Full scale bending tests revealed a 200% improvement in strength compared to timber beams alone. The composite action for low loading levels (<7kN/m^2) was approximately 90% and 30% at failure (Lukaszewska, 2009). Figure 2.26 shows the configuration of the shaped perforated steel sheet.

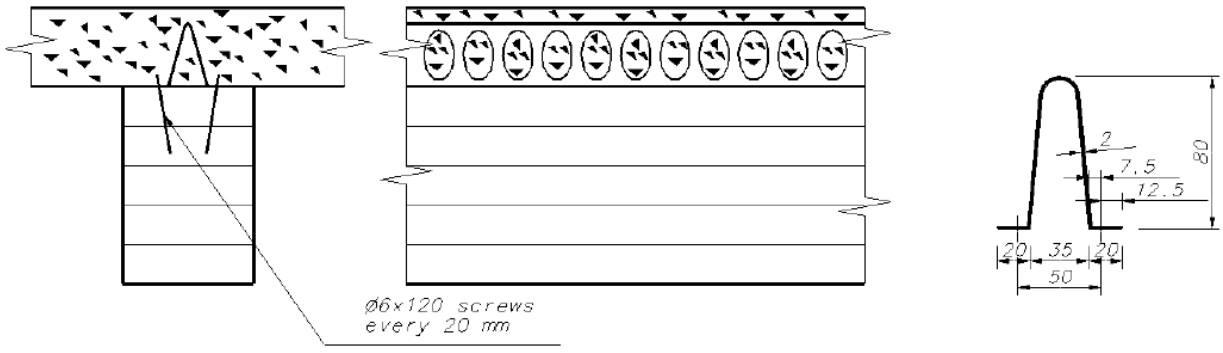

Fig. 2.26 Continuous connector studied by Piazza and Ballerini (Lukaszewska, 2009)

2.3.16 Steel mesh

Extensive testing has been carried out on this type of connector. It is essentially a continuous steel mesh, inserted halfway into a cut in the wood where it is attached by adhesive. The other half is embedded in the concrete, see figure 2.27.

Bathon, Leander, Graf & Markus manufactured 60 push-out test specimens in order to test the peformance of an 80 mm high mesh, inserted halfway into a glulam section and halfway into a standard concrete slab. The specimens were 400 mm long and the failure mechanism observed was primarily due to shearing in the wood. Some specimens however displayed failure in the concrete or in the mesh at the timber-concrete interface (Bathon, Leander, Graf, & Markus, 2000).

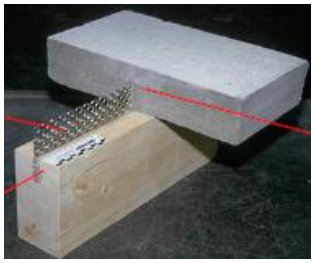

Figure 2.27 Continuous steel mesh (Bathon, Leander, Graf, & Markus)

In another test series performed by Clouston, Bathon and Schreyer, all specimens displayed ductile failure modes due to yielding followed by rupture of the steel mesh. They observed that the mesh performs similarly to a truss. Of the links formed by the steel mesh, the ones under compression yielded and buckled while the ones under tension ruptured. (Clouston, Bathon, & Schreyer, 2005)

Lukaszewska also performed push-out tests on a shear connector of this type. She used concrete of quality C20/25 and a glulam section of Swedish quality L40 (approximately somewhere between the European strength classes GL28 and GL32). As in the tests performed by Bathon, Leander, Graf & Markus, the steel mesh was 80 mm high, 400 mm long and inserted halfway in the glulam sections and halfway in to the concrete slab. A brittle failure resulting from cracks in the concrete along the steel mesh line, followed by yielding and rupturing of the mesh, was observed. (Lukaszewska, 2009) The mechanical parameters determined from push-out tests carried out by the above stated researchers are presented in table 2.13.

	F_{max} [kN]	$k_{0,4}$ [kN/mm]	v [mm]
Bathon, Leander, Graf & Markus	90,0	-	1,8
Clouston, Bathon & Schreyer	111,62	415,46	1,44
Lukaszewska	81,2	483,8	4,0

Table 2.13 Mechanical parameters for a 400 mm long continuous steel mesh

Bathon, Leander, Graf & Markus also performed 4-point bending tests using the steel mesh connector. The beam specimens had spans of 5,4 m, and consisted of concrete slabs and glulam beams with cross sections of 600*70 mm and 100*200 mm respectively. The resulting total average ultimate failure load was 73 kN, with a corresponding vertical displacement of approximately 42 mm (Bathon, Leander, Graf, & Markus, 2000).

2.3.17 Adhesive

Several experiments have been carried out on epoxy-based adhesives for the possible use as a shear connector in timber-concrete composite systems. In the late 1960's, Pincus performed bending tests on 5 composite beams using an epoxy resin compound as connector. The main observation was that there was no slip between the wood and the concrete before the final failure, indicating that full composite action had been achieved. In 1970, Pincus performed 8 more bending tests using adhesive as a connector, this time with added nails along the interface between the timber and concrete to serve as supplementary mechanical shear transfer devices. Pincus concluded from his experiments that efficient timber-concrete composites could be constructed by applying epoxy based adhesive on top of wooden beams and immediately thereafter cast the concrete on the beams. Additionally he concluded that adding nails to the structure could increase the shear capacity of the connection by 50%. (Lukaszewska, 2009)

In 2006, Brunner et al. tested a similar approach, the so called wet-on-wet process, implying that concrete is poured onto the adhesive while the adhesive is still wet. 925 grams/m^2 of a 2-component epoxy based adhesive (SIKA product) was carefully applied at the top of the wooden components, being 3-ply slabs of quality C24. Both self compacting concrete and standard concrete of quality C25/30 were used as top component in the various push-out tests. The strength-parameters presented in table 2.14 were determined. (Brunner, Romer, & Schnuriger, 2007)

Concrete	Shear strength [N/mm^2]
Standard C25/30	2,97
Self compacting concrete C25/30	2,10

Table 2.14 Shear capacity determined by Brunner, Romer, & Schnuriger

For more convenient comparison with the previously investigated mechanical connectors, table 2.15 presents equivalent values to those presented in table 2.14.

Concrete	F_{max} [kN]
Standard C25/30	29,7
Self compacting concrete C25/30	21,0

*Table 2.15 Shear capacities for a 100*100 mm area equivalent to the values presented in table 2.14*

Additional observations made was that the optimal time interval between mixing of the adhesive and pouring of the concrete, given normal conditions (20^0C, RH=50-60%), was approximately 90 minutes. Pouring of concrete before 90 minutes lead to exaggerated displacement of the adhesive. Pouring after 90 min on the other hand reduced the bonding between the materials significantly. (Brunner, Romer, & Schnuriger, 2007)

2.4 Survey of currently employed timber-concrete composite solutions

2.4.1 The HBV-system

The HBV-building system is a result of the testing carried out by Clouston, Bathon, & Schreyer, see section 2.3.16. It includes wall-, floor and roof elements, see figure 2.28. The continuous steel mesh that connects the concrete to the wood is embedded halfway into the concrete and halfway into a sawn slot in the wooden beam. The mesh also serves as support for the reinforcement web that is cast into the concrete. The adhesive used to attach the mesh in the slot is fire resistant up to approximately 200^0C and needs 30 minutes to cure. (Clouston, Bathon, & Schreyer, 2005)

Figure 2.28 The HBV-hybrid-rib-element for commercial housing (Bathon, 2007)

The system includes different variations of the principal structure, suitable for residential and commercial buildings. (Bathon, 2007)

2.4.2 M-section-system

This system utilizes the square concrete plug reinforced with a lag screw, see section 2.3.8. Each semi-prefabricated element is 2400 mm wide and consists of a plywood board (that eventually acts as permanent formwork for the cast in situ 65 mm thick concrete slab) and LVL-girders with cross sections of 400*63 mm. The girders are placed at a spacing of 1200 mm. (Deam, Yeoh, Fragiacomo, Buchanan, Crews, & Haskell, 2008). Figure 2.29 shows a cross section of a semi-prefabricated M-panel.

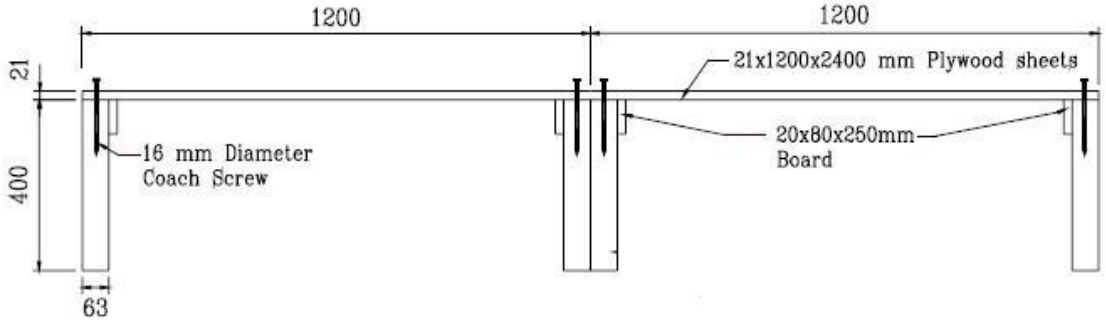

Figure 2.29 Cross section of M-panel
(Deam, Yeoh, Fragiacomo, Buchanan, Crews, & Haskell, 2008)

The centre beam is constituted by a double girder. When the elements are put in place next to each other, the single girders at the end of each element connect into double girders by means of nails, thus creating a uniform platform for the casting of the concrete slab, see figure 2.30. A steel reinforcement mesh provides shrinkage control for the concrete slab.

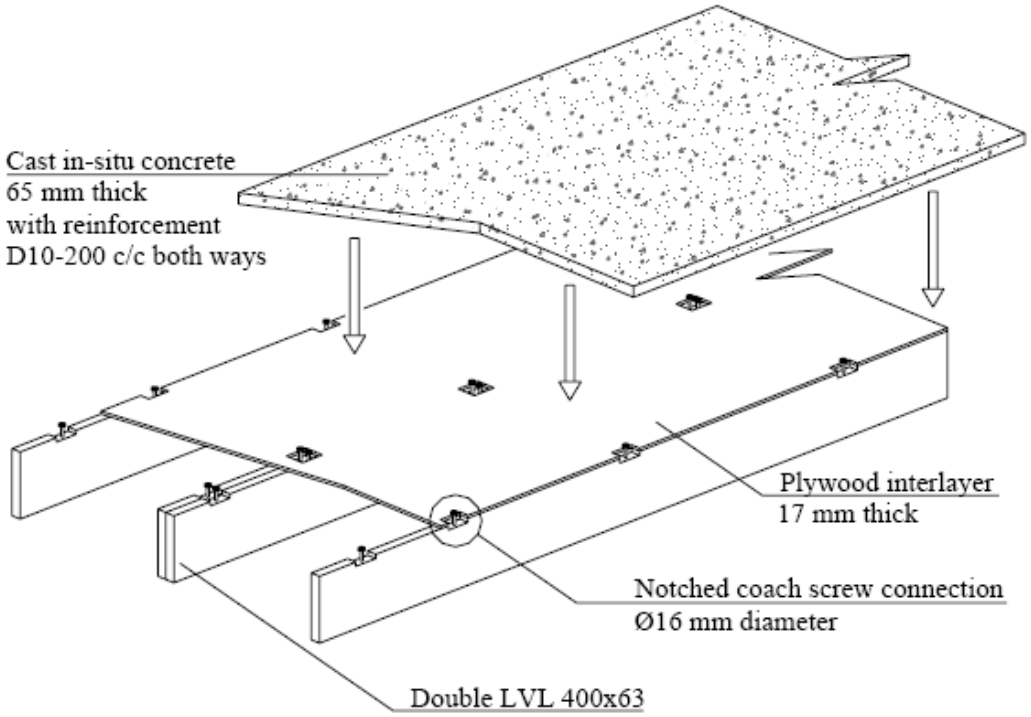

Figure 2.30 M-section with concrete slab
(Deam, Yeoh, Fragiacomo, Buchanan, Crews, & Haskell, 2008)

The sides of the connector are equipped with 20*50*250 mm boards to prevent concrete leakage upon casting. The solution enables spans up to 10 meters requiring only 6-8 connectors along each girder. (Deam, Yeoh, Fragiacomo, Buchanan, Crews, & Haskell, 2008)

2.4.3 The SEPA 2000-system solution

The SEPA-2000 is a result from experiments conducted at VTT Building Technology in Finland. The system, approved by the Finnish Ministry of the Environment, includes two solutions. One is a cast in situ solution and the other is a prefabricated solution, with the concrete cast upside down eliminating the need of formwork. Instead of rectangular wooden beams, wooden trusses are used (see figure 2.31), enabling transverse piping within the floor. (SEPA GROUP)

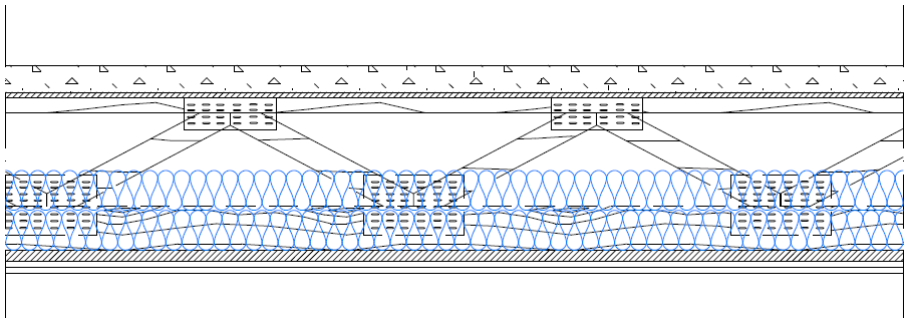

Figure 2.31 Trusses in the SEPA-2000 system (SEPA GROUP)

The concrete is connected to the wood through the use of nail-plate-connectors, see figure 2.32. Spans up to 8 m are possible. With somewhat reduced span lengths, the SEPA-2000 performs satisfactorily as a continuous system as well. (Lukaszewska, 2009)

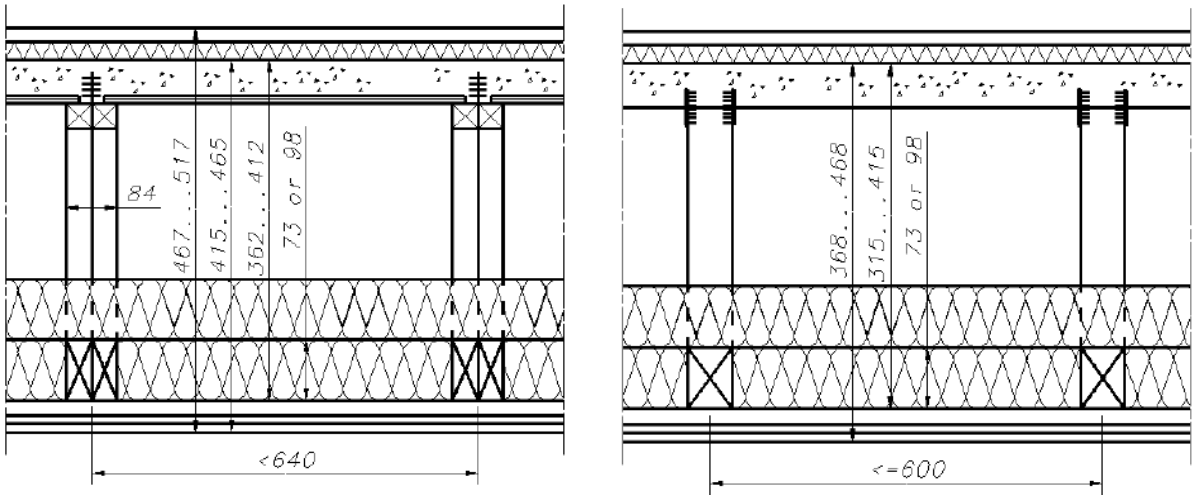

Figure 28. The SEPA-2000 system (Lukaszewska, 2009)

2.4.4 Other solutions

In addition to the above accounted for various prefabricated and semi-prefabricated solutions, other, in-situ solutions are sometimes used. The shear connectors employed for these solutions include the SFS-screw, regular screws and nails. Regular nails and screws are mostly used for restoration purposes however.

2.5 Survey of proposed enhancement-methods for timber-concrete composite structures

2.5.1 Use of lightweight concrete

To use lightweight concrete in a timber-concrete composite floor could be a possible way to reduce its weight. An even bigger reduction of the overall weight of a building would thus be achieved. The experimental results of E. Steinberg, R. Selle and T. Faust suggest that a decrease in a timber-concrete composite's dead weight by approximately 15% could be achieved by using lightweight concrete instead of regular concrete. (Steinberg, Selle, & Faust, 2003)

However, the lower capacity of lightweight concrete would increase the risk of failure in the concrete. This risk is further increased by lightweight concrete's higher tendency to split as a result of the forces concentrated around the shear connectors.

2.5.2 Use of steel-fiber-reinforced concrete

Steel fibre reinforced concrete is more ductile and better on redistributing stresses than normal concrete. As a result, a steel fibre reinforced concrete slab is more resistant to flexural action. Once a crack is initiated, the better redistribution of stresses may also prevent brittle failure from occurring. This can enable a reduction of the slab thickness or alternatively an increase in the spacing of timber girders. (Tajnik, Dobrila, & Premrov, 2007)

Additionally, Holschemacher, Klotz and Weibe demonstrated through experiments that the shear capacity as well as the initial slip modulus of shear connectors could be increased if steel fibre reinforced concrete was used. (Tajnik, Dobrila, & Premrov, 2007)

2.5.3 Use of carbon-strip-reinforcement

Tajnik, Dobrila and Premrov studied the effect of adding a carbon strip at the bottom of the timber component, in composite beams using dowels as shear connectors. For the studied beams, the timber was the component decisive for the ultimate loading capacity, and the idea was that the carbon strip would act as tensile reinforcement, enabling an increase in bending stiffness without increasing the cross section of the timber component.

By performing numerical examples they concluded that the adding of a carbon strip increases the bending stiffness, moment capacity and shear capacity of composite structures. Table 2.16 presents the average improvements concluded in the study. (Tajnik, Dobrila, & Premrov, 2007)

Bending stiffness		Moment capacity		Shear capacity	
Short term	Long term	Short term	Long term	Short term	Long term
+11,1%	+17,6%	+15%	+23,9%	+3,61%	4,66%

Table 2.16 Average improvements with the adding of carbon strip

However, adding carbon fiber strips at the bottom of timber beams is expensive. It also requires a higher quality of workmanship than traditional reinforcements. An economic analysis made by Stevens and Criner showed practical applicability for bridges of longer spans, the application of carbon fiber strips in composite floors is probably too expensive to be considered. (Tajnik, Dobrila, & Premrov, 2007)

3 Evaluation of timber-concrete composite solutions

3.1 General

Apart from fulfilling the first objective, this chapter is an important step towards reaching thesis's the second objective, as stated in section 1.2. The evaluation serves as a platform for choosing a potentially efficient solution for further testing.

There are two factors that govern the overall efficiency of a timber-concrete composite solution; structural performance and economy. If a solution lacks good structural performance, user safety can not be guaranteed. On the other hand, if a solution is not economical, large scale production is not possible regardless of the structural performance.

Both structural performance and economy of a solution are very much related to the connection in the composite floor. For example, rationalizing production is crucial for the economy. Choosing a connection that allows for an effective rationalization to take place is therefore a key step in achieving a good economy. Also, we saw in chapter 2.1 that the structural performance is governed by the stiffness, strength and post-peak performance of the shear connector. In other words, it all comes down to the shear connector.

Due to the critical role of the connection when it comes to achieving an efficient solution, this evaluation centers around the shear connectors. Both structural performance and economic aspects are considered. Thus, the factors that are considered in the evaluation are:

- Slip modulus
- Shear capacity
- Ductility
- Ability to achieve economic solutions

The evaluation includes the shear connectors described in the survey in chapter 2, which also provides the basic structural data for the connections in terms of stiffness, strength and post-peak performance.

The concept of achieving an economic solution should be clarified; as was stated in the beginning, the ability to rationalize production is crucial. Effective rationalization in the production of timber-concrete composite floors involves using a reasonably cheap connector, installing it quickly, and achieving effective logistics. The quickness of the installation of the connector is highly dependant on the number of steps that is required to complete the installation. For example, a nail requires only one step to be installed, while a connection that involves separate parts require several steps to be installed. Therefore, the time needed for installation could be seen as a function of the general simplicity of the connector.

The effectiveness of the logistics depends primarily on the level of ease of handling and the time needed for completion in situ.

3.2 Execution

A complete evaluation involving all the possible solutions with the shear connectors included in the survey of chapter 2 was considered unrealistic. The first step in the evaluation process was thus to disregard from the connectors that seemed unsuitable at a first glance. Nevertheless, this was done considering the factors pointed out in section 3.1. The connectors that passed the first sorting are listed below together with a brief motivation.

SFS-screws: (refer to section 2.3.2)
The SFS-screws show a reasonably good structural performance with regard to stiffness and strength. A composite floor using SFS-screws should therefore be able to satisfy the demands on span length in office buildings (8-10m). The only disadvantage from a structural performance-perspective is the failure mode. The average failure mode observed by Deam, Fragiacomo, & Buchanan was classified as brittle. Faust and Selle however reported that failure when using standard concrete is always due to either the pulling out of the screw from the wood or the shearing off of the screw. It is unclear what type of failure mode the pulling out of the screw from the wood should be considered as.

SFS-screws are readily available and should be obtainable at a reasonably low cost. Only one step is needed for the installation and Deam, Fragiacomo, & Buchanan report that the SFS-screws remain uninfluenced by the presence of an interlayer.

Reinforcement bars: (refer to section 2.3.5)
Reinforcement bars constitute simple connectors, they could be obtained and sawn into sections at a low price. They display a reasonably good structural performance with regard to shear capacity and slip moduli. There is a need to pre-drill holes for the insertion of the connectors, but two steps is not considered to big of a hinder for rationalization to be possible.

Flat steel lock connector: (refer to section 2.3.6).
The flat steel lock connector displays high shear capacity and low slip. The connectors can thus be placed at a considerable spacing reducing the total amount of connectors needed. Furthermore they are simple in their design and could probably be obtained at a low price. The two steps needed for installation ((1)sawing cuts, (2)inserting connectors) are not considered to hinder rationalization from taking place.

Square concrete plug reinforced with a lag screw: (refer to section 2.3.8)
This connector displays extremely good structural performance in every respect, the stiffness is high as is the shear capacity, and the post peak performance is excellent. It does however require 4 steps for installation, cutting of the dimple, pre-drilling hole for the screw, inserting the screw, covering the sides of the dimple to prevent concrete leakage upon casting. The many steps are partly compensated for by the fact that only 6-8 connectors are needed in a span of 8-10 meters. The fact that this connector is currently employed in a system in New Zealand strengthens the hypothesis that a rationalized production with this connector is possible.

Dimple/plug reinforced with lag screw and steel pipe combined:
Though not as strong as the square concrete plug with lag screw reinforcement, this is still a strong connector and rationalization might even be a bit easier. The round plug can be drilled quickly and this is true regardless of the presence of an interlayer. The connection also displays good post-peak performance. (refer to section 2.3.10)

Steel mesh: (refer to section 2.3.16)
This type of connector has displayed very good structural performance in tests in terms of strength and stiffness. Various types of failure modes have been observed. The installation of the connector involves 3 steps, cutting of the slot, application of adhesive and insertion of the steel mesh.

By the time the first sorting was completed it had been established that the timeframe and funding for this project did not allow for more than two solutions to be tested. Thus, only two of the five connectors discussed above could be chosen, and a decision had to be made about which connectors to proceed with. The decision was founded on the following factors:

- A solution involving a steel mesh is already employed in countries nearby
- SFS-screws, lag screws and reinforcement bars were thought to be the easiest to obtain
- Screws are easier to install than reinforcement bars
- A square reinforced concrete notch have performed extremely well in tests and have proved to work successfully in a system in New Zealand

With these factors in mind, it was decided to proceed investigating solutions involving the SFS-screws and the square concrete plugs.

4 Testing

4.1 General

Two full scale bending tests were performed on specimens. The shear connectors employed were square concrete plugs armed with a lag screw and SFS-screws. The load was applied in two points as illustrated in figure 4.1 (4-point bending tests):

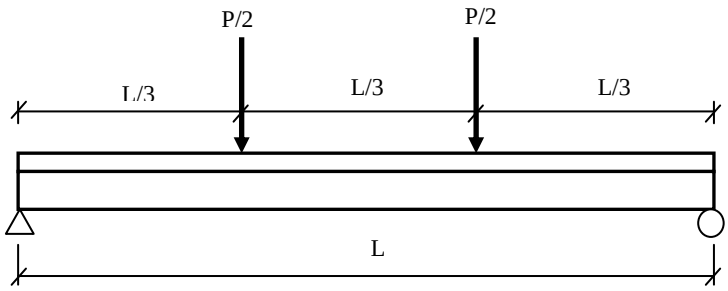

Figure 4.1 Schematic setting of a 4-point bending test

Each test specimen was 2400 mm wide and 7200 mm long, resulting in 7000 mm spans when placed on supports. The wooden part in each specimen was composed of four Swedish glulam beams of strength class L40 (approximately equivalent to GL28/GL32), placed at a spacing of 600 mm. Different glulam cross sections were used for the two floors. For the test specimen using SFS-screws as shear connector, glulam cross sections of 115*225 mm were used. For the other test specimen, 56*270 cross sections were used. The depth of the slab was 80 mm and the concrete used was a high performance, self-compacting concrete for quick curing, with a maximum aggregate size of 16 mm. Three concrete cubes measuring 150*150 mm were compressed to failure in order to establish the compressive strength of the concrete. The average cube strength was 70,1 MPa, corresponding to f_{cm}=65,56 MPa (EN 1992-1-1 (Design of Concrete Structures)). The concrete and the glulam beams were separated by a 21 mm thick plywood interlayer.

The SFS-screw-connection consisted of pairs of screws placed at a spacing of 125 mm. The screws within each pair had a 30 mm distance between them, and were tilted at 45- and 135 degree angles relative to the horizontal plane.

The reinforced concrete plugs were placed at 1000 mm spacing along the floor length. Each plug was 38 mm deep with a cross section of 50*56 mm. The screw used was a 150 mm long Φ12 lag screw. The lag screws were inserted to a depth of 90 mm in pre-drilled holes with 9 mm diameters, leaving 60 mm of the screws to be embedded in the concrete, of which approximately 22 mm remained above the surface of the plywood interlayer.

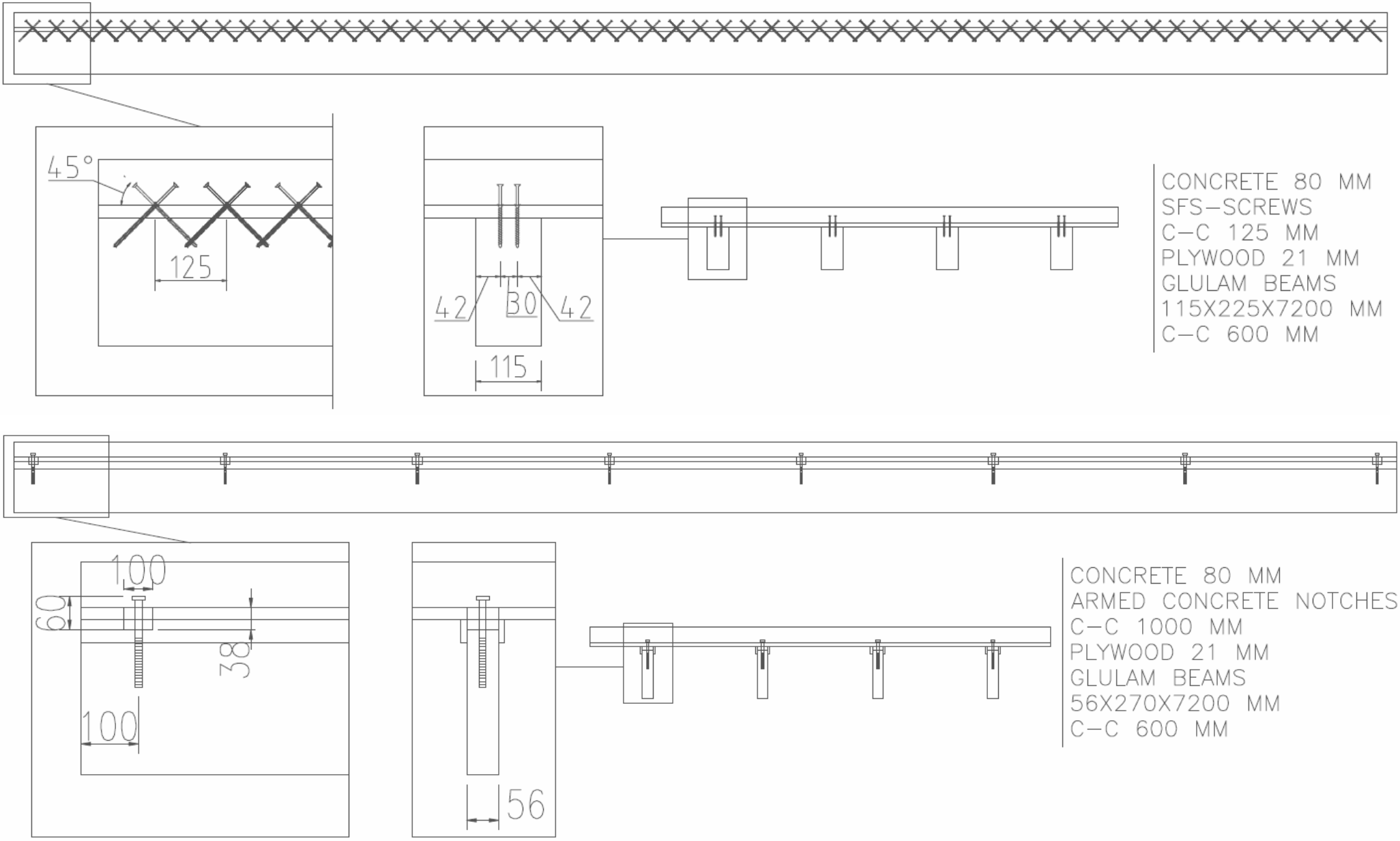

Figure 4.2 Top: Test specimen with SFS-connectors. Bottom: Test specimen with concrete notch-type connectors

4.2 Execution

Figure 4.3 illustrates the principal setup that was used for the full scale bending tests. The point-loads were applied over the whole width of the floor using an arrangement of steel I-beams, as is illustrated in figures 4.5 and 4.6. Due to a misunderstanding, the steel beams perpendicular to the load direction were placed at a spacing of 2,40 m instead of 2,33. This was of no significance for the tests and was therefore not corrected.

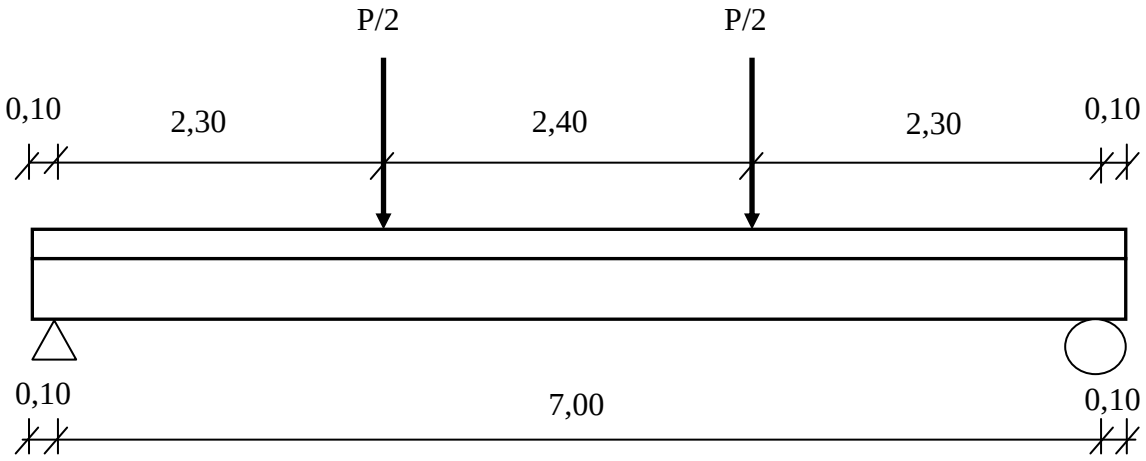

Figure 4.3 Setting used in full scale bending tests

In order to register displacements, measuring-devices were placed according to figure 4.4, where devices a-i registered vertical displacements while devices j-k registered horizontal displacement between concrete slab and the glulam beams.

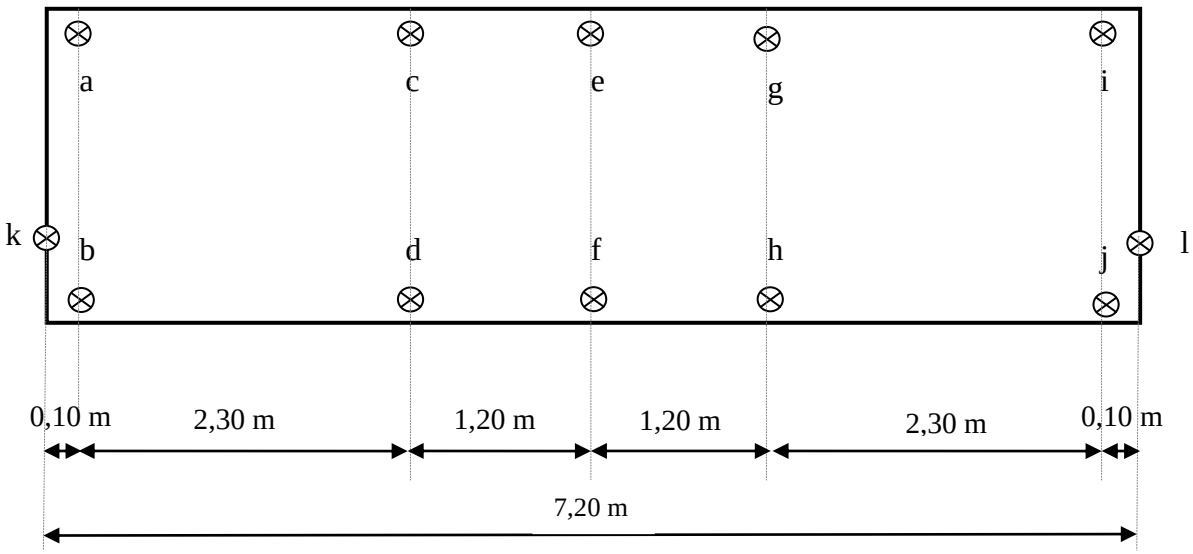

Figure 4.4 The positioning of measuring-devices as seen from above.

Figure 4.5 Top: Rig used for testing of the floor using SFS-screw connectors. Bottom: Rig used for testing of the floor using the plug-type connection

Loading was carried out according to the loading protocol recommended by EN 26891. Hence, the load was first increased to 40% of the estimated failure load where it was kept constant for 30 seconds. After decreasing the load to approximately 10% of estimated failure load, loading was again kept constant for 30 seconds. Finally the load was increased until failure occurred. Vertical displacements were measured continuously by devices (a-i).

The beam arrangement used to apply the point loads were to heavy to be disregarded in the calculations. Table 4.1 summarizes the weight of the beams used.

Beam	L [m]	ρ [kg/m]	m [kg]
HEA300	5,30	88	466,4
IPE300	3,99	42,2	168,4
IPE300	4,24	42,2	178,9
		Σ	813,7

Table 4.1 Additional weight from beam arrangement

This corresponds to the adding of approximately 4 kN at the position of each point load, see figure 4.3.

The centre-deflection was obtained as the average vertical displacement at the centre minus the average deformation at the supports. The local deflection of the floor-section located between the concentrated loads was obtained as the average vertical displacement at the centre, minus the average vertical displacement at the points of impact of the concentrated loads:

$$Centre\ deflection = ef - \frac{ab + ij}{2}$$

$$Local\ centre\ deflection = ef - \frac{cd + gh}{2}$$

Where,

a, b, c, d, e, f, g, h, i, j - vertical displacement/deformation recorded by devices a, b, c, d, e, f, g, h, i and j

ef, ab, i j, cd, gh - calculated average of deflection/deformation recorded by devises e & f, a & b, i & j, c & d and g & h respectively

It should be mentioned how the vertical displacement due to dead load was obtained; before the lifting and placing of the specimens on their supports, a device that registered vertical displacements in the middle third of the specimens had been installed. Assuming constant bending curves throughout the floor specimens, these displacements were used to estimate the total vertical displacements. It is important to remember that part of the displacement obtained in this way is due to the dynamic effects that came into play when lifting the floor and lowering it to its supports.

4.3 Results

Tests specimen 1, SFS-connector

Figure 4.6 shows the load-displacement curve recorded during the experiment. Only the additional load from the jack is considered (dead load and steel beams are disregarded). The abrupt ending of the curve was a result of the test specimen falling off from its supports during loading. By drawing a straight line, a slight deviation becomes visible at an additional load of approximately 235 kN. This corresponds fairly well to the additional load at which shear connector-failure starts to occur according to Girhammar's simplified approach if the actual moment arm due to interlayer thickness is considered (refer to appendix A).

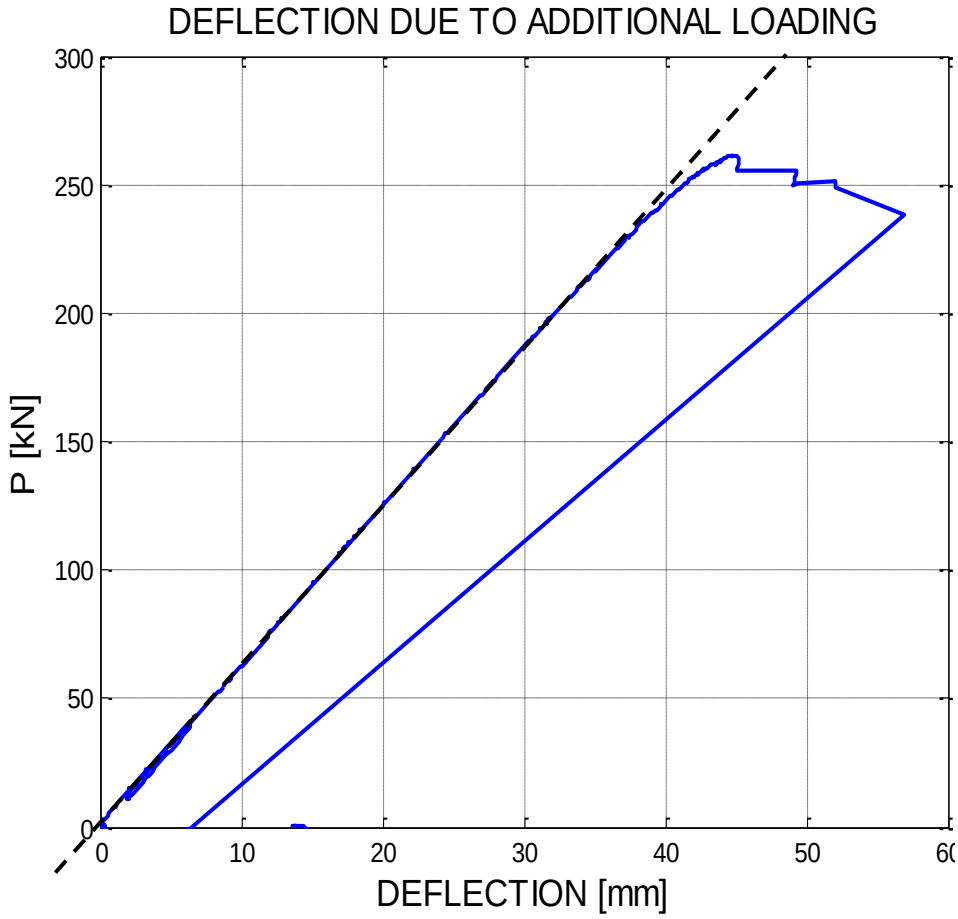

Figure 4.6 Load-displacement curve of specimen with SFS-screws

As stated in section 4.3, the load due to the beam arrangement was 8 kN. The displacement due to dead weight was estimated to 8,5 mm. Hence, the failure load was roughly 270 kN, corresponding to a deflection of approximately 52,5 mm (44+8,5). No sign of damage was visible afterwards, confirming the hypothesis that failure was initiated in the shear connectors.

Test specimen 2, Concrete plug-connector

Figure 4.7 shows the load-displacement curve recorded during the experiment. The curve is more or less linear up to a load of about 64 kN where it is assumed that the connectors started to fail. This is confirmed by the fact that the slope of the second part of the curve corresponds well to the bending stiffness given no composite action (refer to appendix B). At an additional load of approximately 120 kN, bending failure occurred in three of the glulam beams, resulting in an abrupt drop of the load-deflection curve, see figure 4.7 and 4.8.

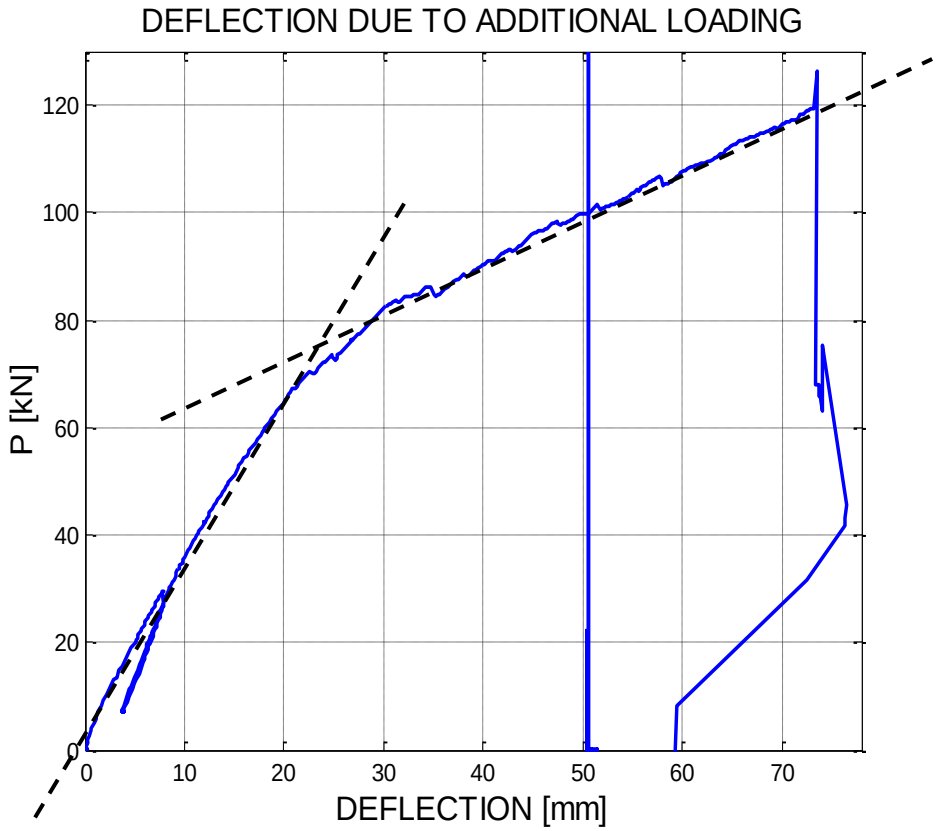

Figure 4.7 Load-displacement curve of specimen with concrete plug connectors

The vertical displacement due to dead weight was estimated to 14 mm. Hence, a total deflection of ~88 mm was observed at corresponding ultimate failure load of 128 (120+8) kN.

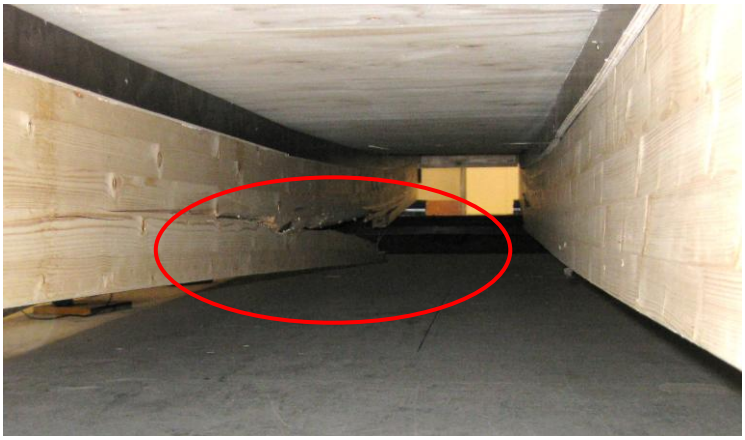

Figure 4.8 Final failure mode

Efficiency of the shear connectors:

When considering the contribution of dead weight as well as the weight of the beam arrangement, the following diagrams could be drawn for the two floor-specimens:

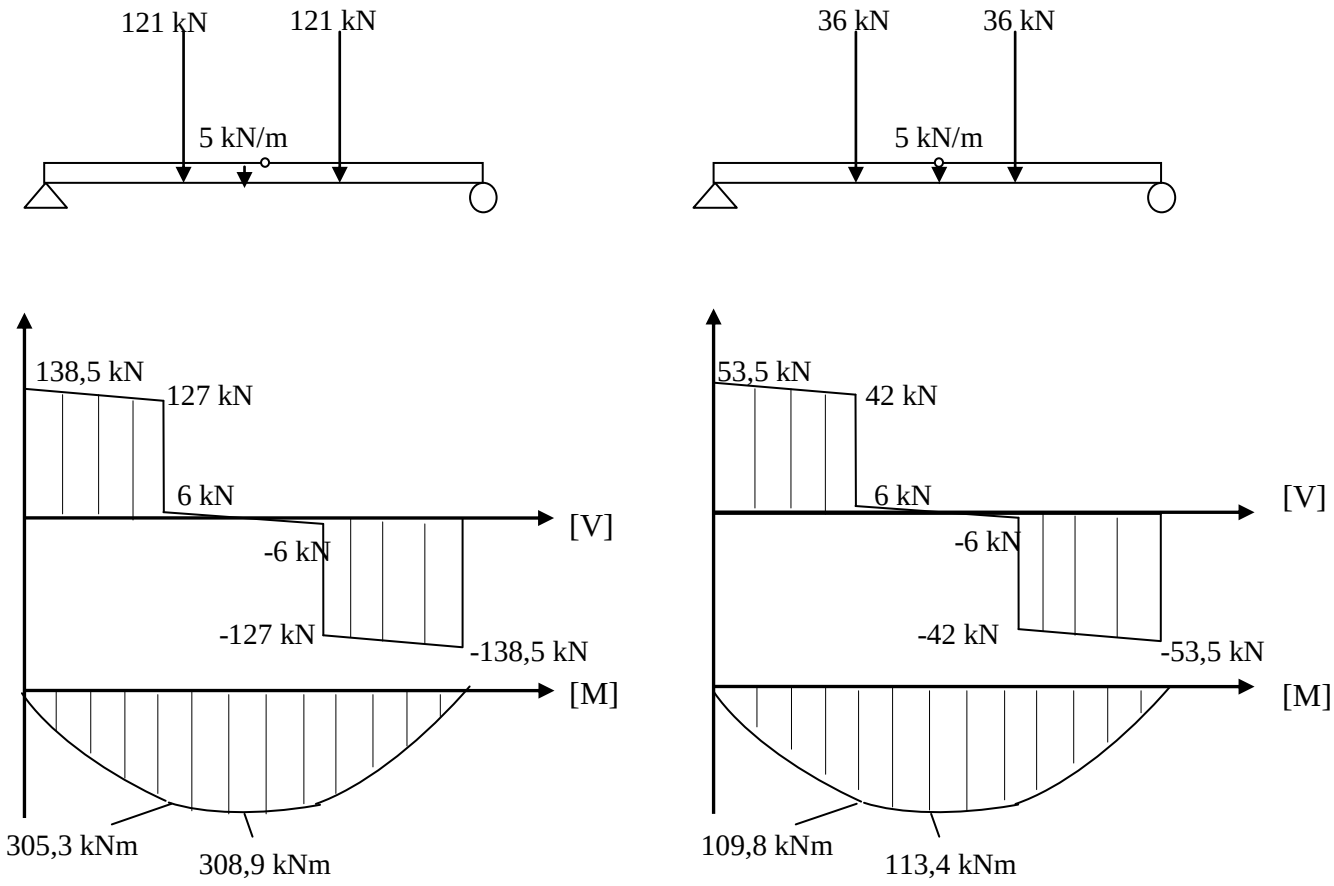

Figure 4.9 Left: Diagrams for specimen 1. Right: Diagrams for specimen 2

It is apparent from figure 4.9 that the floor-section between the point loads is practically unaffected by shear forces. Hence, the efficiency of the connectors could be assessed by comparing the center-piece bending stiffness with the overall bending stiffness. Equations for calculating the actual bending stiffness were thus derived. This was done by using beam-table-load cases.

Upon using beam tables to derive the actual bending stiffness, the vertical displacements "$v_{overall}$" and "$v_{center\text{-}piece}$" were defined as illustrated in figure 4.10. Figure 4.11 illustrates the load cases that were used.

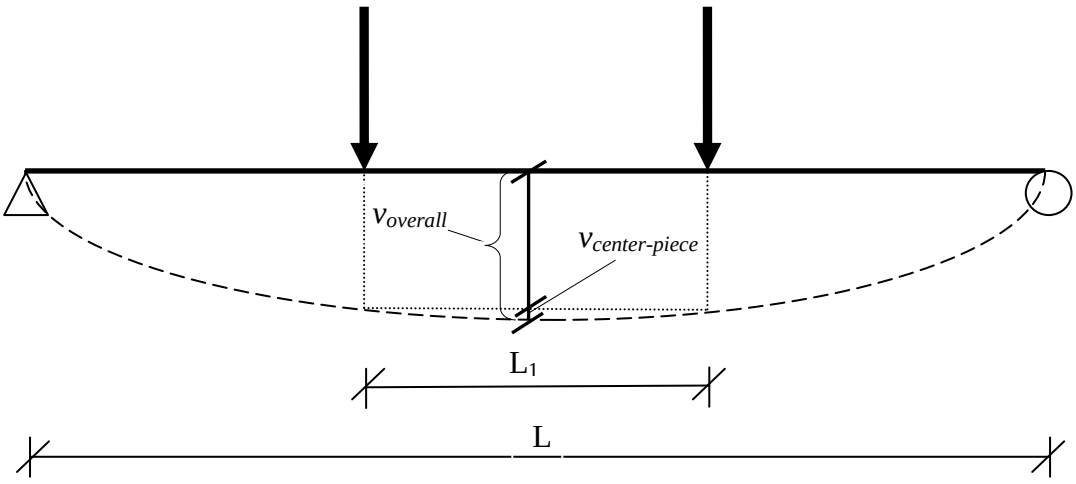

Figure 4.10 "$v_{overall}$" and "$v_{center\text{-}piece}$"

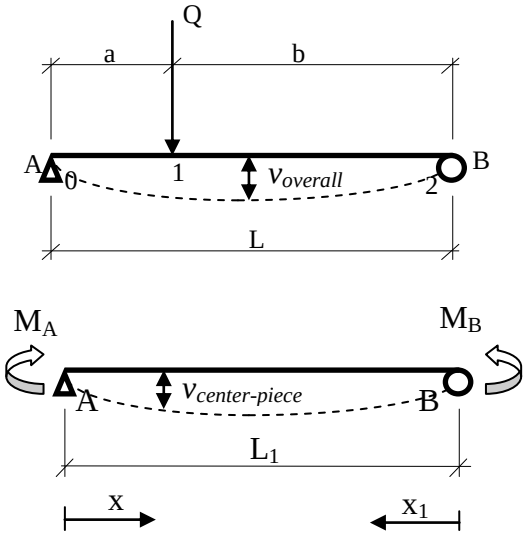

$$v_{overall} = \frac{Qa(3L^2-4a^2)}{48EI}$$

$$v_{center-piece} = \frac{L_1}{6EI}\left(M_A x_1\left(1-\frac{x_1^2}{L_1^2}\right)+M_B x \quad \left(1-\frac{x^2}{L_1^2}\right)\right)$$

Figure 4.11 Load cases used for obtaining actual bending stiffness.
<u>Top</u>: Load case used to determine the overall bending stiffness of the floor.
<u>Bottom</u>: Load case used to determine the bending stiffness of the floor center-piece.

In the actual case, two concentrated loads were present. The symmetry of the loading however enabled the overall deflection to be expressed by simply doubling the effect of the top load case in figure 4.11. Considering also that for the actual case, a, L, x, x_1 and L_1 were constants ($a = 2{,}3\ m,\ L = 7\ m,\ L_1 = 2{,}4\ m,\ x = x_1 = L_1/2 = 1{,}2\ m$), and that M_A=M_B, the equations in figure 4.11 could be rewritten so that equations 4.1 and 4.2 were obtained:

$$v_{overall} = 2 * \left(6{,}03\frac{Q}{EI}\right) \qquad \text{(Eq. 4.1)}$$

$$v_{center\ piece} = 0{,}72\frac{M_A}{EI} \qquad \text{(Eq. 4.2)}$$

Expressions for the actual bending stiffness of the floor specimens could then be derived through the reorganization of equations 4.1 and 4.2 into equation 4.3 and 4.4:

$$EI_{overall} = 2 * \left(6{,}03 \frac{Q}{v_{overall}}\right) \quad \text{(Eq. 4.3)}$$

$$EI_{center\ piece} = 0{,}72 \frac{M_A}{v_{center\ piece}} \quad \text{(Eq. 4.4)}$$

In order to obtain the necessary indata to the above equations, data from the full scale bending experiments was used to plot the diagrams presented in figure 4.12 below.

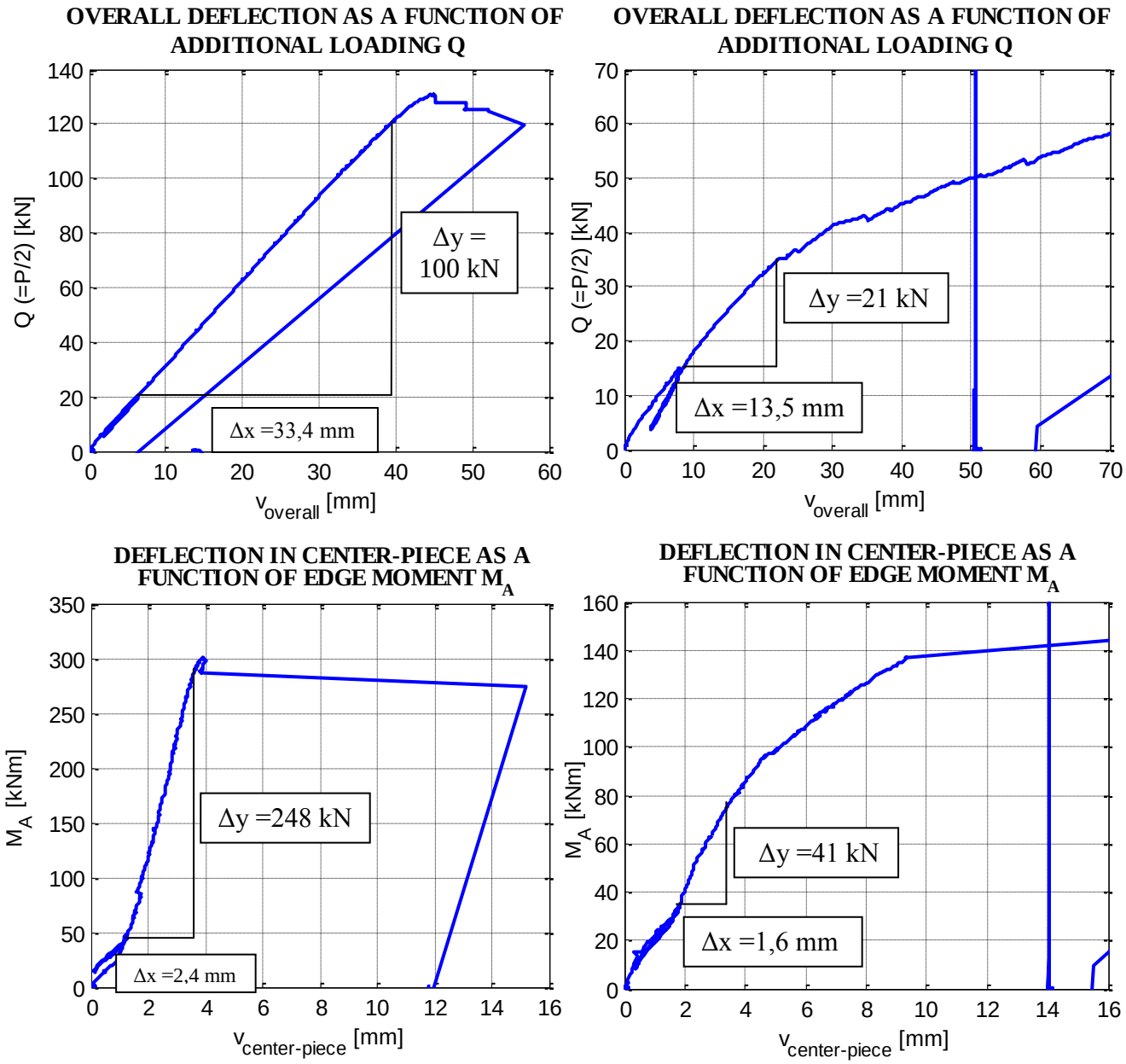

Figure 4.12 Diagrams for obtaining indata to equations 4.3 and 4.4
Left: Specimen with SFS-screws.Right: Specimen with reinforced concrete plugs

Table 4.2 presents the actual bending stiffness that was finally obtained by inserting indata from figure 4.12 into equations 4.3 and 4.4. For comparison, the rightmost two columns provide the corresponding theoretical non- composite- and fully composite bending stiffness (refer to appendix B).

	$EI_{overall}$ [MNm^2]	$EI_{centre\text{-}piece}$ [MNm^2]	$EI_{non\text{-}composite}$ [MNm^2]	$EI_{full\ composite}$ [MNm^2]
SFS-system	36,11	74,4	9,60	43,84
Conc. notch-system	18,76	18,5	8,70	33,06

Table 4.2 Bending stiffness of test specimens. The part of table with thicker lines shows the actual bending stiffness recorded from the experiments.

As is apparent from studying table 4.2, the calculated actual bending stiffness of the floor centre-piece, in the case of the SFS-screw connection, is considerably higher than that of the theoretically full composite bending stiffness for the same connection. This is of course not possible in reality, and the reason for this error was not fully clarified. It should however be emphasized that the Young's moduli of wood and concrete, used to calculate the theoretical non-composite and fully composite bending stiffness for the specimens, were estimated values taken from the literature. Another source of error could of course be the reading of the diagrams in figure 4.11. Last but not least, the de facto small displacements in the beam centre pieces may also have contributed to the error, since small displacements increase the likelihood of measuring-errors occurring. The explanation is thought to be a combination of the above stated factors.

Eventually, another method to evaluate the effectiveness of the connection had to be chosen. The following formula proposed by Gutkowski (Lukaszewska, 2009), was chosen for the evaluation of the effectiveness of the connection:

$$Efficiency = \frac{D_N - D_I}{D_N - D_C} \qquad \text{(Eq. 4.3)}$$

Where,

D_N Theoretical deflection for the corresponding beam with no composite action
D_C Theoretical deflection for corresponding beam with full composite action
D_I The actual measured deflection of the composite beam

Using theoretical and actual bending stiffness together with the expression previously described for the overall deflection, the required input-data for equation 4.3 could be obtained. Efficiencies were then estimated according to the following:

SFS-screws:

$$D_N = 2 * \left(\frac{100*10^3*2,3(3*7^2-4*2,3^2)}{48*9,60*10^6}\right) = 0,126m$$

$$D_C = 2 * \left(\frac{100*10^3*2,3(3*7^2-4*2,3^2)}{48*43,84*10^6}\right) = 0,028m$$

$$D_I = 0,0334\ m$$

$$\Rightarrow Efficiency = \frac{0,126-0,0334}{0,126-0,028} = \underline{0,945}$$

Reinforced concrete plugs:

$$D_N = 2 * \left(\frac{21*10^3*2,3(3*7^2-4*2,3^2)}{48*8,70*10^6}\right) = 0,029m$$

$$D_C = 2 * \left(\frac{21*10^3*2,3(3*7^2-4*2,3^2)}{48*33,06*10^6}\right) = 0,007$$

$$D_I = 0,0135\ m$$

$$\Rightarrow Efficiency = \frac{0,029-0,0135}{0,029-0,007} = \underline{0,705}$$

It is obvious that a sufficient efficiency can be achieved with the first type of connector (SFS-screws). The second type of connection did not prove to be as efficient. The efficiency of this connection would be higher if the connectors were placed at a smaller spacing. However, considering the amount of work that is needed for the installation of each connector, a smaller spacing would have come at the cost of a less rationalized product.

The theoretical bending stiffness, resulting from calculations accounted for in appendix A, depend on whether or not the extra distance between the sub-elements due to the interlayer thickness is taken into consideration. As stated earlier, the strength parameters of SFS-screws remain uninfluenced by the presence of an interlayer (refer to section 3.2), and the increased internal moment arm resulting from the interlayer thickness thereby gives rise to a larger bending stiffness. However, even when choosing the more realistic approach of considering the interlayer thickness, the calculated theoretical bending stiffness was slightly less than the actual bending stiffness achieved in the experiments (EI_{actual}=36,1, $EI_{calculated}$=32,5, for test specimen 1). This could be due to various

reasons; friction between the materials is disregarded in the calculations but in reality it probably contributes somewhat to the bending stiffness achieved. Also, the lifting-devices that can be seen in figure 4.5 may have served as a type of extra connectors, slightly increasing the bending stiffness. Again, it should be emphasized that the Young's moduli of wood and concrete, used to calculate the theoretical bending stiffness, were taken from the literature and not derived from experiments for the particular case.

Shear connectors are more exposed to shear forces the stiffer the composite structure is (refer to section 2.1.2). For a composite structure in which the connectors are decisive for the overall failure, an increased bending stiffness should therefore be synonymous with a decreased load capacity. This was in fact also the case. For the specimen with the SFS-screw connection, there was a -5,8 % difference between the estimated failure load and the failure load observed (P_{actual}= 235 kN, $P_{calculated}$=248,65). Even so this is considered an acceptable difference. In short, the theoretical and actual results are close enough for the method of analysis to be considered acceptable and valid.

Moreover, if the analysis is made anew, using a modified bending stiffness corresponding to the actual value observed, the obtained values for failure load and deflection will match up almost exactly to the observed values.

5 Proposed timber-concrete composite floor system

As a result of the evaluation and testing that was carried out in this project, the following timber-concrete composite system is proposed:

5.1 Configuration and materials

The system is based on semi-prefabricated wooden panels. Each panel is 2400 mm wide and consists of four glulam beams connected to an 18 mm thick plywood board. The beams are of strength class GL28/GL32 and the centre distance between them is 600 mm. The shear connector is constituted by SFS-screws installed pair-wise at a constant spacing along the beam lengths. A minimum distance of 30 mm is required between the beam edge and the screws, and the distance between the screws within a pair must be 30 mm, see figure 5.1.

Indeed, from a rationalization perspective it is advantageous to make production as uniform as possible, i.e. avoiding too many variables, however, the attractiveness of the product must also be considered. If a certain degree of flexibility is not maintained, the product will not be able to attract enough buyers. In order to increase the possibility to satisfy customer's various structural and architectural demands, module-length, connector-spacing, glulam-dimensions and concrete height- and strength class can be varied. Table 5.1 provides the intervals:

Variable	Interval
L	6,0-9,6 m
s	0,2-0,4 m
h_{glulam}	0,18-0,405 m
w_{glulam}	0,09-0,14 m
$h_{concrete}$	0,06-0,10 m
f_{ck}	25-40 MPa

Table 5.1 Variables in the proposed system

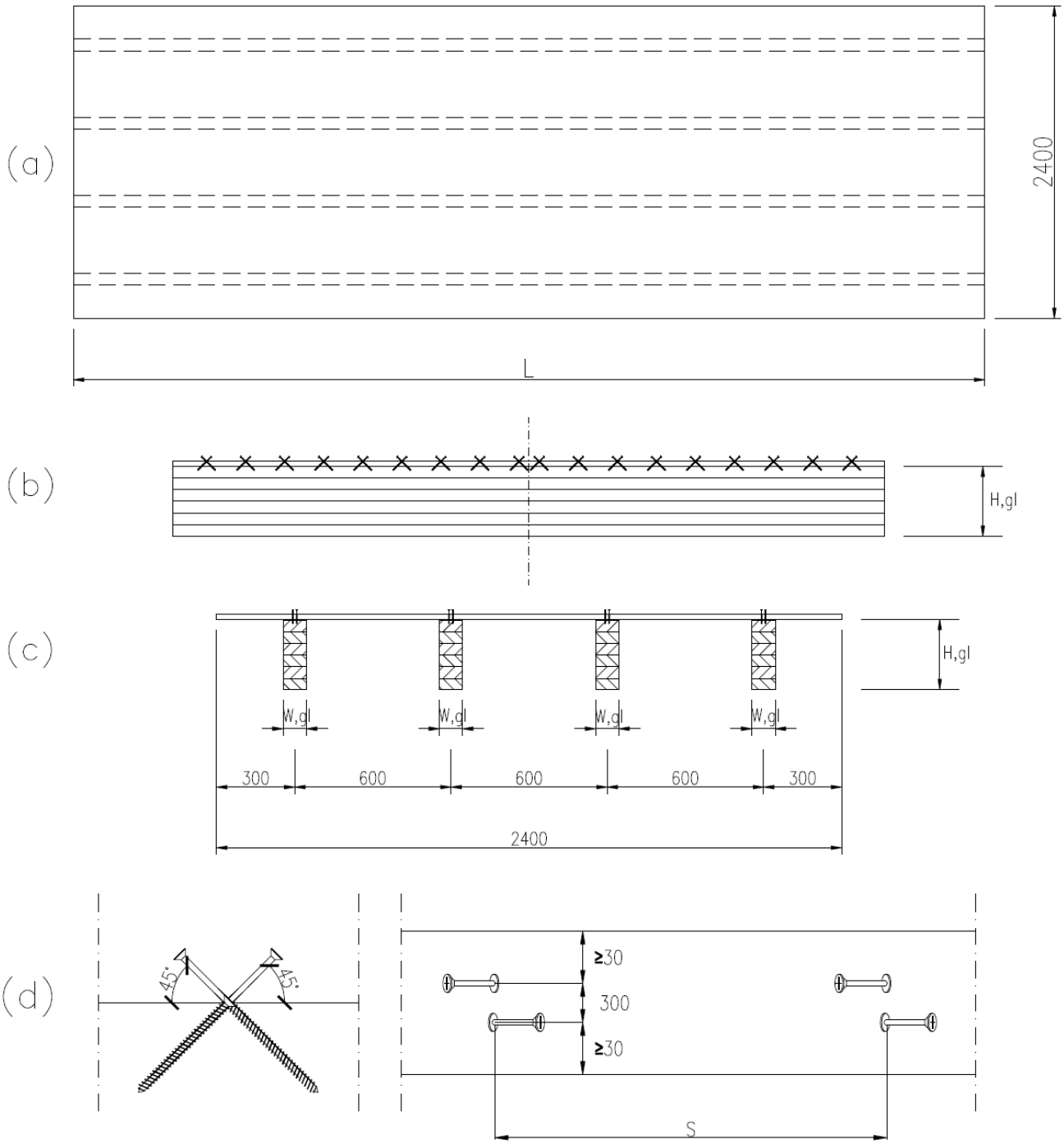

Figure 5.1 Principal configuration of semi-prefabricated module
(a)View from above (b)View from the side (c)Cross-section (d) Shear connector

5.2 Design

The design is conducted as described in section 2.2.2. It is recommended that Girhammar's simplified approach is used to calculate the stresses since this makes it easier to consider the effect of the interlayer thickness. Long term effects are considered using the effective modulus method.

The design could be carried out very quickly using a computer program. Such a program would work as follows: The user specifies the expected moment action after which the program runs the design procedure for a large number of alternative dimensions and material qualities (the intervals are specified in table 5.1). The program then displays the different solutions that can sustain the specified moment. This enables the picking of the alternative that fits the demands of the customer best.

Two illustrative design examples that uses Girhammar's simplified approach are provided in section 5.5.

5.3 Manufacturing and delivery

Production can be rationalized effectively. The proposed method is summarized as follows:

Manufacturing

1 Glulam beams of standard dimensions and 18 mm thick plywood boards measuring 1200*2400 mm are stored in a dry environment.

2 When the design procedure has uncovered the required beam dimensions, beams of the prescribed dimensions are placed on belt conveyors moving at a constant rate. Sawing of the beams and application of the SFS-screws can then take place automatically with machines especially designed for that purpose. The process is simplified considerably by the fact that the plywood boards already have the desired width.

3 Metal hooks for easier in situ-lifting could also be screwed on to the modules during the assembly.

Loading, delivery and unloading (See figure 5.2 & 5.3)

The configuration and light weight of the semi-prefabricated panels allows for effective logistics:

1 The panels are packed pair-wise. The packing is carried out so that the girders of the two panels are positioned next to each other. This way, a lot of space is saved.
2 The panels in each pair are tied together and loaded on a truck. Girders are placed between each pair so that the shear connectors are not damaged during the transportation.
3 Before the transport starts, all panels are fastened properly with fastening belts.
4 At the construction site the panel-pairs are lifted from the truck and lowered to the ground. After untying the panels, the top panel can be lifted and mounted in the building. While the top panel is being put into place, the bottom panel is turned over into position for lifting as well. When both panels are in place, the procedure is repeated until all panels are in place and the truck is empty.

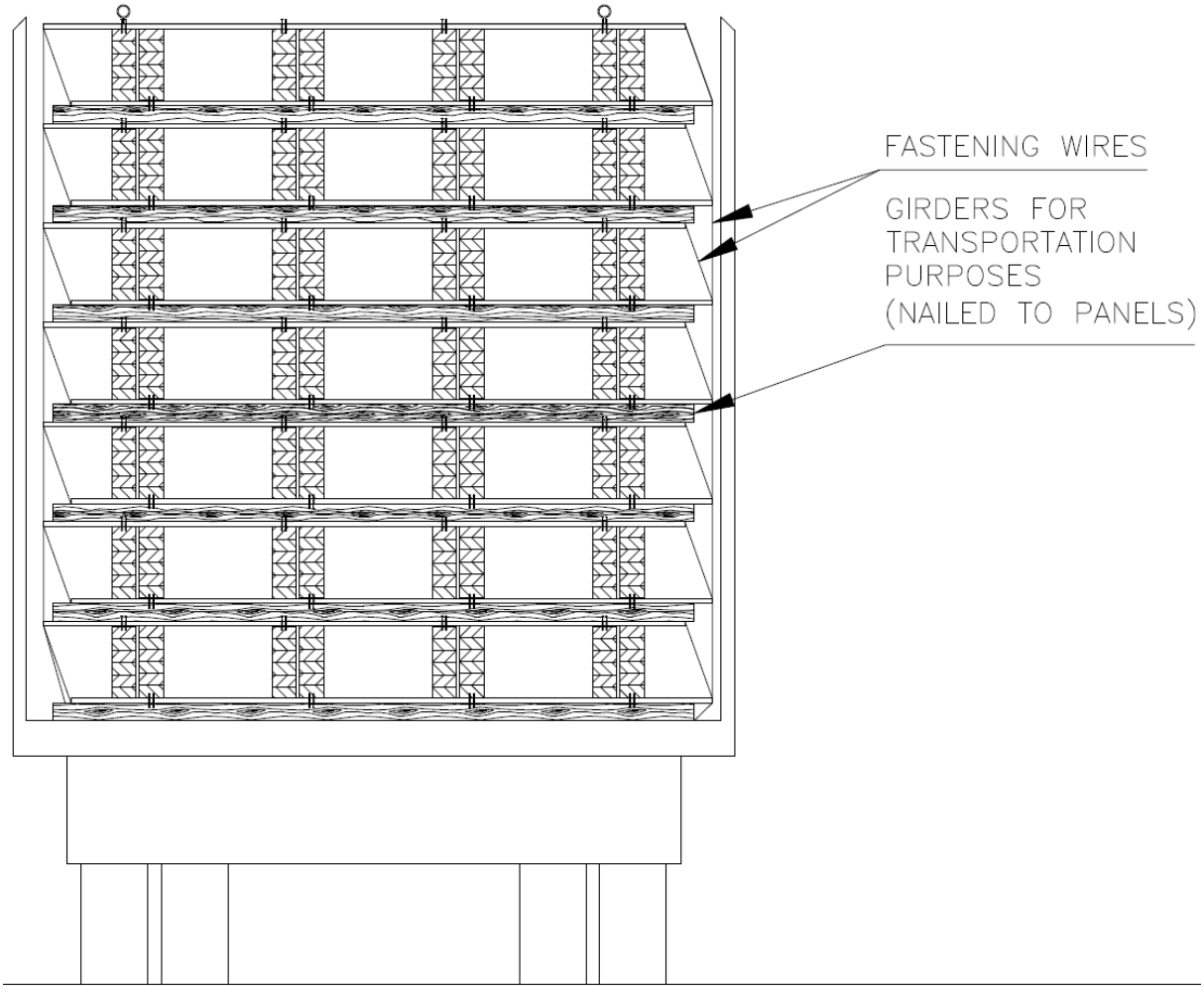

Figure 5.2 Truck loaded with panels for delivery to the construction site

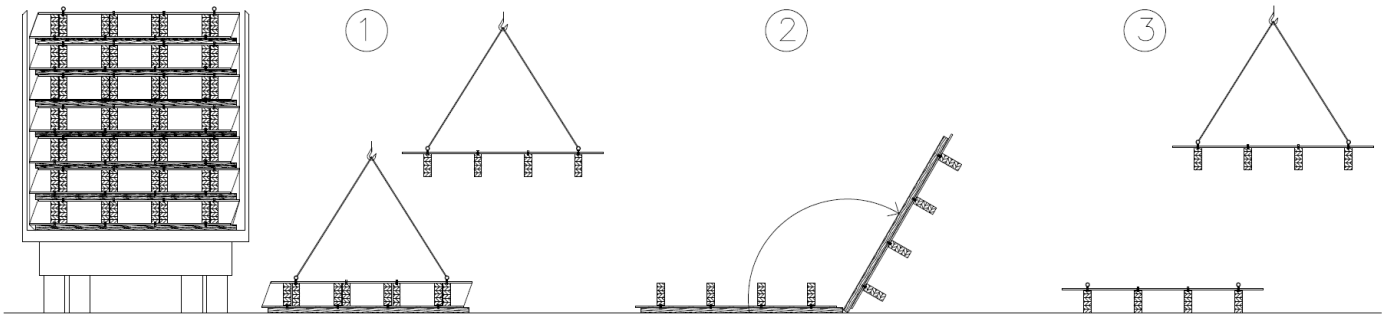

Figure 5.3 Unloading and lifting of the panels

(1)Unloading and unpacking of a pair of panels
(2) Turning of the second panel while the first panel is being put into place
(3)Lifting the second panel into place

5.4 Installation of the system

For the niche that this project focuses upon (light multistory office building), buildings are likely to have steel skeletons or glulam frames. It is also possible that the horizontal skeleton-parts are composed by glulam beams that transport the load on to the vertical components of the skeleton. This section presents the proposed method of installation of the system, together with some suggestions of how to connect the panels to steel frames and glulam beams.

The installation of this system can be summarized as follows:

1. The panels are lifted and put into position next to each other, forming a continuous platform for the casting of the concrete
2. If necessary, the panels are connected to the rest of the structure using screws or bolts
3. The slab is cast on the panels using a high performance concrete for quick curing *

*Before casting, vertical propping should be placed midway under the panels in order to prevent unnecessary deflection during the curing of the concrete. These supports could be removed after a few days.

Connection to a steel frame:

UPE-beams or welded box-beams could be used to connect the panels to a steel frame. Figure 5.4 illustrates a possible way to connect the panels to a steel column using a UPE beam. Alternatively, the UPE beam could be placed between the steel columns. The connection requires that the UPE beams are applied to the panel edges before the panels are lifted into position (step 1). Holes must then be prepared in beforehand in the UPE -beam as well as in the column to enable both the application of the UPE-beams to the panel edges and a quick assembly with bolts to the skeleton of the building.

Figure 5.5 shows how a welded box beam could function as a continuous support for the floor system in question. Such a beam is best used in the interior of a building, as is implied in figure 5.5. However, if placed in the exterior walls of a building, a welded box beam could also serve as an alternative to the connection seen in figure 5.4.

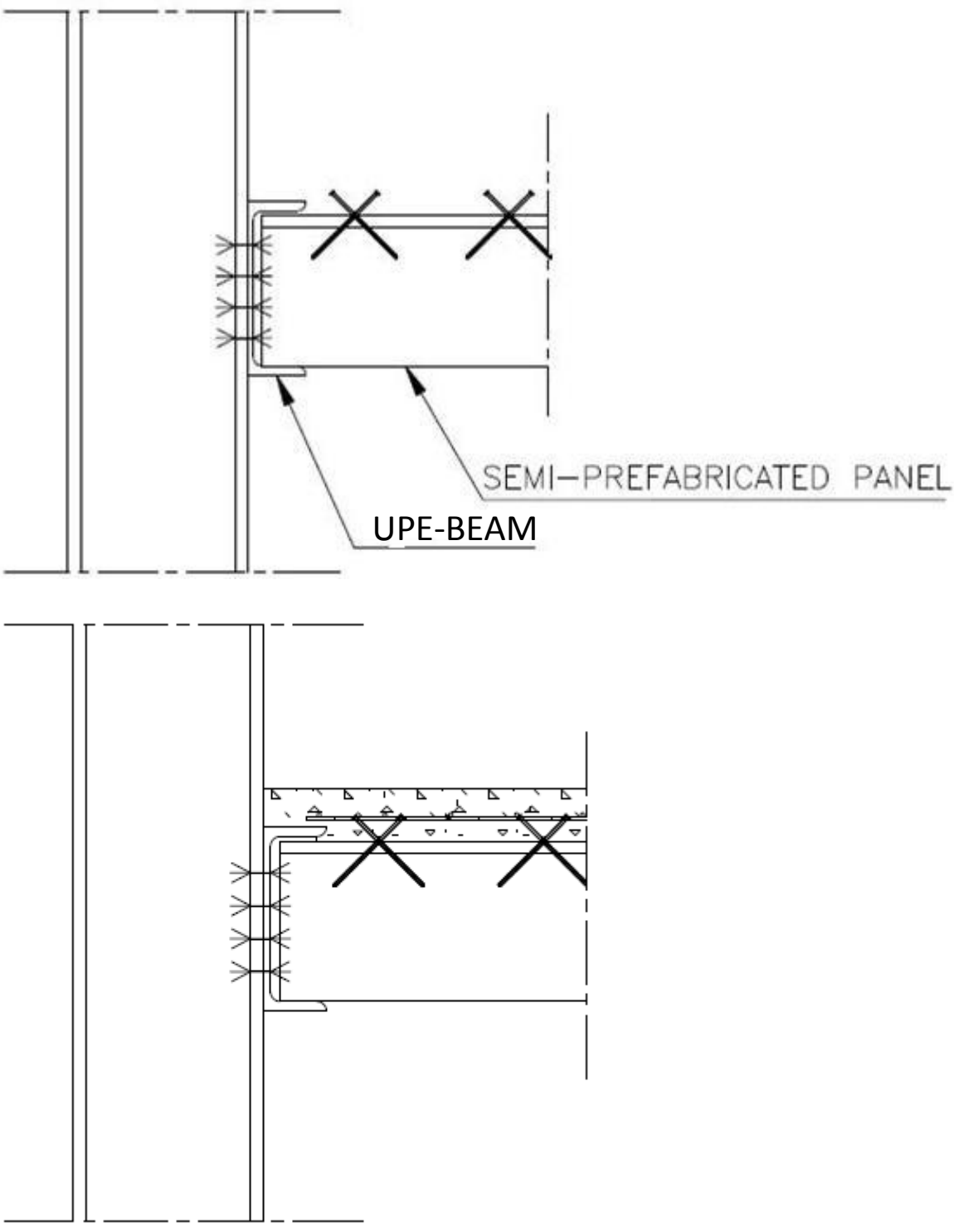

Figure 5.4 connection to a steel column using a UPE-beam.

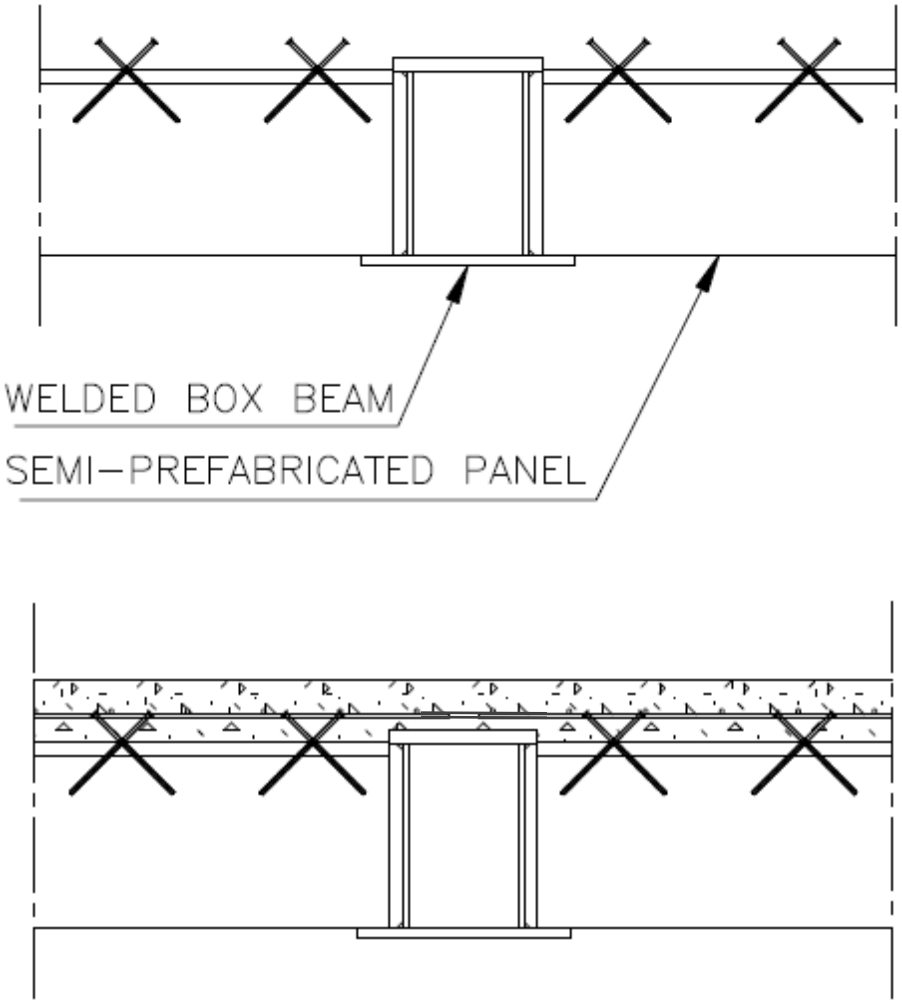

Figure 5.5 Continuous support for panels using a welded box-beam
Top: Before casting of the concrete. Bottom: After casting of the concrete.

Connection to a glulam beam:
The panels could be connected to a glulam beam as is illustrated in figure 5.6. The steel fastening devises should then be applied to the panels before step 1 in the installation process. When the panels have been placed in the right position, they are screwed to the glulam beams.

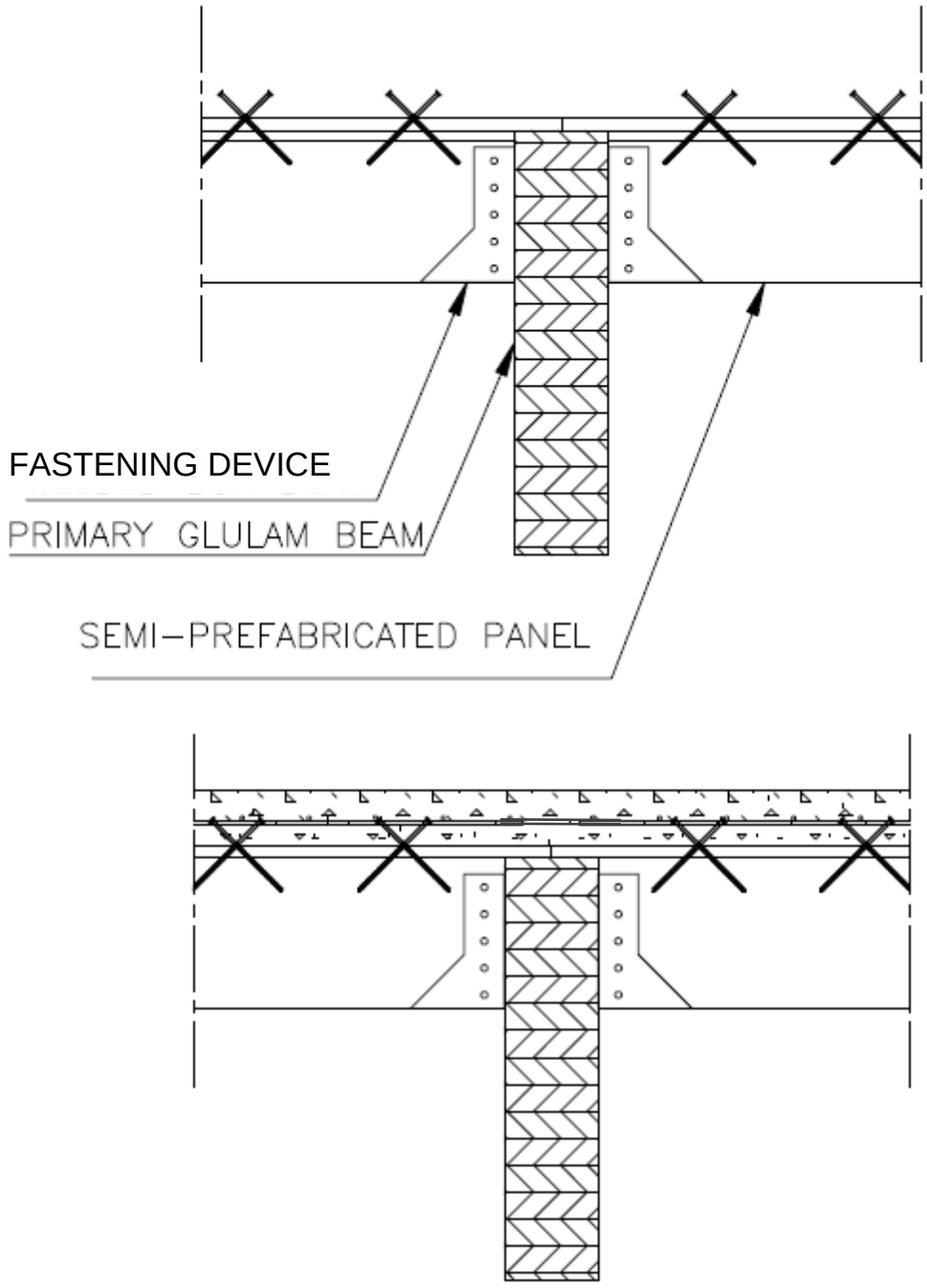

Figure 5.6 Connection to a glulam beam.
Top: Before casting of the concrete. Bottom: After casting of the concrete.

5.5 Design examples

As stated earlier, the design of a timber-concrete composite floor is a repetitive procedure in which a floor is first assumed and then analyzed. To do this by hand would be require a significant amount of work. Thus, in the examples below, floors that fulfill the requirements have already been found using a Matlab program. Instead, the examples constitute double-checks carried out by hand in accordance with the European code; EN 1990:2002 (Basis of structural design), EN 1991-1-1:2001 (Actions on structures – Part 1-1), EN 1992-1-1 (Design of concrete structures), EN1995-1-1 (Design of timber structures, Part 1-1). The method of analysis chosen for the examples is Girhammar's simplified approach. Dead weight is considered in both examples.

Where the European code allows for it, the Swedish "Boverkets konstruktionsregler 2003" has been used to obtain loads.

5.5.1 Case 1: Floor in office building

An office building is to be constructed and the contractor wishes for the 9 m long floor slabs to be of a timber-concrete composite type.

General assumptions

General effects are considered through an evenly imposed characteristic load of *3,0 kN/m*^{2}. Local effects are considered through a concentrated load of *4,5kN*. General and local effects are not investigated simultaneously (EN 1991-1-1, *(*Actions on structures)).

The life span of the building is assumed to be 50 years and the average relative humidity inside is taken as 40%. The floor that is assumed for the analysis is presented below (i.e. pre-chosen by a computer program):

Concrete:
C40/50

Glulam beams:
L40 (GL32)

SFS-screws:
c/c 225 mm

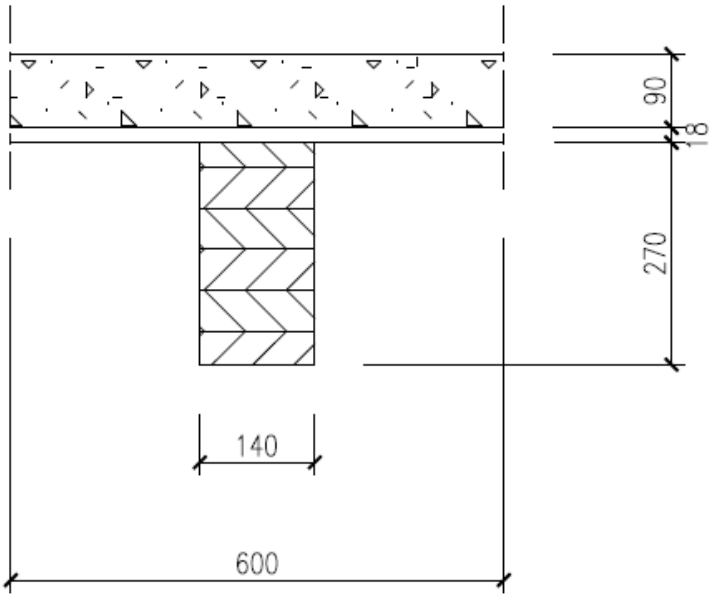

Design of the composite floor

Estimation of long term moduli:

As accounted for in section 2.2.2, the design includes short term- as well as long term verifications. Long term moduli must therefore be estimated according to equations 2.4-2.6 (Refer also to appendix C for how to determine the creep coefficients).

Concrete

$\varphi(t,t_0) = \varphi_0 * \beta_c(t,t_0)$ (creep factor)

⇨

$h_0 = \frac{2*600*90}{600} = 180$

$a_1 = \left[\frac{35}{48}\right]^{0,7} = 0{,}802$

$a_2 = \left[\frac{35}{48}\right]^{0,2} = 0{,}939$

$a_3 = \left[\frac{35}{48}\right]^{0,5} = 0{,}854$

$\varphi_{RH} = \left[1 + \frac{1-40/100}{0{,}1*180^{1/3}} * 0{,}802\right] * 0{,}939 = 1.739$

$\beta(f_{cm}) = \frac{16{,}8}{\sqrt{48}} = 2{,}425$

$\beta(t_0) = \frac{1}{(0{,}1+28^{0,20})} = 0{,}488$

⇨ $\varphi_0 = \varphi_{RH} * \beta(f_{cm}) * \beta(t_0) = 1.739 * 2{,}425 * 0{,}488 = 2{,}059$

$\beta_H = 1{,}5(1 + (0{,}012 * 40)^{18}) * 90 + 250 * 0{,}854 = 483{,}48 \leq 1500 * 0{,}854$

$=> \beta_H = 483{,}48$

⇨ $\beta_c(t - t_o) = \left[\frac{50*365-28}{483{,}48 +50*365-28}\right]^{0,3} = 0{,}992$

⇨ $\varphi(t,t_0) = 2{,}059 * 0{,}994 = 2{,}043$

⇨ $\boxed{E_{c,fin} = \frac{35\ GPa}{1+2{,}043} = 11{,}50\ GPa}$

Glulam beams & shear connectors:

The deformation factor k_{def} is found in table 3.2 of EN1995-1-1 (Design of timber structures). The deformation factor of the timber is thus taken as:

k_{def} = 0,60

⇨ $\boxed{E_{glulam,fin} = \frac{14{,}47\ GPa}{1+0{,}60} = 9{,}04\ GPa}$

⇨ $\boxed{k_{ser,fin} = \frac{14{,}4\ MN/m}{1+0{,}60} = 9{,}0 MN/m}$

Hence, using values of k_{mod} and k_h chosen in accordance with EN1995-1-1 (Design of timber structures), the necessary input-data for the design are:

Concrete C35/40

$f_{ccd} = 40MPa/1{,}5 = 26{,}67MPa$

$E_{cm}(t) = 35\ GPa$

$E_{c,fin} = 11{,}50\ GPa$

SFS-screws

$k_u = 12{,}7MN/m$

$k_{ser} = 14{,}4MN/m$

$k_{ser,fin} = \frac{9{,}0MN}{m}$

$F_{max} = 18{,}5\ kN$

Glulam beams

$f_{ttd} = 1{,}083 * 0{,}8 * 23MPa/1{,}25 = 15{,}94MPa$

$f_{tmd} = 1{,}083 * 0{,}8 * 33MPa/1{,}25 = 22{,}87MPa$

$E_{0,mean} = 14{,}47\ GPa$

$E_{glulam,fin} = 9{,}04\ GPa$

Analysis

The ultimate limit state control is performed as a control of the cross sectional normal stresses, see equations 2.1 & 2.2 in section 2.2.2. The normal stresses can be divided into two separate parts, stress resulting from bending (σ_m) and stress resulting from axial force (σ_c or σ_t) . These are obtained using equations 5.1 & 5.2:

$$\sigma_c = -\sigma_t = \frac{N}{A} = \frac{N}{b*h} \quad \text{(Eq. 5.1)}$$

$$\sigma_m = \frac{M}{w} = \frac{6*M}{b*h^2} \quad \text{(Eq. 5.2)}$$

N and M in equations 5.1 and 5.2 are obtained using equations 2.21-2.23 (see section 2.2.4). It therefore follows that equations 2.1 & 2.2 can be rewritten and expressed as in equations 5.3 & 5.4:

$$f_{ccd} \geq \frac{M}{b_1 h_1}\left(\frac{\left(1-\frac{EI_0}{EI_{eff}}\right)}{r} + \frac{6*E_1 I_1}{h_1 * EI_{eff}}\right) \quad \text{(Eq. 5.3)}$$

$$1 \geq \frac{M}{b_2 h_2}\left(\frac{\left(1-\frac{EI_0}{EI_{eff}}\right)}{r*f_{ttm}} + \frac{6*E_2 I_2}{h_2 * EI_{eff} * f_{tmm}}\right) \quad \text{(Eq. 5.4)}$$

The shear connector can be controlled using a combination of equations 2.24 and 2.26 (see section 2.2.4):

$$\left(1-\frac{EI_0}{EI_{eff}}\right) * \frac{s}{r} * V_d \leq F_{max} \quad \text{(Eq. 5.5)}$$

As opposed to the ultimate limit state, the control of the serviceability limit state is carried out by controlling the deflection. When the effective bending stiffness for the composite floor is known, the deflection can be checked using standard equations available in constructional handbooks. In this example, a maximum allowed deflection of L/250 is chosen.

The short- and long term verification is conducted according to section 2.2.2.
Since Girhammars simplified approach is the method chosen in the examples, in-data for the various limit state controls, in terms of EI_0 and EI_{eff}, are first calculated. Table 5.1 presents the results.

	EI_0 [Nm^2]	EI_{eff} [Nm^2]
$E_{cm}(t), E_{0,mean}, k_u$	$4{,}562 * 10^6$	$13{,}213 * 10^6$
$E_{cm}(t), E_{0,mean}, k_{ser}$	$4{,}562 * 10^6$	$13{,}729 * 10^6$
$E_{c,fin}, E_{t,fin}, k_{ser,fin}$	$2{,}495 * 10^6$	$7{,}665 * 10^6$

Table 5.1 In-data for the various limit state verifications in terms of EI_0 and EI_{eff}

Short term ultimate limit state analysis:

Action effects are expressed as:

$$\sigma_{inst} = \sigma^{F_{d,u}}\left(E_{cm}(t), E_{0,mean}, k_u\right)$$

With ψ- and γ-factors tabulated in Annex A1 of EN 1990:2002 (Basis of structural design), and with only one variable load acting at a time, the ultimate limit state design load combination becomes.

$$F_{d,u} = \sum_{j\geq 1} 1{,}35 * G_{k,j} + 1{,}5 * Q_{k,1}$$

The actions in terms of bending moment and shear force then becomes:

<u>For the evenly imposed load, $Q_k = 3{,}0$ kN/m^2</u>

$$M_{gen.}^{F_{d,u}} = \frac{(1{,}35*(0{,}6*0{,}09*25+0{,}14*0{,}27*5)+1{,}5*0{,}6*3{,}0)*9^2}{8} = 48{,}37\ kNm$$
$$V_{gen.}^{F_{d,u}} = \frac{(1{,}35*(0{,}6*0{,}09*25+0{,}14*0{,}27*5)+1{,}5*0{,}6*3{,}0)*9}{2} = 21{,}5\ kN$$

<u>For the concentrated load, $Q_k = 4{,}5$ kN</u>

$$M_{loc.}^{F_{d,u}} = 1.35 * \frac{(0{,}6*0{,}09*25+0{,}14*0{,}27*5)*9^2}{8} + 1{,}5 * \frac{4{,}5*9}{4} = \underline{36{,}35\ kNm}$$
$$V_{loc.}^{F_{d,u}} = 1.35 * \frac{(0{,}6*0{,}09*25+0{,}14*0{,}27*5)*9}{2} + 1{,}5 * \frac{4{,}5}{2} = \underline{10{,}65\ kN}$$

Hence, the evenly imposed load is critical. Insertion of M=48,37 kNm and V=21,5 kN in equations 5.3-5.5 gives:

$$f_{ccd} = 26{,}27 * 10^6 \geq \frac{48{,}37*10^3}{0{,}6*0{,}09}\left(\frac{\left(1-\frac{4{,}562*10^6}{13{,}213*10^6}\right)}{0{,}198} + \frac{6*35*10^9*3{,}645*10^{-5}}{0{,}09*13{,}213*10^6}\right) =$$
$$8{,}73 * 10^6 \quad OK!$$

$$1 \geq \frac{48{,}37}{0{,}14*0{,}27}\left(\frac{\left(1-\frac{4{,}562*10^6}{13{,}213*10^6}\right)}{0{,}198*15{,}94*10^6} + \frac{6*14{,}47*10^6*2{,}296*10^{-4}}{0{,}27*13{,}213*10^6*22{,}87*10^6}\right) = 0{,}578\ OK!$$

$$\left(1-\frac{4{,}562*10^6}{13{,}213*10^6}\right) * \frac{0{,}225}{0{,}198} * 21{,}5 * 10^3 = 16{,}0\ kN < F_{max} = 18{,}5\ kN\ OK!$$

Short term serviceability limit state analysis

Action effects are expressed as:

$$u_{inst} = u^{F_{d,r}}\left(E_{cm}(t), E_{0,mean}, k_{ser}\right)$$

The characteristic load combination is;

$$F_{d,r} = \sum_{j\geq 1} 1{,}0 * G_{k,j} + 1{,}0 * Q_{k,1}$$

Deflection can now be calculated using standard equations available in constructional handbooks:

<u>For the evenly imposed load, $Q_k = 3{,}0\ kN/m^2$</u>

$$\delta_{gen.}^{F_{d,r}} = \frac{5*(1{,}00*(0{,}6*0{,}09*25+0{,}14*0{,}27*5)+1{,}0*0{,}6*3{,}0)*10^3*9^4}{384*EI_{eff}} = \underline{285249{,}7/EI_{eff}}$$

<u>For the concentrated load, $Q_k = 4{,}5\ kN$</u>

$$\delta_{loc.}^{F_{d,r}} = \frac{5*(1.0*(0{,}6*0{,}09*25+0{,}14*0{,}27*5)*10^3)*9^4}{384*EI_{eff}} + \frac{(1{,}0*4{,}5*10^3)*9^3}{48*EI_{eff}} = 199820{,}0/EI_{eff}$$

Hence, the evenly imposed load is critical. Insertion of $EI_{eff} = 13{,}729 * 10^6$gives:

$$\delta = \frac{285249{,}7}{13{,}729*10^6} = 0{,}0208m < 0{,}030m\ \ OK!$$

Long term ultimate limit state analysis

Action effects are expressed as:

$$\sigma_{fin} = \sigma^{F_{d,p}}\left(E_{c,fin}, E_{t,fin}, k_{ser,fin}\right) + \sigma^{F_{d,u}-F_{d,p}}\left(E_{cm}(t), E_{0,mean}, k_u\right)$$

The load combinations for the long term ultimate limit state analysis are as follows (refer to section 2.2.2):

$$F_{d,p} = \sum_{j\geq 1} 1{,}0 * G_{k,j} + 0{,}3 * Q_{k,1}$$

$$F_{d,u} - F_{d,p} = \sum_{j\geq 1}(1{,}35 - 1{,}0) * G_{k,j} + (1{,}5 - 0{,}3) * Q_{k,1}$$

Action effects in terms of bending moment and shear force are thus:

<u>For the evenly imposed load, $Q_k = 3{,}0\ kN/m^2$</u>

$$M_{gen.}^{F_{d,p}} = \frac{(1{,}0*0{,}6*0{,}09*25+0{,}14*0{,}27*5+0{,}3*0{,}6*3{,}0)*9^2}{8} = 21{,}05\ kNm$$
$$M_{gen.}^{F_{d,u}-F_{d,p}} = \frac{(0{,}35*(0{,}6*0{,}09*25+0{,}14*0{,}27*5)+1{,}2*0{,}6*3{,}0)*9^2}{8} = 27{,}32\ kNm$$

$$V_{gen.}^{F_{d,p}} = \frac{(1{,}0*0{,}6*0{,}09*25+0{,}14*0{,}27*5+0{,}3*0{,}6*3{,}0)*9}{2} = 9{,}36\ kN$$
$$V_{gen.}^{F_{d,u}-F_{d,p}} = \frac{(0{,}35*(0{,}6*0{,}09*25+0{,}14*0{,}27*5)+1{,}2*0{,}6*3{,}0)*9}{2} = 12{,}13\ kN$$

<u>For the concentrated load, $Q_k = 4{,}5$ kN</u>

$$M_{loc.}^{F_{d,p}} = 1.0 * \frac{(0{,}6*0{,}09*25+0{,}14*0{,}27*5)*9^2}{8} + 0{,}3 * \frac{4{,}5*9}{4} = \underline{18{,}62\ kNm}$$
$$M_{loc.}^{F_{d,u}-F_{d,p}} = 0{,}35 * \frac{(0{,}6*0{,}09*25+0{,}14*0{,}27*5)*9^2}{8} + 1{,}2 * \frac{4{,}5*9}{4} = \underline{17{,}60\ kNm}$$

$$V_{loc.}^{F_{d,p}} = 1{,}0 * \frac{(0{,}6*0{,}09*25+0{,}14*0{,}27*5)*9}{2} + 0{,}3 * \frac{4{,}5}{2} = \underline{7{,}60\ kN}$$
$$V_{loc.}^{F_{d,u}-F_{d,p}} = 0{,}35 * \frac{(0{,}6*0{,}09*25+0{,}14*0{,}27*5)*9}{2} + 1{,}2 * \frac{4{,}5}{2} = \underline{5{,}12\ kN}$$

Hence, the evenly imposed load is critical. Equations 5.3-5.5 give:

$$f_{ccd} = 26{,}27 * 10^6 \geq \frac{21{,}05 * 10^3}{0{,}6*0{,}09}\left(\frac{\left(1-\frac{2{,}495*10^6}{7{,}665*10^6}\right)}{0{,}198} + \frac{6*11{,}5*10^9*3{,}645*10^{-5}}{0{,}09*7{,}665*10^6}\right) +$$
$$\frac{27{,}32 * 10^3}{0{,}6*0{,}09}\left(\frac{\left(1-\frac{4{,}562*10^6}{13{,}213*10^6}\right)}{0{,}198} + \frac{6*35*10^9*3{,}645*10^{-5}}{0{,}09*13{,}213*10^6}\right) = \ 7{,}727MPa \ \ OK!$$

$$1 \geq \frac{21{,}05*10^3}{0{,}14*0{,}27}\left(\frac{\left(1-\frac{2{,}495*10^6}{7{,}665*10^6}\right)}{0{,}198*15{,}94*10^6} + \frac{6*9{,}04*10^9*2{,}296*10^{-4}}{0{,}27*7{,}665*10^6*22{,}87*10^6}\right) +$$
$$\frac{27{,}32*10^3}{0{,}14*0{,}27}\left(\frac{\left(1-\frac{4{,}562*10^6}{13{,}213*10^6}\right)}{0{,}198*15{,}94*10^6} + \frac{6*14{,}47*10^9*2{,}296*10^{-4}}{0{,}27*13{,}213*10^6*22{,}87*10^6}\right) = 0{,}592\ OK!$$

$$F_{s,eff} = \left(1 - \frac{2{,}495*10^6}{7{,}665*10^6}\right) * \frac{0{,}225}{0{,}198} * 9{,}36 * 10^3 + \left(1 - \frac{4{,}562*10^6}{13{,}213*10^6}\right) * \frac{0{,}225}{0{,}198} *$$
$$12{,}13 * 10^3 = 16{,}205\ kN\ OK!$$

Long term serviceability limit state analysis

Action effects are expressed as:

$$u_{fin} = u^{F_{d,p}}\left(E_{c,fin}, E_{t,fin}, k_{ser,fin}\right) + u^{F_{d,r}-F_{d,p}}\left(E_{cm}(t), E_{0,mean}, k_{ser}\right)$$

The load combinations for the long term serviceability limit state analysis are as follows (refer to section 2.2.2):

$$F_{d,p} = \sum_{j\geq 1} 1{,}0 * G_{k,j} + 0{,}3 * Q_{k,1}$$

$$F_{d,r} - F_{d,p} = (1{,}0 - 0{,}3) * Q_{k,1}$$

Deflection:

<u>For the evenly imposed load, $Q_k = 3{,}0$ kN/m^2</u>

$$\delta_{gen.}^{F_{d,p}} = \frac{5*(1{,}00*(0{,}6*0{,}09*25+0{,}14*0{,}27*5)+0{,}3*0{,}6*3{,}0)*9^4}{384*EI_{eff}} = 177608{,}32/EI_{eff}$$
$$\delta_{gen.}^{F_{d,r}-F_{d,p}} = \frac{5*(0{,}7*0{,}6*3{,}0)*9^4}{384*EI_{eff}} = 107641{,}41/EI_{eff}$$

For the concentrated load, $Q_k = 4{,}5$ kN

$$\delta_{loc.}^{F_{d,p}} = \frac{5*(1{,}00*(0{,}6*0{,}09*25+0{,}14*0{,}27*5)*9^4}{384*EI_{eff}} + \frac{(0{,}3*4{,}5)*9^3}{48*EI_{eff}} = 131496/EI_{eff}$$

$$\delta_{loc.}^{F_{d,r}-F_{d,p}} = \frac{(0{,}7*4{,}5*10^3)*9^3}{48*EI_{eff}} = 47840/EI_{eff}$$

It is unclear if it is the evenly distrusted load or the concentrated load that will cause the critical deflection. Both cases are investigated.

$$\delta = \frac{177608{,}32}{7{,}665*10^6} + \frac{107641{,}41}{13{,}213*10^6} = 0{,}030$$

$$\delta = \frac{131496}{7{,}665*10^6} + \frac{47840}{13{,}213*10^6} = 0{,}0208$$

Both deflections are within the limit of L/300=0,030 OK!

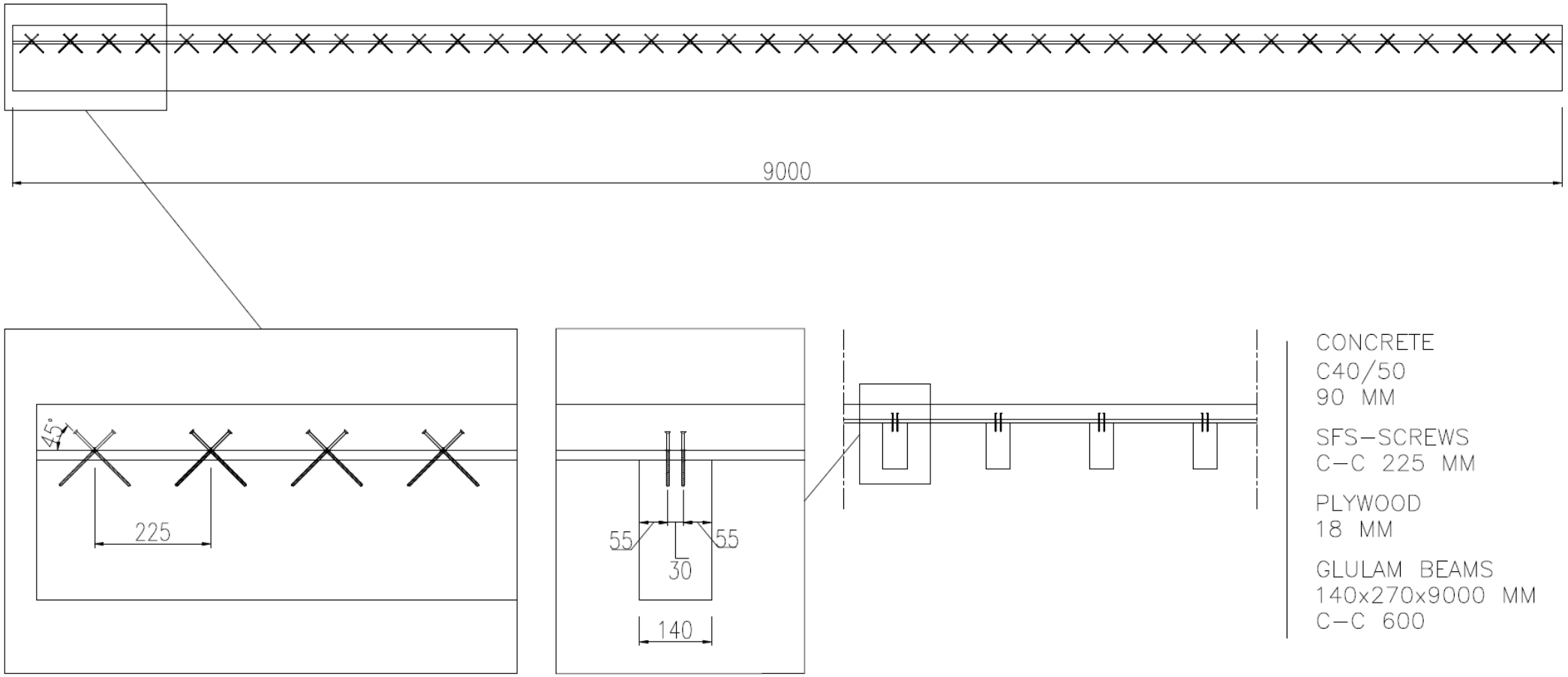
9000
45°
225
55
55
30
140
CONCRETE
C40/50
90 MM
SFS–SCREWS
C–C 225 MM
PLYWOOD
18 MM
GLULAM BEAMS
140x270x9000 MM
C–C 600

5.5.2 Case 2: Floor in multistory car park

A multistory car park with 7 meter floor spans is to be constructed and the contractor wants the slabs to be of a timber-concrete composite type.

General assumptions

The Swedish code BKR 03 specifies the following actions that are in compliance with the intervals provided by the European code:

General effects due to traffic loads in car parks are considered through an evenly distributed characteristic load of *2,0 kN/m*^{2}. Local effects are considered through a concentrated load of *10 kN*, acting on an area of 100*100 mm. General and local effects are not investigated simultaneously.

It is assumed that the service life of the car park is 50 years and that the yearly average relative humidity outdoors is 80 %. The floor that is assumed for the analysis is presented below (i.e. pre-chosen by a computer program):

Concrete:
C40/50

Glulam beams:
L40 (GL32)

SFS-screws:
c/c 225 mm

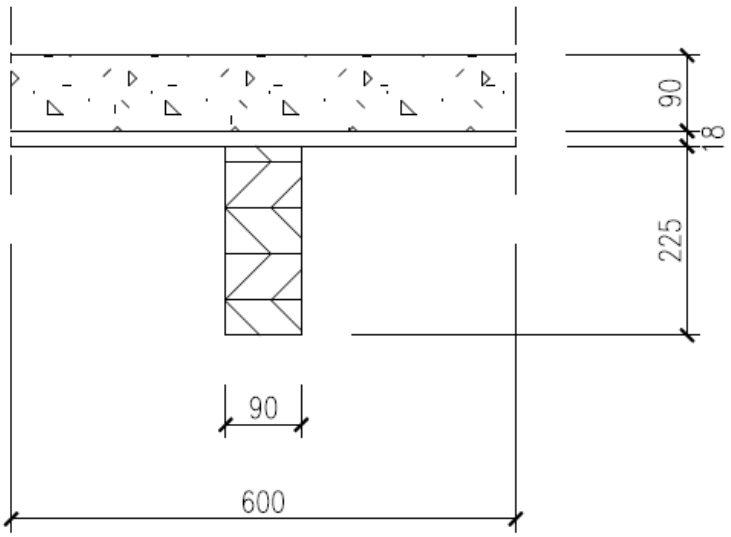

Design of concrete slab

Due to the amplitude of the concentrated load and the aggressive alkali environment in car parks, the concrete slab needs to be checked as an individual component before designing the composite floor as a whole. The following controls are carried out; bending, punching and crack-width.

Choice of reinforcement and slab thickness

Since shrinking of the concrete slab induces tensions that reduce the overall bending capacity of the composite floor, shrinking needs to be reduced as much as possible. The aggressive environment also calls for crack-reduction. Thus, a dense reinforcement web of Φ6 100*100 mm is chosen. For construction simplicity, the web is placed so that the bars going in the main direction are located at the slab-centre. EN 1992-1-1 (Design of concrete structures) specifies the minimum cover c_{nom}, (provided that the casting is carefully monitored) for the slab in question to 35 mm. The smallest slab thickness possible is therefore 2*(35+6/2+6)=88 mm. Hence, *h=90 mm* is chosen, => d=45 mm.

Bending:

Only the short term ultimate limit state is considered. EN 1990 (Basis of structural design*)* gives:

<u>General effects ($Q_k = 2{,}0\ kN/m^2$)</u>

$$E_d = 1{,}35 * 0{,}09 * 25\frac{kN}{m^3} + 1{,}5 * 2{,}0\frac{kN}{m^2} = 3{,}04\frac{kN}{m^2} + 3\frac{kN}{m^2}$$

Maximum span-bending moment:

$$M_d = M_4 = 0{,}0772 * \frac{3{,}04kN}{m} * 0{,}6^2m + 0{,}0996 * \frac{3{,}00kN}{m} * 0{,}6^2m = = 0{,}192\ kNm$$

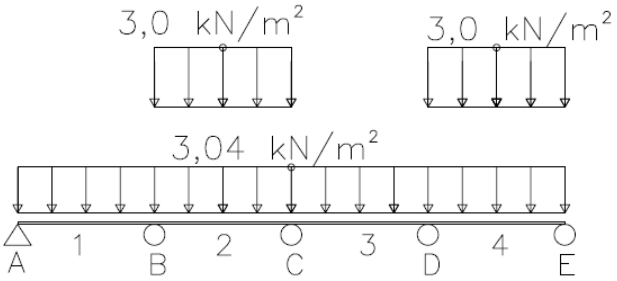

Maximum support-bending moment:

$$M_d = M_B = -0{,}1071 * \frac{3{,}04kN}{m} * 0{,}6^2m - 0{,}1205 * \frac{3{,}0kN}{m} * 0{,}6^2m = = -0{,}25\ kNm$$

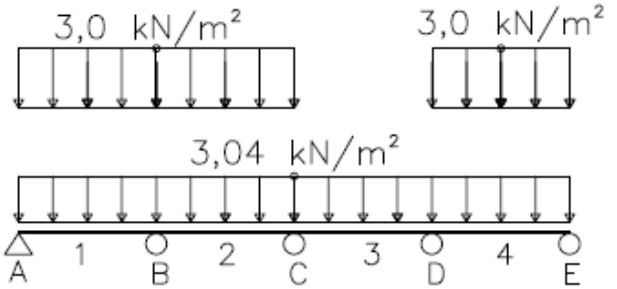

Local effects (Q_k = 10,0 kN)

Due to the limited area of 100*100 mm upon which the concentrated load acts, an equivalent resulting bending moment per meter strip has to be calculated. This may be done using an influence surface diagram:

$n = 4 =>$

$\Delta Q = 1{,}5 * \frac{10{,}0}{4} kN = 3{,}75\ kN$

$Contour = 5{,}5$

$K = \frac{Contour}{8\pi} = 0{,}219$

$=> M = n * \Delta Q * K =$
$= 4 * 3{,}75kN * 0{,}219$
$= 3{,}285\ kNm$

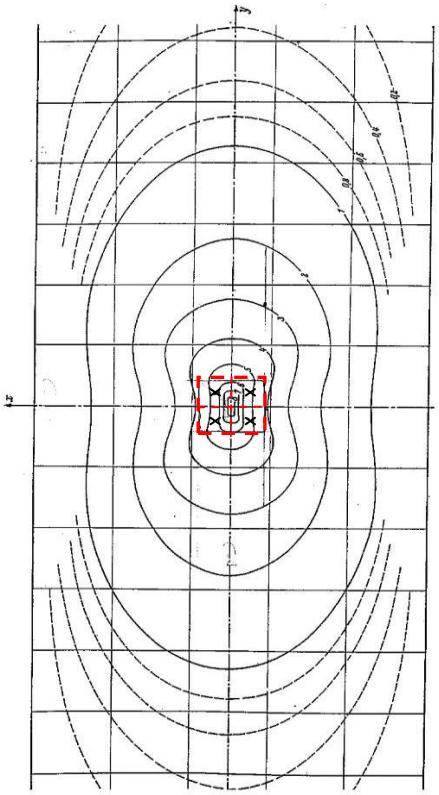

The influence diagram applies for a single simply supported plate strip. The equivalent load for use on a continuous strip is calculated.

$M = \frac{P*L}{4} =>$

$P = \frac{4*M}{L} = \frac{4*3{,}285\ kNm}{0{,}6m} = 21{,}90\ kN/m$

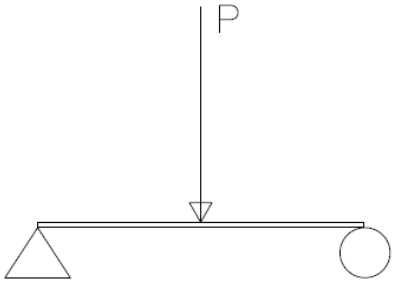

Maximum span-bending moment:

$$M_d = M_1 = 0{,}0772 * 3{,}04\frac{kN}{m} * 0{,}6^2 + 0{,}2098 * 21{,}90kN * 0{,}6m = = 2{,}84\ kNm$$

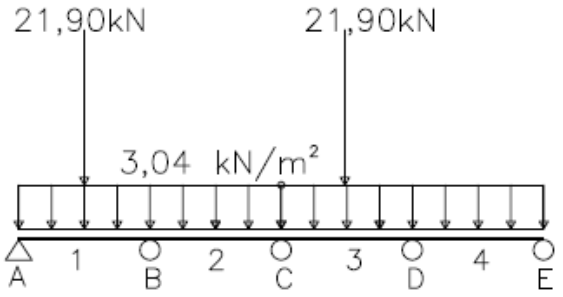

Maximum support-bending moment:

$$M_d = M_B = -0{,}1071 * \frac{3{,}04kN}{m} * 0{,}6^2m - 0{,}1808 * 21{,}90kN * 0{,}6m = -2{,}49\ kNm$$

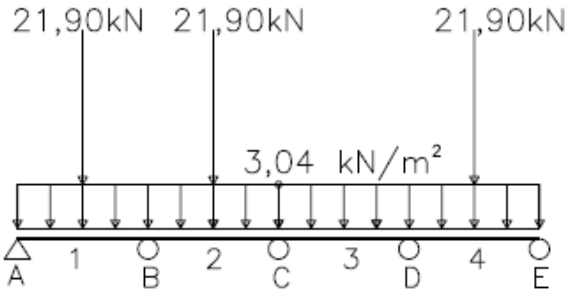

Local effects give the largest bending moments:

$M_{d,field} = 2{,}84\ kNm$
$M_{d,support} = -2{,}49\ kNm$

Since the reinforcement is placed in the slab centre, positive and negative bending moment capacities are the same and only one control is needed. The design is conducted according to EN 1992-1-1 (Design of concrete structures)*:*

$A_s = 10 * \pi * 0{,}3^2 = 2{,}83\ cm^2/m$

$f_{yd} = \frac{f_{yk}}{\gamma_s} = \frac{500}{1{,}15} = 434{,}78\ MPa$
$f_{cd} = \frac{\alpha_{cc} f_{ck}}{\gamma_c} = \frac{1{,}0*35}{1{,}5} = 23{,}33\ MPa$

$\sigma_s = f_{yd}$ is assumed

$F_s = A_s * f_{yd} = 2{,}83 * 10^{-4} * 434{,}78 * 10^6 = 123{,}04\ kN$
$F_c = \lambda * x * b * \eta * f_{cd}$
$F_c = F_s$

$\Rightarrow x = \frac{123{,}04*10^3}{0{,}8*1{,}0*1{,}0*23{,}33*10^6} = 0{,}0066\ m$

$M_{Rd} = 123{,}04 * 10^3(0{,}045 - 0{,}5 * 0{,}8 * 0{,}0066) = 5{,}21\ kNm$

5,21 kNm > 2,44 kNm >2,135kNm=> OK

Control of the assumption that the reinforcement has yielded:

$$\varepsilon_{s,1} = \varepsilon_{c,2}\left(\frac{d}{x} - 1\right) = 0{,}0035\left(\frac{0{,}045}{0{,}0066} - 1\right) = 0{,}020$$

$$\varepsilon_{sy} < \varepsilon_{s,1} = 0{,}20 < \varepsilon_{ud} = 0{,}9 * \varepsilon_{uk} = 0{,}9 * 0{,}025 = 0{,}0225 => OK$$

Punching:

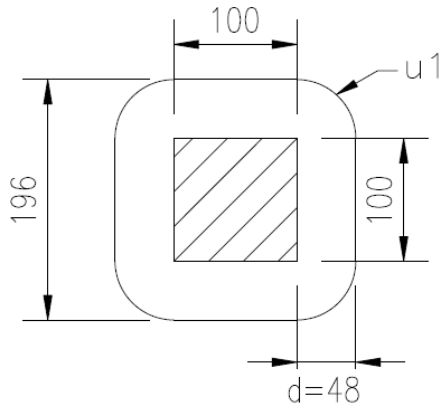

$$V_E \leq V_u$$

$$V_u = \eta * u_1 * d * f_{v,1}$$

$$f_{v,1} = 0{,}45 * \xi * (1 + 50 * \rho) * f_{ct}$$

$$d = 0{,}5\left(d_x + d_y\right) = 0{,}5 * (0{,}045 + 0{,}051) = 0{,}048m$$

$$u_1 = 4 * 0{,}1 + 2 * \pi * 0{,}043 = 0{,}701\ m$$

$$\rho = \sqrt{\rho_x \rho_y} = \rho_x = \frac{A_{sx}}{A_{cx}} = \frac{2 * \pi * 0{,}03^2}{0{,}048 * 0{,}701 - 2 * \pi * 0{,}03^2} = 0{,}20$$

$$0{,}20 > 0{,}01 => \rho = 0{,}01$$

$$f_{v,1} = 0{,}45 * 1{,}4 * (1{,}0 + 50 * 0{,}01) * 1{,}8 * 10^6 = 1{,}701\ MPa$$

⇨ $V_u = 1{,}0 * 0{,}701m * 0{,}048m * 1{,}701\ MPa$ *=57,24 kN >15 kN => OK!*

Crack-width:

The control is carried out in accordance with EN 1992-1-1 (Design of concrete structures).

$$\left.\begin{aligned} w_k &= s_{r,max}(\varepsilon_{sm}-\varepsilon_{cm}) \\ s_{r,max} &= 3{,}4*c+\frac{0{,}425*k_1*k_2*\phi}{\rho_{p,eff}} \\ \varepsilon_{sm}-\varepsilon_{cm} &= \max\left(\frac{\sigma_s-k_t\frac{f_{ct,eff}}{\rho_{p,eff}}(1+\alpha_e*\rho_{p,eff})}{E_s};0{,}6\frac{\sigma_s}{E_s}\right) \end{aligned}\right\} =>$$

$$\sigma_s=\frac{F_s}{A_s}=\frac{M/(d-0{,}4x)}{A_s}=\frac{2{,}84*10^3/(0{,}045-0{,}4*0{,}0066)}{10*\pi*0{,}003^2}=237{,}12\ MPa$$

$$\alpha_e=\frac{E_s}{E_{cm}}=\frac{200*10^9}{34*10^9}=5{,}88$$

$$A_{c,eff}=1m*h_{c,ef}=1m*\left(\min\left(2{,}5(h-d);\frac{h-x}{3};\frac{h}{2}\right)-A_s\right)=$$

$$=1m*(0{,}0278-10*\pi*0{,}003^2)=0{,}0275m^2$$

$$\rho_{p,eff}=\frac{A_s}{A_{c,eff}}=\frac{10*\pi*0{,}003^2}{0{,}0275}=0{,}0103$$

$$k_t=0{,}4\ (Long\ term\ loading)$$

$$\varepsilon_{sm}-\varepsilon_{cm}=\frac{237{,}12*10^6-0{,}4*\frac{3{,}2*10^6}{0{,}0103}*(1+5{,}88*0{,}0103)}{200*10^9}=5{,}27*10^{-4}$$

$$5{,}27*10^{-4}<0{,}6\frac{237{,}12*10^6}{200*10^9}=7{,}11*10^{-4} => \varepsilon_{sm}-\varepsilon_{cm}=7{,}11*10^{-4}$$

$$s_{r,max}=3{,}4*0{,}042+\frac{0{,}425*0{,}8*0{,}5*0{,}006}{0{,}0103}=0{,}242$$

$$w_k=0{,}242*7{,}11*10^{-4}=1{,}72*10^{-4}m\approx 0{,}17\ mm => OK$$

The concrete slab performs satisfactorily.

Design of the composite floor

Except for the additional control of the concrete slab as such, the design of the deck in the car park is principally the same as the design of the office floor, refer to section 5.5.1. However, here the limit of acceptable deflection is set to L/250.

Estimation of long term moduli:

Concrete

$$\varphi(t,t_0) = \varphi_0 * \beta_c(t,t_0)$$

⇨

$$h_0 = \frac{2*600*90}{2*600} = 90$$

$$\varphi_{RH} = 1 + \frac{1-80/100}{0{,}1*90^{1/3}} = 1{,}446$$

$$\beta(f_{cm}) = \frac{16{,}8}{\sqrt{43}} = 2{,}562$$

$$\beta(t_0) = \frac{1}{(0{,}1+28^{0{,}20})} = 0{,}488$$

⇨ $\varphi_0 = \varphi_{RH} * \beta(f_{cm}) * \beta(t_0) = 1{,}44 * 2{,}560 * 0{,}488 = 1{,}81$

$$\beta_H = 1{,}5(1 + (0{,}012 * 80)^{18}) * 90 + 250 = 449{,}7 \leq 1500 => \beta_H = 449{,}7$$

⇨ $\beta_c(t-t_o) = \left[\frac{50*365-28}{449{,}7+50*365-28}\right]^{0{,}3} = 0{,}993$

⇨ $\varphi(t,t_0) = 1{,}81 * 0{,}993 = 1{,}797$

⇨ $\boxed{E_{c,fin} = \frac{34\ GPa}{1+1{,}797} = 12{,}16\ GPa}$

Glulam beams & shear connectors:
The deformation factor k_{def} is found in table 3.2 of EN 1995-1-1 (Design of timber structures). The deformation factor of the timber is thus taken as:

k_{def} = 0,80

⇨ $\boxed{E_{glulam,fin} = \frac{14{,}47\ GPa}{1+0{,}80} = 8{,}04\ GPa}$

⇨ $\boxed{k_{ser,fin} = \frac{14{,}4\ MN/m}{1+0{,}8} = 8{,}0 MN/m}$

With k_{mod} and k_h chosen in accordance with EN 1995-1-1 (Design of timber structures), the necessary in-data for the design procedure are:

Concrete C35/40
$f_{ccd} = 35MPa/1{,}5 = 23{,}33MPa$
$E_{cm}(t) = 34\ GPa$
$E_{c,fin} = 12{,}16\ GPa$

SFS-screws
$k_u = 12{,}7MN/m$
$k_{ser} = 14{,}4MN/m$
$k_{ser,fin} = 8{,}0MN/m$

Glulam beams
$f_{ttd} = 1{,}1 * 0{,}8 * 23MPa/1{,}25 = 16{,}19MPa$
$f_{tmd} = 1{,}1 * 0{,}8 * 33MPa/1{,}25 = 23{,}23MPa$
$E_{0,mean} = 14{,}47\ GPa$
$E_{glulam,fin} = 8{,}04\ GPa$

Analysis

In-data in terms of EI_0 and EI_{eff}, for the various limit state controls are first calculated using Girhammars simplified approach (Refer to section 2.2.4). Table 5.2 presents the result for the slab in question.

	EI_0 [Nm^2]	EI_{eff} [Nm^2]
$E_{cm}(t), E_{0,mean}, k_u$	$2{,}476 * 10^6$	$6{,}796 * 10^6$
$E_{cm}(t), E_{0,mean}, k_{ser}$	$2{,}476 * 10^6$	$7{,}035 * 10^6$
$E_{c,fin}, E_{t,fin}, k_{ser,fin}$	$1{,}130 * 10^6$	$3{,}555 * 10^6$

Table 5.2 In-data in terms of EI_0 and EI_{eff} for the various limit state verifications

Short term ultimate limit state analysis

Action effects are expressed as:

$$\sigma_{inst} = \sigma^{F_{d,u}}\left(E_{cm}(t), E_{0,mean}, k_u\right)$$

With ψ- and γ-factors tabulated in Annex A1 of EN 1990 (Basis of structural design2), and with only one variable load acting at a time, the ultimate limit state design load combination is written as:

$$F_{d,u} = \sum_{j\geq 1} 1{,}35 * G_{k,j} + 1{,}5 * Q_{k,1}$$

Action effects in terms of bending moment and shear force then become:

<u>For the evenly imposed load, $Q_k = 2{,}0$ kN/m^2</u>

$$M_{gen.}^{F_{d,u}} = \frac{(1{,}35*0{,}6*0{,}9*25+1{,}5*0{,}6*2{,}0)*7^2}{8} = 22{,}19\ kNm$$
$$V_{gen.}^{F_{d,u}} = \frac{(1{,}35*0{,}6*0{,}9*25+1{,}5*0{,}6*2{,}0)*7}{2} = 12{,}68\ kN$$

<u>For the concentrated load, $Q_k = 10{,}0$ kN</u>

$$M_{loc.}^{F_{d,u}} = 1.35 * \frac{0{,}6*0{,}09*25*7^2}{8} + 1{,}5 * \frac{10{,}0*7}{4} = \underline{37{,}41\ kNm}$$
$$V_{loc.}^{F_{d,u}} = 1.35 * \frac{0{,}6*0{,}09*25*7}{2} + 1{,}5 * \frac{10{,}0}{2} = \underline{13{,}88\ kN}$$

The concentrated load is critical. Insertion of M=37,41 kNm and V=13,88 kN in equations 5.3-5.5 gives:

$$f_{ccd} = 26{,}27 * 10^6 \geq \frac{37{,}41*10^3}{0{,}6*0{,}09}\left(\frac{\left(1-\frac{2{,}476*10^6}{6{,}796*10^6}\right)}{0{,}1755} + \frac{6*34*10^9*3{,}645*10^{-5}}{0{,}09*6{,}796*10^6}\right) =$$
$$10{,}93 * 10^6 \quad OK!$$

$$1 \geq \frac{37{,}41*10^3}{0{,}09*0{,}225}\left(\frac{\left(1-\frac{2{,}476*10^6}{6{,}796*10^6}\right)}{0{,}1755*16{,}19*10^6} + \frac{6*14{,}47*10^9*8{,}543*10^{-5}}{0{,}225*6{,}796*10^6*23{,}23*10^6}\right) = 0{,}799 \quad OK!$$

$$\left(1-\frac{2{,}476*10^6}{6{,}796*10^6}\right) * \frac{0{,}2}{0{,}1755} * 13{,}88 * 10^3 = 10{,}054\ kN \leq F_{max} = 18{,}5\ kN \quad OK!$$

Short term serviceability limit state analysis

Action effects are expressed as:

$$u_{inst} = u^{F_{d,r}}\left(E_{cm}(t), E_{0,mean}, k_{ser}\right)$$

The characteristic load combination is written as:

$$F_{d,r} = \sum_{j\geq 1} 1{,}0 * G_{k,j} + 1{,}0 * Q_{k,1}$$

Deflection:

<u>For the evenly imposed load, $Q_k = 2{,}0\ kN/m^2$</u>

$$\delta_{gen.}^{F_{d,r}} = \frac{5*(*1.0*0{,}6*0{,}09*25*10^3+1{,}0*0{,}6*2{,}0*10^3)*7^4}{384*EI_{eff}} = \underline{79720{,}7/EI_{eff}}$$

<u>For the concentrated load, $Q_k = 10{,}0\ kN$</u>

$$\delta_{loc.}^{F_{d,r}} = \frac{5*(1.0*0{,}6*0{,}09*25*10^3)*7^4}{384*EI_{eff}} + \frac{(1{,}0*10*10^3)*7^3}{48*EI_{eff}} = 42276{,}53/EI_{eff}$$

The evenly imposed load is critical. Insertion of $EI_{eff} = 7{,}035 * 10^6$ gives:

$$\delta = \frac{79720{,}7}{7{,}035*10^6} = 0{,}011m < \frac{7}{250} = 0{,}028m\ \ OK!$$

Long term ultimate limit state analysis

Action effects are expressed as:

$$S_{fin} = S^{F_{d,p}}\left(E_{c,fin}, E_{t,fin}, k_{ser,fin}\right) + S^{F_{d,u}-F_{d,p}}\left(E_{cm}(t), E_{0,mean}, k_u\right)$$

The load combinations for the long term ultimate limit state analysis are as follows (refer to section 2.2.2):

$$F_{d,p} = \sum_{j\geq 1} 1{,}0 * G_{k,j} + 0{,}6 * Q_{k,1}$$

$$F_{d,u} - F_{d,p} = \sum_{j\geq 1}(1{,}35 - 1{,}0) * G_{k,j} + (1{,}5 - 0{,}6) * Q_{k,1}$$

Action effects in terms of bending moment and shear force are thus:

For the evenly imposed load, $Q_k = 2{,}0\ kN/m^2$

$$M_{gen.}^{F_{d,p}} = \frac{(1{,}0*0{,}6*0{,}09*25+0{,}6*0{,}6*2{,}0)*7^2}{8} = 12{,}68\ kNm$$
$$M_{gen.}^{F_{d,u}-F_{d,p}} = \frac{(0{,}35*0{,}6*0{,}09*25+0{,}9*0{,}6*2{,}0)*7^2}{8} = 9{,}51\ kNm$$

$$V_{gen.}^{F_{d,p}} = \frac{(1{,}0*0{,}6*0{,}09*25+0{,}6*0{,}6*2{,}0)*7}{2} = 7{,}25\ kN$$
$$V_{gen.}^{F_{d,u}-F_{d,p}} = \frac{(0{,}35*0{,}6*0{,}09*25+0{,}9*0{,}6*2{,}0)*7}{2} = 5{,}43\ kN$$

For the concentrated load, $Q_k = 10{,}0\ kN$

$$M_{loc.}^{F_{d,p}} = 1.0 * \frac{0{,}6*0{,}09*25*7^2}{8} + 0{,}6 * \frac{10{,}0*7}{4} = \underline{18{,}77\ kNm}$$
$$M_{loc.}^{F_{d,u}-F_{d,p}} = 0{,}35 * \frac{0{,}6*0{,}09*25*7^2}{8} + 0{,}9 * \frac{10{,}0*7}{4} = \underline{18{,}64\ kNm}$$

$$V_{loc.}^{F_{d,p}} = 1{,}0 * \frac{0{,}6*0{,}09*25*7}{2} + 0{,}6 * \frac{10{,}0}{2} = \underline{7{,}73\ kN}$$
$$V_{loc.}^{F_{d,u}-F_{d,p}} = 0{,}35 * \frac{0{,}6*0{,}09*25*7}{2} + 0{,}9 * \frac{10{,}0}{2} = \underline{6{,}15\ kN}$$

The concentrated load is critical. Insertion of values gives:

$$f_{ccd} = 26{,}27 * 10^6 \geq \frac{18{,}77*10^3}{0{,}6*0{,}09}\left(\frac{\left(1-\frac{1{,}130*10^6}{3{,}555*10^6}\right)}{0{,}1755} + \frac{6*12{,}16*10^9*3{,}645*10^{-5}}{0{,}09*3{,}555*10^6}\right) +$$
$$\frac{18{,}64*10^3}{0{,}6*0{,}09}\left(\frac{\left(1-\frac{2{,}476*10^6}{6{,}796*10^6}\right)}{0{,}1755} + \frac{6*34*10^9*3{,}645*10^{-5}}{0{,}09*6{,}796*10^6}\right) = 9{,}687 * 10^6 \quad OK!$$

$$1 \geq \frac{18{,}77*10^3}{0{,}09*0{,}225}\left(\frac{\left(1-\frac{1{,}130*10^6}{3{,}555*10^6}\right)}{0{,}1755*16{,}19*10^6} + \frac{6*8{,}04*10^9 8{,}543*10^{-5}}{0{,}225*3{,}555*10^6*23{,}23*10^6}\right) +$$
$$+\frac{18{,}64*10^3}{0{,}09*0{,}225}\left(\frac{\left(1-\frac{2{,}476*10^6}{6{,}796*10^6}\right)}{0{,}1755*16{,}19*10^6} + \frac{6*14{,}47*10^9 8{,}543*10^{-5}}{0{,}225*6{,}796*10^6*23{,}23*10^6}\right) = 0{,}83 < 1 \quad OK!$$

$$\left(1-\frac{1{,}130*10^6}{3{,}555*10^6}\right)*\frac{0{,}2}{0{,}1755}*7{,}73*10^3 + \left(1-\frac{2{,}476*10^6}{6{,}796*10^6}\right)*\frac{0{,}2}{0{,}1755}*6{,}15*10^3 =$$
$$= 10{,}46*10^3 \leq F_{max} = 18{,}5*10^3\ OK!$$

Long term *serviceability limit state analysis*

Action effects are expressed as:

$$u_{fin} = u^{F_{d,p}}\left(E_{c,fin}, E_{t,fin}, k_{ser,fin}\right) + u^{F_{d,r}-F_{d,p}}\left(E_{cm}(t), E_{0,mean}, k_{ser}\right)$$

The load combination for the long term ultimate limit state analysis is as follows (refer to section 2.2.2):

$$F_{d,r} - F_{d,p} = (1{,}0 - 0{,}6) * Q_{k,1}$$

$$F_{d,p} = \sum_{j\geq 1} 1{,}0 * G_{k,j} + 0{,}6 * Q_{k,1}$$

The deflection can thus be calculated:

<u>For the evenly imposed load, $Q_k = 2{,}0$ kN/m^2</u>

$$\delta_{gen.}^{F_{d,p}} = \frac{5*(1.0*0{,}6*0{,}09*25*10^3+0{,}6*0{,}6*2{,}0*10^3)*7^4}{384*EI_{eff}} = 64714{,}45/EI_{eff}$$
$$\delta_{gen.}^{F_{d,r}-F_{d,p}} = \frac{5*(0{,}4*0{,}6*2{,}0*10^3)*7^4}{384*EI_{eff}} = 15006{,}25/EI_{eff}$$

<u>For the concentrated load, $Q_k = 10{,}0$ kN</u>

$$\delta_{loc.}^{F_{d,p}} = \frac{5*(1.0*0{,}6*0{,}09*25*10^3)*7^4}{384*EI_{eff}} + \frac{(0{,}6*10)*7^3}{48*EI_{eff}} = 42247{,}95/EI_{eff}$$
$$\delta_{loc.}^{F_{d,r}-F_{d,p}} = \frac{(0{,}4*10*10^3)*7^3}{48*EI_{eff}} = 28583{,}33/EI_{eff}$$

It is unclear if it is the evenly distrusted load or the concentrated load that will cause the critical deflection. Both cases are therefore investigated.

$$\delta = \frac{64714{,}45}{3{,}555*10^6} + \frac{15006{,}25}{7{,}035*10^6} = 0{,}020$$

$$\delta = \frac{42247{,}95}{3{,}555*10^6} + \frac{28583{,}33}{7{,}035*10^6} = 0{,}016$$

Both deflections are within the limit of L/250=0,028 OK!

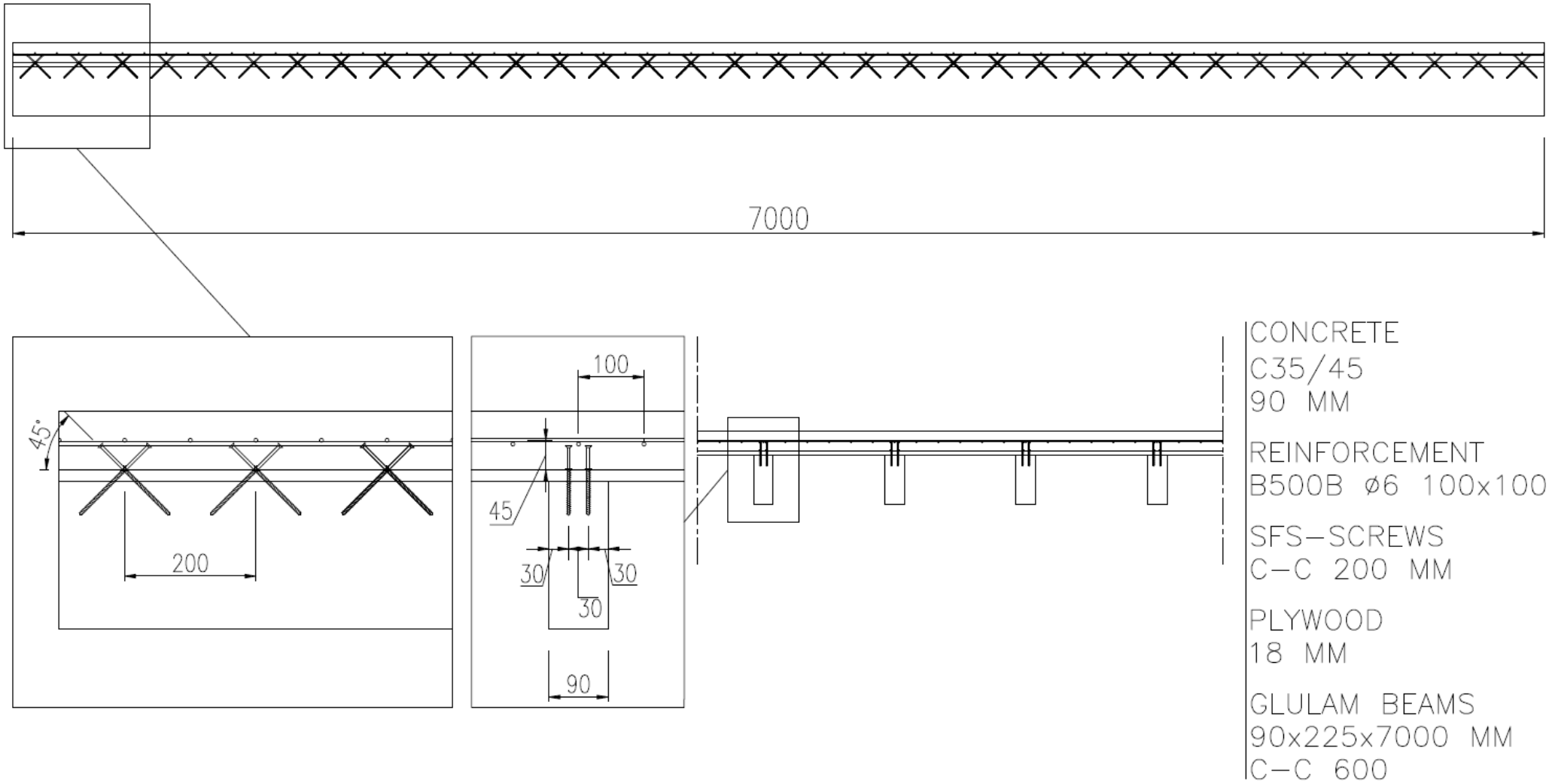
7000
45°
200
100
45
30
30
30
90
CONCRETE
C35/45
90 MM
REINFORCEMENT
B500B ø6 100x100
SFS–SCREWS
C–C 200 MM
PLYWOOD
18 MM
GLULAM BEAMS
90x225x7000 MM
C–C 600

6 Conclusions & Discussion

Timber-concrete composite floors were investigated and evaluated. Focus was mainly put on the shear connectors due to their critical role in composite structures. Some possible performance-enhancement methods of timber-concrete composites were also briefly touched upon, but they were either too expensive or in the need of further research before implementation.

The evaluation eventually lead to further examination of two shear connectors, one a was a square reinforced concrete plug and the other a connector consisting of two SFS- screws inclined in different directions. It was thus concluded from practical experiments that light and stiff composite floors can be achieved when using SFS-screws as connectors. Considering the degree of agreement between the theoretical estimations of the load capacity, and the experimental values, it was also established that the method of analysis was valid.

Having concluded the above, a timber-concrete composite system using SFS-screws as connectors was proposed. The proposed system was based on semi-prefabricated wooden panels that could be manufactured almost automatically. The panels would be 2,4 m wide and available in lengths of 6,0-9,6 m. Their configuration and light weight would also enable efficient logistics. At the construction site, the panels would be installed next to each other, thus forming a continuous platform upon which concrete could be cast. High performance concrete for quick curing was suggested to reduce construction time.

After the extensive literature review that was performed in the beginning of this work, it was also clear that further research is needed on several areas in the field of timber-concrete composite engineering. Especially, the long term performance of timber-concrete composites needs more investigation. Unfortunately, the necessary resources in terms of time required to investigate this matter, were lacking. It would also be interesting to learn about the performance of the connectors if lightweight concrete is used. Only a few of the connectors examined in this work have been tested with lightweight concrete (refer to section 2.3).

7 References

Literature

Dias, A.M.P.G. (2005). “Mechanical behavior of timber-concrete composite joints”. PhD thesis, Delft University of Technology, The Netherlands.

Aicher, H. & Reinhardt, W. (2000). “Joints in Timber Structures”. Rilem Publications, pp 301-309.

Aicher H., Klöck, W., Dill Langer, G., & Radovic, B. (2003). “Nails and nailplates as shear connectors for timber-concrete composite constructions”. Otto-Graf-Journal vol. 14, 2003.

Bathon, L. A. (2007) “Green Technologies for Structural Retrofit and Prefabrications with Wood”. Power-Point presentation at UMass 2007 Wood Structures Symposium, University of Massachusetts.

Bathon, Leander, Graf & Markus. (2000) “A continuous wood-concrete-composite system”. Proceedings of the World Conference on Timber Engineering, 2000.

Benitez, M. F. (2000). “Development and testing of timber/concrete shear connectors”. Proceedings of the World Conference on Timber Engineering, 2000.

Boverket. (2003) ”Regelsamling för konstruktion - Boverkets konstruktionsregler BKR, byggnadsverkslagen, och byggnadsverksförordningen”.

Branco, M., Cruz, J.S., Piazza, M. (2009) “Experimental analysis of laterally loaded nailed timber-to-concrete connections”. Construction and Building Materials vol. 23, 2009.

Brunner, M., Romer, M., & Scnuriger, M. (2007). ”Timber-concrete composites with an adhesive connector (wet on wet process)”. Materials and structures, vol. 40, pp. 119-126, 2007.

Clouston, P., Bathon, L. A., & Schreyer, A. (2005). “Shear and Bending Performance of a Novel Wood–Concrete”. Journal of structural engineering, vol 131 pp. 1402-1412.

Deam, B. L., Fragiacomo, M., & Buchanan, A. H. (2008). "Connections for composite concrete slabs and LVL flooring systems". Materials and Structures vol. 41, no 3, pp. 495-507, 2008.

Deam, B.L., Yeoh, D., Fragiacomo, M., Buchanan, A. H. Crews, K., & Haskell, J. (2008) "Development of Semi-Prefabricated Timber-Concrete Composite Floors in Australasia". 10th World Conference of Timber Engineering, Miyazaki, Japan, 2008.

Girhammar, U. (2009). "A simplified analysis method for composite beams with an interlayer slip". International Journal of Mechanical Sciences vol. 51, 2009.

Lukaszewska, E. (2009). "Development of Prefabricated Timber-Concrete Composite Floors". PhD thesis, Luleå University of Technology, Sweden.

EN 1990 Eurocode-Basis of structural design. CEN, 2002.

EN 1991-1-1. Eurocode-Actions on structures – Part 1-1. CEN, 2001.

EN 1992-1-1. Eurocode-Design of concrete structures – Part 1. CEN, 2002.

EN 1995-1-1. Eurocode-Design of timber structures – Part 1-1. CEN, 2002

SFS intec. "Secure, individual and cost-effective timber/concrete joints by SFS intec". Product sheet.

Steinberg, E., Selle, R., & Faust, T. (2003). "Connectors for Timber–Lightweight Concrete Composite Structures". Journal of structural engineering, vol 129 , No 11 pp. 1538-1545, 2003.

Tajnik, Dobrila, & Premrov. (2007). "Analysis of composite T beam composed of timber, concrete and carbon strip". WSEAS TRANSACTIONS on APPLIED and THEORETICAL MECHANICS, Issue 9, Volume 2, September, 2007.

Weaver, C. A. (2002). "Behavior of FRP-reinforced Glulam-concrete composite bridge girders". MS Thesis in Civil and Environmental engineering. University of Maine, 2002.

Internet sources

SEPA GROUP, 2010-05-15,
http://www.sepa.fi/SV/ovriga-produkter/tra-betong-kombiplatta.html

Appendix A.

Theoretical failure loads and deflections in full scale bending experiments

Indata:

Concrete

The compression capacity of a 0,15 x 0,15 m cube was established as the mean value of three compression experiments to 70,074 MPa. Using this as a reference value, interpolating between material property-values in table in prEN 1992-1-1 (Design of concrete structures), resulted in the following parameters:

E_{cm} = 38,32 GPa
f_{ccm}= 65,56 MPa
f_{ctm} = 4,3 MPa

Glulam beams

The characteristic material properties for the timber were obtained from the Swedish *BKR 03*.

E_{tk}=13 GPa (Young's modulus for calculation of deformation properties)
f_{mk}=33 MPa (For bending parallel to the grain direction)
f_{tk}=23 MPa (For bending parallel to the grain direction)

In the case of bending- and tensile-capacity, effects of sample size had to be taken in consideration. This was done by multiplying with the factor k_h.
For $h \leq 300\ mm$, $k_h = 1{,}15$:

F_{mk}=33*1,15=37,95 MPa
F_{tk}=23*1,15=26,45 MPa

Finally, the average material strength properties could be obtained through the use of equation A1.

$$f_k = e^{-1{,}65*cov} * f_m \qquad \text{(Eq. A1)}$$

Where *cov* = 0,2 is the coefficient of variation. Hence, the following average material properties were obtained for timber:

$E_{tm} = E_{tm} = 13{,}0 * 10^9\ Pa$ => E_{tm}=13,0 GPa
$f_{tm} = \frac{f_{tk}}{e^{-1{,}65*cov}} = \frac{26{,}45*10^6}{e^{-1{,}65*0{,}2}} = 36{,}79 * 10^6\ Pa$ => f_{tm}=36,79 MPa
$f_{mm} = \frac{f_{mk}}{e^{-1{,}65*cov}} = \frac{37{,}95*10^6}{e^{-1{,}65*0{,}2}} = 52{,}79 * 10^6\ Pa$ => f_{mm}= 52,79 MPa

SFS-connector

Screw-pairs were placed at a spacing of 0,125 m. The following parameters apply for each pair of screws (Deam, Fragiacomo, & Buchanan, 2008):

$K_{0,4}$=14,4 kN/mm
$K_{0,6}$=12,7 kN/mm
$K_{0,8}$=11,9 kN/mm

F_{max}=18,5 kN

Given the connector's linear load displacement curve almost up to failure observed in the literature, $K_{0,4}$ was considered the most realistic value to use in calculations.

Concrete notch-connector

The concrete notch-connectors are placed at a spacing of 1,0 m. The following parameters apply for one connector (Deam, Fragiacomo, & Buchanan, 2008):

$K_{0,4}$=297,0 kN/mm
$K_{0,6}$=197,3 kN/mm
$K_{0,8}$=148,5 kN/mm

F_{max}=54,9 kN

General:

The dead weight of the floor is calculated in table A1:

	Number of elements	Dimensions, (b*h*l) [m]	Density [kg/m^3]	Weight [kg]
Concr. slab	1	2,4*0,08*7	2400	3225,6
Plywood interl.	1	2,4*0,021*7	530	187,0
Gl. Beam (SFS)	4	0,115*0,225*7	500	362,3
Gl. Beam (Notch)	4	0,056*0,270*7	500	211,68
			$\sum_{SFS}$	3774,9
			$\sum_{Notch}$	3624,3

Table A1. Dead weight of floor specimens.

The calculated dead weights correspond to evenly distributed loads of 5,29 kN/m and 5,08 kN/m for floor-specimen 1 and 2 respectively. For simplicity reasons, the dead load was taken as 5 kN/m for both cases. Considering also the weight of the steel beams, the following diagrams could be drawn, see figure A1:

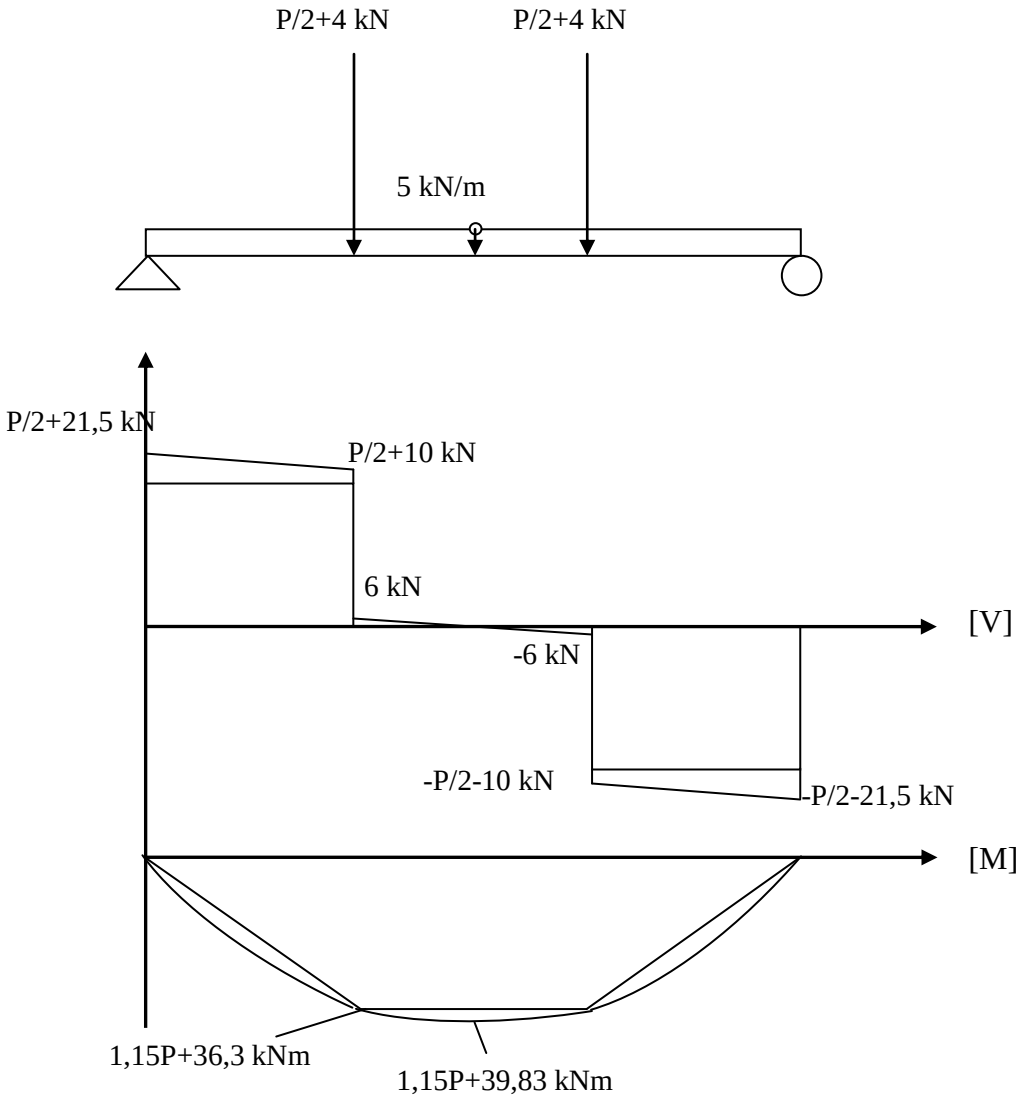

Figure A1. Shear force & bending moment in 4-point bending tests

Test specimen 1, SFS-connector

Using the γ-method:

Insertion of data in equations of the γ-method results in the following:

Area of element cross sections:
$A_1 = 0{,}6 * 0{,}08 = 0{,}048m^2$
$A_2 = 0{,}115 * 0{,}225 = 0{,}0258m^2$

Second moment of inertia of sub-elements:
$I_1 = \frac{0{,}6*0{,}08^3}{12} = 2{,}56 * 10^{-5}m^4$
$I_2 = \frac{0{,}115*0{,}225^3}{12} = 1{,}091 * 10^{-4}m^4$

Composite action achieved:
$\gamma_1 = \frac{1}{1+\frac{\pi^2*38{,}32*10^9*0{,}048*0{,}125}{14{,}4*10^6*7^2}} = 0{,}237$
$\gamma_2 = 1$

Distances from neutral layer to the centroids of the sub-elements:
$a_2 = \frac{0{,}237*38{,}32*10^9*0{,}048*(0{,}08+0{,}225)}{2(0{,}237*38{,}32*10^9 0{,}048+1*13{,}0*10^9*0{,}0258)}$ =0,0861 m
$a_1 = \frac{0{,}08+0{,}225}{2} - 0{,}0861 = 00664$ m

Resulting effective bending stiffness:
$EI_{eff} =$
$38{,}32 * 10^9 * 2{,}56 * 10^{-5} + 0{,}237 * 38{,}32 * 10^9 * 0{,}048 * 00664^2 + 13{,}0 * 10^9 * 1{,}091 * 10^{-4} + 1 * 13{,}0 * 10^9 * 0{,}0258 * 0{,}0861^2 = 6{,}817$ MNm^2

From the illustration below it is clear that the necessary conditions could be expressed through equations A2-A4.

$f_{ccm} \geq \sigma_1 + \sigma_{m,1}$ (eq. A2)

$f_{ctm} \geq \sigma_1 - \sigma_{m,1}$ (eq. A3)

$1 \geq \frac{\sigma_2}{f_{ttm}} + \frac{\sigma_{2,m}}{f_{tmm}}$ (eq. A4)

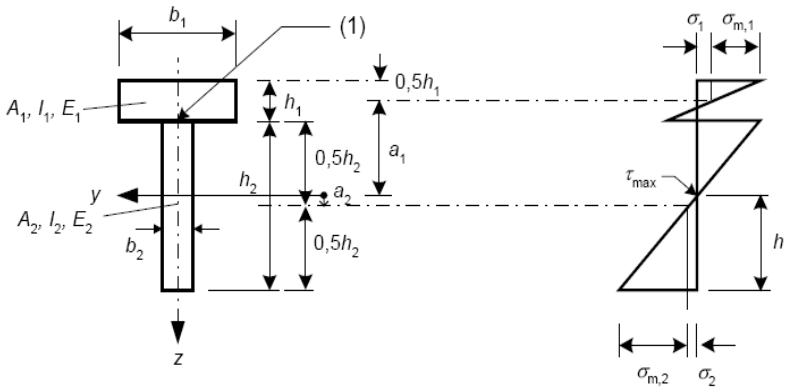

Equations A2-A4 regard failure in concrete due to compression, failure in concrete due to tension, and failure in timber du to a combination of bending and tension.

From equations A2-A4 follows:

$$f_{ccm} \geq \sigma_1 + \sigma_{m,1} = \frac{\gamma E_1 a_1 M}{EI_{ef}} + \frac{0{,}5 E_1 h_1 M}{EI_{ef}} = \frac{E_1 M}{EI_{ef}}(\gamma a_1 + 0{,}5 h_1) \qquad \text{(eq. A5)}$$

$$f_{ctm} \geq \sigma_1 - \sigma_{m,1} = \left|\frac{\gamma E_1 a_1 M}{EI_{ef}} - \frac{0{,}5 E_1 h_1 M}{EI_{ef}}\right| = \frac{E_1 M}{EI_{ef}} * |\gamma a_1 - 0{,}5 h_1| \qquad \text{(eq. A6)}$$

$$1 \geq \frac{\sigma_2}{f_{ttm}} + \frac{\sigma_{2,m}}{f_{tmm}} = \frac{\gamma_2 E_2 a_2 M}{EI_{ef} f_{ttm}} + \frac{0{,}5 E_2 h_2 M}{EI_{ef} f_{tmm}} = \frac{E_2 M}{EI_{ef}}\left(\frac{\gamma_2 a_2}{f_{ttm}} + \frac{0{,}5 h_2}{f_{tmm}}\right) \qquad \text{(eq. A7)}$$

If M is extracted, equations A5-A7 become,

$$M \leq \frac{EI_{ef} f_{ccm}}{E_1(\gamma a_1 + 0{,}5 h_1)} \qquad \text{(eq. A8)}$$

$$M \leq \frac{EI_{ef} f_{ctm}}{E_1 * |\gamma a_1 - 0{,}5 h_1|} \qquad \text{(eq. A9)}$$

$$M \leq \frac{EI_{ef}}{E_2\left(\frac{a_2}{f_{ttm}} + \frac{0{,}5 h_2}{f_{tmm}}\right)} \qquad \text{(eq. A10)}$$

In the case of a floor consisting of four composite beams, the equivalents to equations A8-A10 become:

$$M \leq \frac{4 * EI_{ef} f_{ccm}}{E_1(\gamma a_1 + 0{,}5 h_1)} \qquad \text{(eq. A11)}$$

$$M \leq \frac{4 * EI_{ef} f_{ctm}}{E_1 * |\gamma a_1 - 0{,}5 h_1|} \qquad \text{(eq. A12)}$$

$$M \leq \frac{4 * EI_{ef}}{E_2\left(\frac{a_2}{f_{ttm}} + \frac{0{,}5 h_2}{f_{tmm}}\right)} \qquad \text{(eq. A13)}$$

Combining equations A11-A13 with shear forces and bending moments illustrated in figure 1, the following expressions of load capacity can be stated with regard to; compression failure in the concrete, tensile failure in the concrete, and failure in the glulam beams.

$$P_{compr.fail.concr.} = \frac{4*EI_{ef}f_{ccm}}{1{,}15E_1(\gamma a_1+0{,}5h_1)} - 34{,}63 * 10^3 \qquad \text{(eq. A14)}$$

$$P_{tens.fail.concr.} = \frac{4*EI_{ef}f_{ctm}}{1{,}15E_1*|\gamma a_1-0{,}5h_1|} - 34{,}63 * 10^3 \qquad \text{(eq. A15)}$$

$$P_{timber\ failure} = \frac{4*EI_{ef}}{1{,}15E_2\left(\frac{a_2}{f_{ttm}}+\frac{0{,}5h_2}{f_{tmm}}\right)} - 34{,}63 * 10^3 \qquad \text{(eq. A16)}$$

The load on the fastener in a composite beam is taken as:

$$F = \frac{\gamma_1 E_1 A_1 a_1 s_1 V(x)}{EI_{ef}} \qquad \text{(eq. A17)}$$

Hence, the shear force at which failure occurs in the shear connectors could be expressed as:

$$V(x) = \frac{EI_{ef}F_{max}}{\gamma_1 E_1 A_1 a_1 s_1} \qquad \text{(eq. A18)}$$

The loading at which failure starts in the first pair of connectors is thus calculated as:

$$P_{failure\ in\ connector} = \frac{2*4*EI_{ef}F_{max}}{\gamma_1 E_1 A_1 a_1 s_1} - 2 * 21{,}5 * 10^3 \qquad \text{(eq. A19)}$$

Insertion of calculated values in equations A14, A15, A16 and A19 gives

$$P_{compr.fail.concr.} = \frac{4*6{,}817*10^6 65{,}56*10^6}{1{,}15*38{,}32*10^9(0{,}237*0{,}0664+0{,}5*0{,}08)} - 34{,}63 * 10^3 = 693{,}1\ \text{kN}$$

$$P_{tens.fail.concr.} = \frac{4*6{,}817*10^6*4{,}3*10^6}{1{,}15*38{,}32*10^9*|0{,}237*0{,}0664-0{,}5*0{,}08|} - 34{,}63 * 10^3 = 75{,}1\ \text{kN}$$

$$P_{timber\ failure} = \frac{4*6{,}817*10^6}{1{,}15*13{,}0*10^9\left(\frac{0{,}0861}{36{,}79*10^6}+\frac{0{,}5*0{,}225}{52{,}78*10^6}\right)} - 34{,}63 * 10^3 = 373{,}2\ \text{kN}$$

$$P_{failure\ in\ connector} = \frac{2*4*6{,}817*10^6*18{,}5*10^3}{0{,}237*38{,}32*10^9*0{,}048*0{,}0664*0{,}125} - 2 * 21{,}5 * 10^3 = 235{,}7\text{kN}$$

In reality, tensile failure in the concrete only means that micro-cracks will develop. They have little or no effect on the load capacity of the floor. Hence, the failure is due to failure in the shear connectors.

Once the effective bending stiffness is known, the theoretical deflection due to the applied load (dead weight and weight of metal beams excluded) can be estimated by extrapolating an extra concentrated load in the load case illustrated below (Q should be looked upon as one of the concentrated loads in the experiments). Because of the symmetric setup in the bending experiments, the deflection could then be obtained by simply doubling the effect of equation A20.

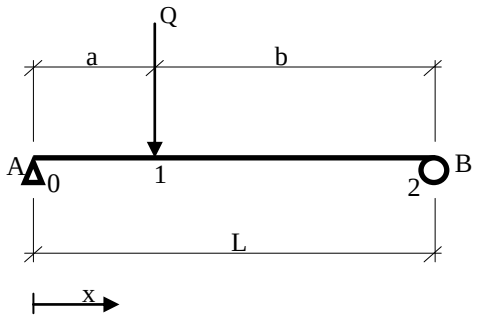

$$v^{1-2} = \frac{Qa(3L^2-4a^2)}{48EI} \qquad \text{(Eq. A20)}$$

Thus, with Q=P/2, $a = 2{,}3$m, L=7m and with a specimen consisting of four beams, each with a bending stiffness of $EI=EI_{eff}=6{,}817 * 10^6 \text{Nm}^2$, thetheoretical deflection becomes:

$$v = 2 * \left(\frac{(235670/2) * 2{,}3 * (3 * 7^2 - 4 * 2{,}3^2)}{48 * 4 * 6{,}817 * 10^6} \right) = \quad 0{,}052\ m$$

EI_{eff}=4*6,817*10^6 Nm^2 =27,27 MNm^2

$P_{\text{failure in shear connector}}$=235,67 kN

$V_{\text{additional loading}}$ = 52 mm

Using Girhammar's simplified method:

Insertion of data in the equations of Girhammar's simplified approach results in the following:

Area of element cross section:

$A_1 = 0{,}6 * 0{,}08 = 0{,}048m^2$

$A_2 = 0{,}115 * 0{,}225 = 0{,}0258m^2$

Second moment of inertia of sub-elements:

$I_1 = \frac{0{,}6*0{,}08^3}{12} = 2{,}56 * 10^{-5}m^4$

$I_2 = \frac{0{,}115*0{,}225^3}{12} = 1{,}091 * 10^{-4}m^4$

The bending stiffness of the corresponding non-composite beam:

$EI_0 = 38{,}32 * 10^9 * 2{,}56 * 10^{-5} + 13{,}0 * 10^9 * 1{,}091 * 10^{-4} = 2{,}40$ MNm^2

The axial stiffness of the corresponding non-composite beam:

$EA_0 = 38{,}32 * 10^9 * 0{,}048 + 13{,}0 * 10^9 * 0{,}0258 = 2{,}175$ GN

The product of the axial stiffness of the sub elements:

$EA_p = 38{,}32 * 10^9 * 0{,}048 * 13{,}0 * 10^9 * 0{,}0258 = 6{,}17 * 10^{17}$ N^2

The bending stiffness of the corresponding fully-composite beam:

$EI_\infty = EI_0 + \frac{EA_p r^2}{EA_0} = 2{,}561 * 10^6 + \frac{6{,}17*10^{17}*0{,}1525^2}{2{,}175*10^9} = 8{,}997$ MNm^2

The non-dimensional shear connector parameter:

$$\alpha L = \sqrt{\frac{(14.4 * 10^6/0{,}125) * 0{,}1525^2}{2{,}40 * 10^6(1 - 0{,}267)}} * 7 = 8{,}634$$

The effective bending stiffness:

$$EI_{eff} \approx \left[1 + \frac{8{,}997*10^6\ /2{,}40*10^6 - 1}{1+(1/\pi)^2(8{,}634)^2}\right]^{-1} * 8{,}997 * 10^6 = 6{,}809 \text{ MNm}^2$$

Internal actions in the sub-elements can be expressed through A22-A23:

$$N_{i,eff} = \left(1 - \frac{EI_0}{EI_{eff}}\right)\frac{M}{r} \quad \text{(eq. A22)}$$

$$M_{i,eff} = \frac{E_i I_i}{EI_{eff}} * M \quad \text{(eq. A23)}$$

Normal stresses due to axial forces and bending moment can thus be expressed as:

$$\sigma = \frac{N}{A} = \frac{N}{b_i h_i} \quad \text{(eq. A24)}$$

$$\sigma = \frac{M}{w} = \frac{6*M}{b_i h_i^2} \quad \text{(eq. A25)}$$

Combining equations A22-A23 with equations A24-A25 leads to the following expressions for stresses resulting from axial forces and bending respectively:

$$\sigma_i = \frac{M*\left(1-\frac{EI_0}{EI_{eff}}\right)}{b_i h_i * r} \quad \text{(eq. A26)}$$

$$\sigma_{m,i} = \frac{6*M*E_i I_i}{b_i * h_i^2 * EI_{eff}} \quad \text{(eq. A27)}$$

The necessary conditions are obtained from inserting equations A26-A27 in equations A2-A4:

$$f_{ccm} \geq \sigma_1 + \sigma_{m,1} = \frac{M*\left(1-\frac{EI_0}{EI_{eff}}\right)}{b_1 h_1 * r} + \frac{6*M*E_1 I_1}{b_1 * h_1^2 * EI_{eff}} = \\ = \frac{M}{b_1 h_1}\left(\frac{\left(1-\frac{EI_0}{EI_{eff}}\right)}{r} + \frac{6*E_1 I_1}{h_1 * EI_{eff}}\right) \quad \text{(eq. A28)}$$

$$f_{ctm} \geq \sigma_1 - \sigma_{m,1} = \left|\frac{M*\left(1-\frac{EI_0}{EI_{eff}}\right)}{b_1 h_1 * r} - \frac{6*M*E_1 I_1}{b_1 * h_1^2 * EI_{eff}}\right| = \\ = \frac{M}{b_1 h_1}\left|\frac{\left(1-\frac{EI_0}{EI_{eff}}\right)}{r} - \frac{6*E_1 I_1}{h_1 * EI_{eff}}\right| \quad \text{(eq. A29)}$$

$$1 \geq \frac{\sigma_2}{f_{ttm}} + \frac{\sigma_{2,m}}{f_{tmm}} = \frac{M * \left(1 - \frac{EI_0}{EI_{eff}}\right)}{b_2 h_2 * r * f_{ttm}} + \frac{6 * M * E_2 I_2}{b_2 * h_2^2 * EI_{eff} * f_{tmm}} = \\ = \frac{M}{b_2 h_2}\left(\frac{\left(1-\frac{EI_0}{EI_{eff}}\right)}{r * f_{ttm}} + \frac{6*E_2 I_2}{h_2 * EI_{eff} * f_{tmm}}\right) \quad \text{(eq. A30)}$$

If M is extracted, equations A28-A30 become

$$M \leq \frac{b_1 h_1 f_{ccm}}{\left(\frac{\left(1-\frac{EI_0}{EI_{eff}}\right)}{r}+\frac{6*E_1 I_1}{h_1 * EI_{eff}}\right)} \quad \text{(eq. A31)}$$

$$M \leq \frac{b_1 h_1 f_{ctm}}{\left|\frac{\left(1-\frac{EI_0}{EI_{eff}}\right)}{r}-\frac{6*E_1 I_1}{h_1 * EI_{eff}}\right|} \quad \text{(eq. A32)}$$

$$M \leq \frac{b_2 h_2}{\left(\frac{\left(1-\frac{EI_0}{EI_{eff}}\right)}{r*f_{ttm}}+\frac{6*E_2 I_2}{h_2 * EI_{eff}*f_{tmm}}\right)} \quad \text{(eq. A33)}$$

Remembering that the floor consists of 4 composite beams, it is clear from figure 1 that the following expressions of load capacity can be stated with regard to; compression failure in concrete, tensile failure in concrete, and failure in glulam beams.

$$P_{compr.fail.concr.} = \frac{4*b_1 h_1 f_{ccm}}{1{,}15*\left(\frac{\left(1-\frac{EI_0}{EI_{eff}}\right)}{r}+\frac{6*E_1 I_1}{h_1 * EI_{eff}}\right)} - 34{,}63 * 10^3 \quad \text{(eq. A34)}$$

$$P_{tens.fail.concr.} = \frac{4*b_1 h_1 f_{ctm}}{1{,}15*\left|\frac{\left(1-\frac{EI_0}{EI_{eff}}\right)}{r}-\frac{6*E_1 I_1}{h_1 * EI_{eff}}\right|} - 34{,}63 * 10^3 \quad \text{(eq. A35)}$$

$$P_{timber\ failure} = \frac{4*b_2 h_2}{1{,}15*\left(\frac{\left(1-\frac{EI_0}{EI_{eff}}\right)}{r*f_{ttm}}+\frac{6*E_2 I_2}{h_2 * EI_{eff}*f_{tmm}}\right)} - 34{,}63 * 10^3 \quad \text{(eq. A36)}$$

The load on a fastener can be taken as:

$$F = \left(1-\frac{EI_0}{EI_{eff}}\right) * \frac{s}{r} * V(x) \quad \text{(eq. A37)}$$

If V(x) is extracted and rewritten according to figure 1, equation A38 is obtained.

$$V(x) = \frac{F}{\left(1-\frac{EI_0}{EI_{eff}}\right)*\frac{s}{r}} \quad \text{(eq. A38)}$$

Hence, according to figure 1, the loading at which failure starts in the first pair of connectors can be expressed as stated in equation A39

$$P_{failure\ in\ shear\ connector} = \frac{2*4*F}{\left(1-\frac{EI_0}{EI_{eff}}\right)*\frac{s}{r}} - 2*21{,}5*10^3 \qquad \text{(eq. A39)}$$

Insertion of calculated values in equations A34, A35, A36 and A39 gives

$$P_{compr.fail.concr.} = \frac{4*0{,}6*0{,}08*65{,}56*10^6}{1{,}15*\left(\frac{\left(1-\frac{2{,}40*10^6}{6{,}817*10^6}\right)}{0{,}1525}+\frac{6*38{,}32*10^9 2{,}56*10^{-5}}{0{,}08*6{,}817*10^6}\right)} - 34{,}63*10^3 =$$

$$= 692{,}6 \text{ kN}$$

$$P_{tens.fail.concr.} = \frac{4*0{,}6*0{,}08*4{,}3*10^6}{1{,}15*\left|\frac{\left(1-\frac{2{,}40*10^6}{6{,}817*10^6}\right)}{0{,}1525}-\frac{6*38{,}32*10^9*2{,}56*10^{-5}}{0{,}08*6{,}817*10^6}\right|} - 34{,}63*10^3 =$$

$$=86{,}9 \text{ kN}$$

$$P_{timber\ failure} = \frac{4*0{,}115*0{,}225}{1{,}15*\left(\frac{\left(1-\frac{2{,}40*10^6}{6{,}817*10^6}\right)}{0{,}1525*36{,}79*10^6}+\frac{6*13{,}0*10^9*1{,}091*10^{-4}}{0{,}225*6{,}817*10^6*52{,}78*10^6}\right)} - 34{,}63*10^3 =$$

$$= 373{,}3 \text{ kN}$$

$$P_{failure\ in\ shear\ connector} = \frac{2*4*18{,}5*10^3}{\left(1-\frac{2{,}40*10^6}{6{,}817*10^6}\right)*\frac{0{,}125}{0{,}1525}} - 2*21{,}5*10^3 = 235{,}8 \text{ kN}$$

Deflection is calculated as before:

$$v = 2*\left(\frac{(235823/2)*2{,}3*(3*7^2-4*2{,}3^2)}{48*4*6{,}809*10^6}\right) = \quad 0{,}052\ m$$

EI_{eff}=4*6,809*10^6 Nm^2= 27,24 MNm^2

$P_{failure\ in\ shear\ connector}$=235,82 kN

$V_{additional\ loading}$= 52 mm

As expected for a simply supported floor, the γ-method and Girhammar's simplified method delivered the same result. However, Girhammar's method also offers a simple way to calculate the more realistic bending moment capacity that follows from taking into consideration the interlayer thickness, and the increased moment arm that follows. If this extra distance is considered by taking the actual correct value of *r=0,1735 m*, instead of $r=r_1+r_2=h_1/2+ h_2/2$, the result becomes:

The bending stiffness of the corresponding fully-composite beam:

$$EI_\infty = EI_0 + \frac{EA_p r^2}{EA_0} = 2{,}40 * 10^6 + \frac{6{,}17*10^{17}*0{,}1735^2}{2{,}175*10^9} = 10{,}96 \text{ MNm}^2$$

The non-dimensional shear connector parameter:

$$\alpha L = \sqrt{\frac{(14.4 * 10^6/0{,}125) * 0{,}1735^2}{2{,}40 * 10^6(1-0{,}219)}} * 7 = 9{,}52$$

The effective bending stiffness:

$$EI_{eff} \approx \left[1 + \frac{1{,}096*10^7\ /2{,}40*10^6-1}{1+(1/\pi)^2(9{,}52)^2}\right]^{-1} * 1{,}096 * 10^7 = 8{,}118 \text{ MNm}^2$$

Insertion of values in equations A34, A35, A36, A39 and A20 gives

$$P_{compr.fail.concr.} = \frac{4*0{,}6*0{,}08*65{,}56*10^6}{1{,}15*\left(\frac{\left(1-\frac{2{,}40*10^6}{8118*10^6}\right)}{0{,}1735}+\frac{6*38{,}32*10^9*2{,}56*10^{-5}}{0{,}08*8{,}118*10^6}\right)} - 34{,}63 * 10^3 =$$

$$= 799{,}44 \text{ kN}$$

$$P_{tens.fail.concr.} = \frac{4*0{,}6*0{,}08*4{,}3*10^6}{1{,}15*\left|\frac{\left(1-\frac{2{,}40*10^6}{8118*10^6}\right)}{0{,}1735}-\frac{6*38{,}32*10^9*2{,}56*10^{-5}}{0{,}08*8118*10^6}\right|} - 34{,}63 * 10^3 =$$

$$= 108{,}84 \text{ kN}$$

$$P_{timber\ failure} = \frac{4*0{,}115*0{,}225}{1{,}15*\left(\frac{\left(1-\frac{2{,}40*10^6}{8118*10^6}\right)}{0{,}1735*36{,}79*10^6}+\frac{6*13{,}0*10^9*1{,}091*10^{-4}}{0{,}225*8118*10^6*52{,}78*10^6}\right)} - 34{,}63 * 10^3 =$$

$$= 418{,}38 \text{ kN}$$

$$P_{failure\ in\ shear\ connector} = \frac{2*4*18{,}5*10^3}{\left(1-\frac{2{,}40*10^6}{8118*10^6}\right)*\frac{0{,}125}{0{,}1735}} - 2 * 21{,}5 * 10^3 = 248{,}646 \text{ kN}$$

$$v = 2 * \left(\frac{(248646/2) * 2{,}3 * (3 * 7^2 - 4 * 2{,}3^2)}{48 * 4 * 8{,}118 * 10^6} \right) = \quad 0{,}046\ m$$

EI_{eff}=4*8,118*10^6 Nm^2= 32,47 MNm^2

$P_{failure\ in\ shear\ connector}$=248,65 kN

$V_{additional\ loading}$= 46 mm

Test specimen 2,Concrete notch-connector

Using the γ-method:

Insertion of input-data in equations of the γ-method gives the following results:

Area of element cross section:
$A_1 = 0{,}6 * 0{,}08 = 0{,}048 m^2$
$A_2 = 0{,}056 * 0{,}270 = 0{,}015 m^2$

Second moment of inertia of sub-elements:
$I_1 = \frac{0{,}6 * 0{,}08^3}{12} = 2{,}56 * 10^{-5} m^4$
$I_2 = \frac{0{,}056 * 0{,}270^3}{12} = 9{,}19 * 10^{-5} m^4$

Composite action achieved:
$\gamma_1 = \frac{1}{1+\frac{\pi^2 * 38{,}32 * 10^9 * 0{,}048 * 1{,}0}{297{,}0 * 10^6 * 7^2}} = 0{,}445$
$\gamma_2 = 1$

Distances from neutral layer to the neutral layers of the sub-elements:
$a_2 = \frac{0{,}445 * 38{,}32 * 10^9 * 0{,}048 * (0{,}08 + 0{,}270)}{2(0{,}445 * 38{,}32 * 10^9 * 0{,}048 + 1 * 13{,}0 * 10^9 * 0{,}015)}$ =0,141 m
$a_1 = \frac{0{,}08 + 0{,}270}{2} - 0{,}141 = 0{,}034$ m

Resulting effective bending stiffness:
$EI_{eff} =$
$38{,}32 * 10^9 * 2{,}56 * 10^{-5} + 0{,}445 * 38{,}32 * 10^9 * 0{,}048 * 0{,}034^2 + 13{,}0 * 10^9 * 9{,}19 * 10^{-5} + 1 * 13{,}0 * 10^9 * 0{,}015 * 0{,}141^2 = 7{,}03$ MNm^2

Insertion of calculated values in equations A34, A35, A36, A39 and A20 gives

$$P_{compr.fail.concr.} = \frac{4 * 7{,}03 * 10^6 * 65.56 * 10^6}{1{,}15 * 38{,}32 * 10^9 * (0{,}445 * 0{,}034 + 0{,}5 * 0.08)} - 34{,}63 * 10^3 = 724{,}8 \text{ kN}$$

$$P_{tens.fail.concr.} = \frac{4 * 7{,}03 * 10^6 * 4{,}3 * 10^6}{1{,}15 * 38{,}32 * 10^9 * |0{,}445 * 0{,}034 - 0{,}5 * 0.08|} - 34{,}63 * 10^3 = 75{,}41 \text{ kN}$$

$$P_{timber\ failure} = \frac{4*7{,}03*10^6}{1{,}15*13{,}0*10^9*\left(\frac{0{,}141}{36.79*10^6}+\frac{0{,}5*0{,}270}{52{,}78*10^6}\right)} - 34{,}63 * 10^3 =$$

$$= 259{,}53 \text{ kN}$$

$$P_{failure\ in\ connector} = \frac{2*4*7{,}03*10^6*54{,}9*10^3}{0{,}445*38{,}32*10^9*0{,}048*0{,}034*1} - 2 * 21{,}5 * 10^3 =$$

$$= 68{,}3 \text{ kN}$$

$$v = 2 * \left(\frac{(68302/2) * 2{,}3 * (3 * 7^2 - 4 * 2{,}3^2)}{48 * 4 * 7{,}03 * 10^6 * 10^6}\right) = \quad 0{,}0146\ m$$

EI_{eff}=4*7,03*10^6 Nm^2= 28,12 MNm^2

$P_{failure\ in\ shear\ connector}$=68,30 kN

$V_{additional\ loading}$= 15 mm

Using Girhammars simplified method:

Insertion of data in the equations of Girhammar's simplified method gives the following results:

Area of element cross section:
$A_1 = 0{,}6 * 0{,}08 = 0{,}048 m^2$
$A_2 = 0{,}056 * 0{,}270 = 0{,}015 m^2$

Second moment of inertia of sub-elements:
$I_1 = \frac{0{,}6 * 0{,}08^3}{12} = 2{,}56 * 10^{-5} m^4$
$I_2 = \frac{0{,}056 * 0{,}270^3}{12} = 9{,}19 * 10^{-5} m^4$

The bending stiffness of the corresponding non-composite beam:
$EI_0 = 38{,}32 * 10^9 * 2{,}56 * 10^{-5} + 13{,}0 * 10^9 * 9{,}19 * 10^{-5} = 2{,}1757$ MNm^2

The axial stiffness of the corresponding non-composite beam:
$EA_0 = 38{,}32 * 10^9 * 0{,}048 + 13{,}0 * 10^9 * 0{,}015 = 2{,}034$ GN

The product of the axial stiffness of the sub elements:
$EA_p = 38{,}32 * 10^9 * 0{,}048 * 13{,}0 * 10^9 * 0{,}015 = 3{,}587 * 10^{17}$ N^2

The bending stiffness of the corresponding fully-composite beam:
$EI_\infty = 2{,}1757 * 10^6 + \frac{3{,}587 * 10^{17} * 0{,}175^2}{2{,}034 * 10^9} = 7{,}614$ MNm^2

The non-dimensional shear connector parameter:

$$\alpha L = \sqrt{\frac{(297 * 10^6 / 1{,}0) * 0{,}175^2}{2{,}1757 * 10^6 \left(1 - \frac{2{,}1757 * 10^6}{7{,}614 * 10^6}\right)}} * 7 = 16{,}94$$

The effective bending stiffness:
$EI_{eff} \approx \left[1 + \frac{7{,}614 * 10^6 / 2{,}1757 * 10^6 - 1}{1 + (1/\pi)^2 (16{,}94)^2}\right]^{-1} * 7{,}614 * 10^6 = 7{,}029$ MNm^2

Insertion of calculated values in equations A34, A35, A36, A39 and A20 gives

$$P_{compr.fail.concr.} = \frac{4*0{,}6*0{,}08*65{,}56*10^6}{1{,}15*\left(\frac{\left(1-\frac{2{,}1757*10^6}{7{,}029*10^6}\right)}{0{,}175}+\frac{6*38{,}32*10^9*2{,}56*10^{-5}}{0{,}08*7{,}029*10^6}\right)} - 34{,}63*10^3 =$$

$$= 72478 \text{ kN}$$

$$P_{tens.fail.concr.} = \frac{4*0{,}6*0{,}08*4{,}3*10^6}{1{,}15*\left|\frac{\left(1-\frac{2{,}1757*10^6}{7{,}029*10^6}\right)}{0{,}175}-\frac{6*38{,}32*10^9*2{,}56*10^{-5}}{0{,}08*7{,}029*10^6}\right|} - 34{,}63*10^3 =$$

$$= 75{,}46 \text{ kN}$$

$$P_{timber\ failure} = \frac{4*0{,}056*0{,}27}{1{,}15*\left(\frac{\left(1-\frac{2{,}1757*10^6}{7{,}029*10^6}\right)}{0{,}175*36{,}79*10^6}+\frac{6*14{,}47*10^9*9{,}19*10^{-5}}{0{,}27*7{,}029*10^6*52.78*10^6}\right)} - 34{,}63*10^3 =$$

$$= 259{,}53 \text{ kN}$$

$$P_{failure\ in\ shear\ connector} = \frac{2*4*54{,}9*10^3}{\left(1-\frac{2{,}1757*10^6}{7{,}029*10^6}\right)*\frac{1{,}0}{0{,}175}} - 2*21{,}5*10^3 =$$

$$= 68{,}3 \text{ kN}$$

$$v = 2*\left(\frac{(68302/2)*2{,}3*(3*7^2-4*2{,}3^2)}{48*4*7{,}029*10^6*10^6}\right) = \quad 0{,}0146\ m$$

EI_{eff}=4*7,029*10^6 Nm^2= 28,12 MNm^2

$P_{failure\ in\ shear\ connector}$=68,30 kN

$V_{additional\ loading}$= 15 mm

If the real distance r=*0,196 m* is considered, the result becomes:

The bending stiffness of the corresponding fully-composite beam:

$$EI_\infty = EI_0 + \frac{EA_p r^2}{EA_0} = 2{,}1757 * 10^6 + \frac{3{,}587*10^{17}*0{,}196^{\,2}}{2{,}034*10^9} = 8{,}997 \text{ MNm}^2$$

The non-dimensional shear connector parameter:

$$\alpha L = \sqrt{\frac{(297 * 10^6/1{,}0) * 0{,}196^{\,2}}{2{,}1757 * 10^6 \left(1 - \frac{2{,}1757 * 10^6}{8{,}997 * 10^6}\right)}} * 7 = 18{,}41$$

The effective bending stiffness:

$$EI_{eff} \approx \left[1 + \frac{8{,}997*10^6\,/2{,}1757*10^6 - 1}{1+(1/\pi)^2(18{,}41)^2}\right]^{-1} * 8{,}997 * 10^6 = 8{,}2638 \text{ MNm}^2$$

Insertion of values in equations A34, A35, A36, A39 and A20 gives,

$$P_{compr.fail.concr.} = \frac{4*0{,}6*0{,}08*65{,}56*10^6}{1{,}15*\left(\frac{\left(1-\frac{2{,}1757*10^6}{8{,}2638*10^6}\right)}{0{,}196} + \frac{6*38{,}32*10^9*2{,}56*10^{-5}}{0{,}08*8{,}2638*10^6}\right)} - 34{,}63 * 10^3 =$$

$$= 829{,}8 \text{ kN}$$

$$P_{tens.fail.concr.} = \frac{4*0{,}6*0{,}08*4{,}3*10^6}{1{,}15*\left|\frac{\left(1-\frac{2{,}1757*10^6}{8{,}2638*10^6}\right)}{0{,}196} - \frac{6*38{,}32*10^9*2{,}56*10^{-5}}{0{,}08*8{,}2638*10^6}\right|} - 34{,}63 * 10^3 =$$

$$= 104{,}93 \text{ kN}$$

$$P_{timber\ failure} = \frac{4*0{,}056*0{,}270}{1{,}15*\left(\frac{\left(1-\frac{2{,}1757*10^6}{8{,}2638*10^6}\right)}{0{,}196*36{,}79*10^6} + \frac{6*13{,}0*10^9*9{,}19*10^{-5}}{0{,}270*8{,}2638*10^6*52{,}78*10^6}\right)} - 34{,}63 * 10^3 =$$

$$= 287{,}98 \text{ kN}$$

$$P_{failure\ in\ shear\ connector} = \frac{2*4*54{,}9*10^3}{\left(1-\frac{2{,}1757*10^6}{8{,}2638*10^6}\right)*\frac{1{,}0}{0{,}196}} - 2 * 21{,}5 * 10^3 =$$

$$= 73{,}835 \text{ kN}$$

$$v = 2 * \left(\frac{(73835/2) * 2{,}3 * (3 * 7^2 - 4 * 2{,}3^2)}{48 * 4 * 8{,}2638 * 10^6 * 10^6}\right) = \quad 0{,}0135\ m$$

$$EI_{eff}=4*8{,}2638*10^{6}\ Nm^{2}=33{,}06\ MNm^{2}$$

$$P_{failure\ in\ shear\ connector}=73{,}84\ kN$$

$$V_{additional\ loading}=13{,}5\ mm$$

Appendix B

Corresponding non composite- and fully composite bending stiffness of test specimens

Test specimen 1, SFS-connector

No composite action:

$$EI_{non\ composite} =$$
$$= E_1 I_1 + E_2 I_2 = 38{,}32 * 10^9 * \frac{0{,}6 * 0{,}08^3}{12} + 13{,}0 * 10^9 * \frac{0{,}115 * 0{,}225^3}{12} =$$
$$= 2{,}4\ MNm^2$$

Full composite action:

(Effective cross section-method)

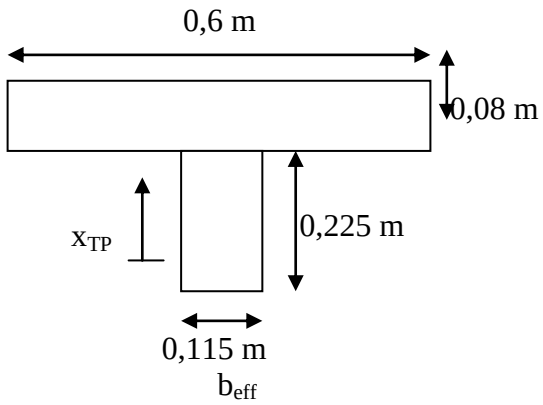

$$E_{concrete} = 38{,}32\ GPa$$
$$E_{timber} = 13{,}0\ GPa$$

$$E_{ref} = E_{concrete} = 38{,}32\ GPa$$

$$b_{eff} = \frac{13{,}0}{38{,}32} * 0{,}115 = 0{,}03901\ m$$

$$A_{eff} = 0{,}08 * 0{,}6 + 0{,}03901 * 0{,}225 = 0{,}0568\ m$$

$$A_{eff} * x_{TP} =$$
$$= 0{,}6 * 0{,}08 * \left(0{,}225 + \frac{0{,}08}{2}\right) + 0{,}03901 * 0{,}225 * \left(\frac{0{,}225}{2}\right) = 0{,}01371$$

$$=> x_{TP} = \frac{0{,}01371}{0{,}0568} = 0{,}2413\ m$$

$$I_{eff} = \frac{0{,}6 * 0{,}08^3}{12} + 0{,}6 * 0{,}08 * \left(0{,}225 + \frac{0{,}08}{2} - 0{,}2413\right)^2 + \frac{0{,}03901 * 0{,}225^3}{12} + 0{,}03901 * 0{,}225 \left(0{,}2413 - \frac{0{,}225}{2}\right)^2 = 2{,}352 * 10^{-4}$$

$$=> EI_{eff} = 38{,}32 * 10^9 * 2{,}352 * 10^{-4} = 9012856{,}6\ Nm^2$$

(The γ −method)

$\gamma = 1$ for full composite action:

$$a_2 = \frac{1{,}0*38{,}32*10^9*0{,}6*0{,}08(0{,}08+0{,}225)}{2(1{,}0*38{,}32*10^9*0{,}6*0{,}08+13{,}0*10^9*0{,}115*0{,}225)} = 0{,}129$$

$$a_1 = \frac{0{,}08 + 0{,}225}{2} - 0{,}129 = 0{,}0235$$

$$I_1 = \frac{0{,}6 * 0{,}08^3}{12} = 2{,}56 * 10^{-5}$$

$$I_2 = \frac{0{,}115 * 0{,}225^3}{12} = 1{,}092 * 10^{-4}$$

$EI_\infty = 38{,}32 * 10^9 * 2{,}56 * 10^{-5} + 38{,}32 * 10^9 * 0{,}6 * 0{,}08 * 0.0235^2 + 13{,}0 * 10^9 * 1{,}092 * 10^{-4} + 13{,}0 * 10^9 * 0{,}115 * 0{,}225 * 0{,}129^2$=9013994,94 N$m^2$

Girhammar's simplified method:
The bending stiffness for full composite action has already been calculated with Girhammar's simplified approach (refer to appendix A-Theoretical failure loads and deflections in full scale bending experiments):

$EI_\infty = 8{,}997 * 10^6 Nm^2$

If prolonged moment arm due to interlayer thickness is considered:

$EI_\infty = 10{,}96 * 10^6 Nm^2$

Table B1 summarizes the non composite- and fully composite bending stiffness for test specimen 1 (SFS connectors). Note that the values have been multiplied by four, since the specimen consists of four beams.

	$EI_{no\ composite\ action}$ [MNm^2]	$EI_{full\ composite\ action}$ [MNm^2]
Standard method	9,60	36,05
γ −method		36,06
Girhammar's method		35,99
Girhammar's method*		43,84

*If the actual moment arm is considered (due to interlayer thickness)

Table B1. Non composite- and fully composite bending stiffness for test specimen 1

Test specimen 2, Reinforced concrete plug-connector

No composite action:

$EI_{non\ composite} =$

$$= E_1 I_1 + E_2 I_2 = 38{,}32 * 10^9 * \frac{0{,}6 * 0{,}08^3}{12} + 13{,}0 * 10^9 * \frac{0{,}056 * 0{,}270^3}{12} =$$

$$= 2{,}1751\ MNm^2$$

Full composite action:

(Effective cross section-method)

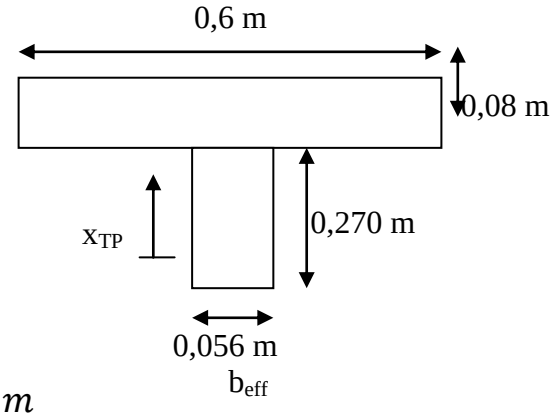

$E_{concrete} = 38{,}32\ GPa$
$E_{timber} = 13{,}0\ GPa$

$E_{ref} = E_{concrete} = 38{,}32\ GPa$

$b_{eff} = \frac{13{,}0}{38{,}32} * 0{,}056 = 0{,}019\ m$

$A_{eff} = 0{,}08 * 0{,}6 + 0{,}019 * 0{,}270 = 0{,}0531\ m$

$A_{eff} * x_{TP} =$

$$= 0{,}6 * 0{,}08 * \left(0{,}270 + \frac{0{,}08}{2}\right) + 0{,}019 * 0{,}270 * \left(\frac{0{,}270}{2}\right) = 0{,}0156$$

$$=> x_{TP} = \frac{0{,}0136}{0{,}0531} = 0{,}29327\ m$$

$$I_{eff} = \frac{0{,}6 * 0{,}08^3}{12} + 0{,}6 * 0{,}08 * \left(0{,}270 + \frac{0{,}08}{2} - 0{,}29327\right)^2 + \frac{0{,}019 * 0{,}270^3}{12} + 0{,}019 * 0{,}270\left(0{,}29327 - \frac{0{,}270}{2}\right)^2 = 1{,}987 * 10^{-4}$$

$$=> EI_{eff} = 38{,}32 * 10^9 * 1{,}987 * 10^{-4} = 7614293{,}12\ Nm^2$$

The $\gamma-$method:

$\gamma = 1$ for full composite action:

$$a_2 = \frac{1{,}0*38{,}32*10^9*0{,}6*0{,}08(0{,}08+0{,}270)}{2(1{,}0*38{,}32*10^9*0{,}6*0{,}08+13*10^9*0{,}056*0{,}270)} = 0{,}158$$

$$a_1 = \frac{0{,}08 + 0{,}270}{2} - 0{,}158 = 0{,}017$$

$$I_1 = \frac{0{,}6 * 0{,}08^3}{12} = 2{,}56 * 10^{-5}$$

$$I_2 = \frac{0{,}056 * 0{,}270^3}{12} = 9{,}19 * 10^{-5}$$

$$EI_\infty = 38{,}32 * 10^9 * 2{,}56 * 10^{-5} + 38{,}32 * 10^9 * 0{,}6 * 0{,}08 * 0{,}017^2 + 13{,}0 * 10^9 * 9{,}19 * 10^{-5} + 13{,}0 * 10^9 * 0{,}056 * 0{,}270 * 0{,}158^2 =$$
$$= 7614190{,}88 \text{ N}m^2$$

Girhammar's simplified method:
The bending stiffness for full composite action has already been calculated with Girhammar's simplified approach (refer to appendix A-*Theoretical failure loads and deflections in full scale bending experiments*):

$EI_\infty = 7{,}614 * 10^6$ Nm^2

If prolonged moment arm due to interlayer thickness is considered:

$EI_\infty = 8{,}2638 * 10^6$ Nm^2

Table B2 summarizes the non composite- and fully composite bending stiffness for test specimen 2 (reinforced concrete notch-connectors). Note that the values have been multiplied by four, since the specimen consists of four beams.

	$EI_{\text{no composite action}}$ [MNm^2]	$EI_{\text{full composite action}}$ [MNm^2]
Standard method	8,70	30,46
$\gamma-$method		30,46
Girhammar's method		30,46
Girhammar's method*		33,06

*If the actual internal moment arm is considered (due to interlayer thickness)

Table B2. Non composite- and fully composite bending stiffness for test specimen 2

Appendix C

Calculating creep coefficients

Creep coefficient of concrete:
The creep coefficient is essentially a function of the concrete age at loading, the time that has passed since loading, the relative humidity of the environment and the strength class of the concrete. It can be calculated using equation C1.

$$\varphi(t, t_0) = \varphi_0 * \beta_c(t, t_0) \quad \text{(Eq. C1)}$$

Where,

φ_0 The notional creep coefficient
$\beta_c(t, t_0)$ Coefficient that describes how creep develops with time after loading

The first term in equation C1 is in turn estimated as

$$\varphi_0 = \varphi_{RH} * \beta(f_{cm}) * \beta(t_0) \quad \text{(Eq. C2)}$$

Where,

φ_{RH} Coefficient that considers the effect of the relative humidity
$\beta(f_{cm})$ Coefficient that considers the concrete strength class
$\beta(t_0)$ Coefficient that considers the concrete age at loading

φ_{RH} is obtained using equation C3:

$$\varphi_{RH} = 1 + \frac{1 - RH/100}{0{,}1 * h_0^{1/3}} \quad \text{for } f_{cm} \leq 35 \text{ MPa}$$
$$\varphi_{RH} = \left(1 + \frac{1 - RH/100}{0{,}1 * h_0^{1/3}} * \alpha_1\right) * \alpha_2 \quad \text{for } f_{cm} > 35 \text{ MPa} \quad \text{(Eq. C3)}$$

where RH is the relative humidity. h_0 in equation C3 is the notional size of the member, it is calculated as.

$$h_0 = \frac{2 * A_c}{u} \quad \text{(Eq. C3)}$$

The coefficients $\beta(f_{cm})$ and $\beta(t_0)$ are calculated using equations C4 and C5,

$$\beta(f_{cm}) = \frac{16{,}8}{\sqrt{f_{cm}}} \qquad \text{(Eq. C4)}$$

$$\beta(t_0) = \frac{1}{(0{,}1+t_0^{0{,}20})} \qquad \text{(Eq. C5)}$$

where f_{cm} denotes the mean compressive strength of the concrete 28 days after casting (in MPa).

The second term in equation C1 can be estimated using the following expression,

$$\beta_c(t-t_o) = \left[\frac{t-t_0}{\beta_H+t-t_0}\right]^{0{,}3} \qquad \text{(Eq. C5)}$$

where "t" is the concrete age in days at the moment considered while "t_0" is the age at loading. β_H in equation C5 is a coefficient that depends on the relative humidity, the notional member size h_0 and the concrete quality. It is estimated using one of the below expressions.

$$\beta_H = 1{,}5(1+(0{,}012RH)^{18}) * h_0 + 250 \leq 1500 \qquad for\ f_{cm} \leq 35\ MPa$$
$$\beta_H = 1{,}5(1+(0{,}012RH)^{18}) * h_0 + 250 * \alpha_3 \leq 1500 * \alpha_3\ for\ f_{cm} > 35\ MPa$$

(Eq. C6)

Factors $\alpha_{1-3}$are obtained as:

$$\alpha_1 = \left[\frac{35}{f_{cm}}\right]^{0{,}7}$$
$$\alpha_2 = \left[\frac{35}{f_{cm}}\right]^{0{,}2} \qquad \text{(Eq. C7)}$$
$$\alpha_3 = \left[\frac{35}{f_{cm}}\right]^{0{,}5}$$

Creep coefficient of timber and shear connectors:
The creep coefficient of the timber and shear connectors is i.e. the timber's deformation factor k_{def}. It depends on the service class which in turn depends on the climate in the local environment. Values of the deformation factor k_{def} can be found in table 3.2 of EC 5 – *Design of timber structures.*

Appendix D

Manufacturing of the test specimens

The manufacturing and assembly of the wooden panels took place at the Setra manufacturing park in Dalarna. After carriage to Lund, application of shear connectors and casting of concrete followed at the "Lund Tekniska Högskola" testing facility.

Figure D1. Manufacturing and assembling of the timber component at the Setra manufacturing Park

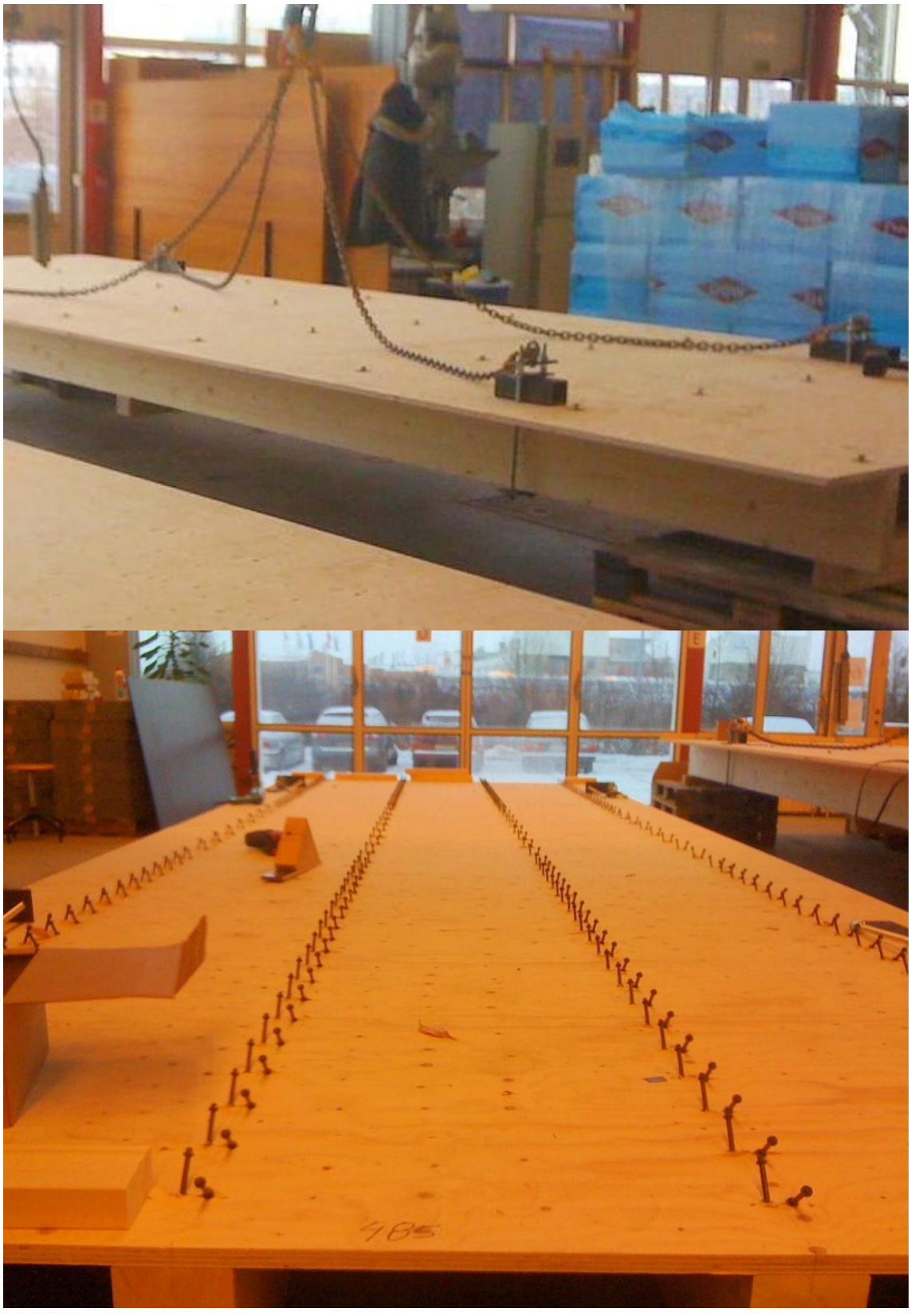

Figure D2. Mounting of shear connectors at the testing facility of "Lunds Tekniska Högskola". Top: Concrete plug-type connection. Bottom: SFS-screw-connection

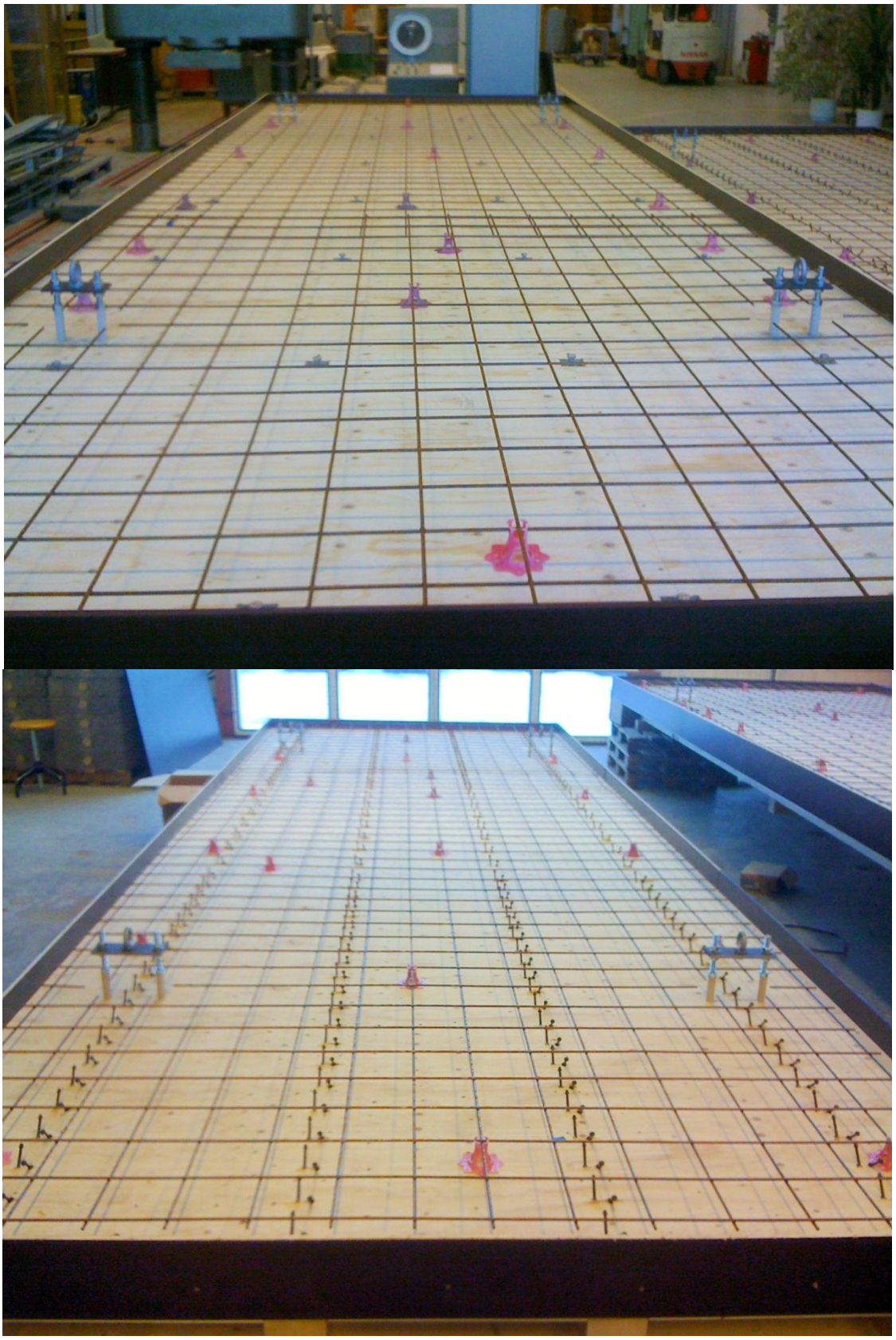

Figure D3. Adding of formwork and reinforcement web for shrinkage reduction

Figure D4. Casting the concrete